Technical Report Documentation Page

1. Report No.	2. Government Accession No.	3. Recipient's Catalog No.
FHWA/TX-96/1409-2F		

4. Title and Subtitle	5. Report Date
THE EFFECTS OF VARIOUS PIPING CONFIGURATIONS ON THE CAPACITY OF A BRIDGE DECK DRAIN	December 1995
	6. Performing Organization Code
7. Author(s)	8. Performing Organization Report No.
Steven Smith and Edward Holley	Research Report 1409-2F
9. Performing Organization Name and Address	10. Work Unit No. (TRAIS)
Center for Transportation Research The University of Texas at Austin 3208 Red River, Suite 200 Austin, Texas 78705-2650	11. Contract or Grant No. Research Study 0-1409
	13. Type of Report and Period Covered
12. Sponsoring Agency Name and Address	Final
Texas Department of Transportation Research and Technology Transfer Office P. O. Box 5080 Austin, Texas 78763-5080	14. Sponsoring Agency Code

15. Supplementary Notes

Study conducted in cooperation with the U.S. Department of Transportation, Federal Highway Administration. Research study title: "Hydraulic Characteristics of Recessed Curb Inlets and Bridge Drains: Phase 2"

16. Abstract

This report describes the effects of the downspout piping on the capacity of a bridge deck drain. Full-scale hydraulic modeling of the drain was performed using two separate physical models to observe the hydraulic behavior of the drain and the influence of various piping configurations on the drain capacity. It was found that the drain behaved under one of two different control regimes for any given set of modeling conditions. Weir control occurred when the drain pan was not completely full and the approach flow was in free-fall over at least a portion of the drain grate. Orifice flow occurred when the drain pan was full so that the flow control was the capacity of the entrance into the drain piping. The capacity of the drain is greater for weir flow than for orifice flow. Thus, the downspout piping above the vent affected the capacity of the drain by influencing the flow at which the transition from weir to orifice control occurred. All vertical piping which followed a piping elbow never flowed full, so the location of the first elbow was found to have significant impact on the drain capacity because this elbow affected the total head on the drain due to the drain piping system. This report presents details of these results with conclusions and design recommendations.

In addition, the results in this report and two previous reports were used to determine the accuracy of calculating the drain flow as the minimum of weir flow using HEC-12 and orifice flow using a constant orifice coefficient and the head across the orifice at the entrance to the drain piping. For most of the conditions, the calculations overestimated the capacity of the drain. The error was as much as 120% just for weir flows or 65% when taking the minimum of weir and orifice controlled flows.

17. Key Words	18. Distribution Statement
Flush depressed curb inlets, bridge deck drains, hydraulic behavior, bridge drain piping	No restrictions. This document is available to the public through the National Technical Information Service, Springfield, Virginia 22161.

19. Security Classif. (of this report)	20. Security Classif. (of this page)	21. No. of Pages	22. Price
Unclassified	Unclassified	139	

THE EFFECTS OF VARIOUS PIPING CONFIGURATIONS ON THE CAPACITY OF A BRIDGE DECK DRAIN

by

Steven Smith
Edward R. Holley

Research Report 0-1409-2F

Research Project 0-1409
Hydraulic Characteristics of Recessed Curb Inlets and Bridge Drains
Phase 2

conducted for the

Texas Department of Transportation

in cooperation with the

U.S. Department of Transportation
Federal Highway Administration

by the

CENTER FOR TRANSPORTATION RESEARCH
Bureau of Engineering Research
THE UNIVERSITY OF TEXAS AT AUSTIN

December 1995

IMPLEMENTATION STATEMENT

1) The drains which have been tested have a larger flow capture capacity when operating under weir control than under orifice control at the outlet from the drain pan.

2) Deeper drains pans with larger outlet pipes maintain weir control for larger captured flow rates.

3) When feasible, straight vertical piping should be connected directly to the outlet from the drain pan. This straight vertical pipe should be as long as possible before a vent and before an elbow. This type of vertical piping provides additional head for draining the pan and keeping the drain operating under weir conditions.

4) It is highly desirable that physical model tests be conducted for drains before their installation to develop empirical calibration information rather than calculating the captured flow rate. Some of the problems with the calculations are (a) calculated flows tend to overestimate the actual captured flow rates, (b) flows calculated from HEC-12 for conditions known to be under weir control were as much as 2.25 times the measured flows, (c) orifice coefficients calculated from the experimental results for flows known to be under orifice control increased with increasing flow rates and varied by almost a factor of 2, (d) the orifice coefficients were different for the same drain installed in two different orientations where one was rotated 180° from the other, (e) taking the calculated capacity as the smaller flow from weir control using HEC-12 and orifice control using an average orifice coefficient of 0.57, the calculations indicated orifice control for flows known to be under weir control, and (f) the problem noted in (e) kept the error in the calculations to a maximum of about 65% overestimation of the captured flow.

Prepared in cooperation with the Texas Department of Transportation and the
U.S. Department of Transportation, Federal Highway Administration.

DISCLAIMERS

NOT INTENDED FOR CONSTRUCTION, BIDDING, OR PERMIT PURPOSES

E. R. Holley
Research Supervisor

SUMMARY

This report describes the effects of the downspout piping on the capacity of a bridge deck drain. Full-scale hydraulic modeling of the drain was performed using two separate physical models to observe the hydraulic behavior of the drain and the influence of various piping configurations on the drain capacity. It was found that the drain behaved under one of two different control regimes for any given set of modeling conditions. Weir control occurred when the drain pan was not completely full and the approach flow was in free-fall over at least a portion of the drain grate. Orifice flow occurred when the drain pan was full so that the flow control was the capacity of the entrance into the drain piping. The capacity of the drain is greater for weir flow than for orifice flow. Thus, the downspout piping above the vent affected the capacity of the drain by influencing the flow at which the transition from weir to orifice control occurred. All vertical piping which followed a piping elbow never flowed full, so the location of the first elbow was found to have significant impact on the drain capacity because this elbow affected the total head on the drain due to the drain piping system. This report presents details of these results with conclusions and design recommendations.

In addition, the results in this report and two previous reports were used to determine the accuracy of calculating the drain flow as the minimum of weir flow using HEC-12 and orifice flow using a constant orifice coefficient and the head across the orifice at the entrance to the drain piping. For most of the conditions, the calculations overestimated the capacity of the drain. The error was as much as 120% just for weir flows or 65% when taking the minimum of weir and orifice controlled flows.

TABLE OF CONTENTS

IMPLEMENTATION STATEMENT iii
SUMMARY v

CHAPTER 1. INTRODUCTION 1
1.1 Background 1
1.2 Objectives 2
1.3 Method of Study 2

CHAPTER 2. LITERATURE REVIEW 3
32.1 Introduction 3
2.2 Modified Manning's Equation 3
2.3 Grate Inlets 5
2.4 One-Dimensional Hydraulics (Daugherty et al., 1985) 6
2.5 Piping Effects on Drain Capacity (Holley et al., 1992) 8
2.6 Vortices 12

CHAPTER 3. EXPERIMENTAL METHODS 15
3.1 Introduction 15
3.2 Drain 2B 15
3.3 Large Model 16
3.3.1 Large Model Size and Construction 17
3.3.2 Large Model Hydraulic System 19
3.3.3 Large Model Instrumentation 21
3.3.4 Large Model Roughness 22
3.4 Small Model 24
3.4.1 Small Model Size and Construction 24
3.4.2 Small Model Hydraulic System 26
3.4.3 Small Model Instrumentation 26
3.4.4 Small Model Roughness 27
3.5 Venturi Meter 27
3.6 V-Notch Weirs 30
3.6.1 Large Model Carryover Weir 32
3.6.2 Large Model Captured Flow Weir 33
3.6.3 Outside Weir 35
3.6.4 Small Model Carryover Weir 36
3.7 Swirl Meter 37
3.7.1 Swirl Meter Dimensions 38
3.7.2 Swirl Angle 40

CHAPTER 4. EXPERIMENTAL RESULTS 41
4.1 Introduction 41
4.2 Large Model Tests 41
4.2.1 Experimental Methods 41
4.2.2 Large Model Test Results 45
4.2.2.1 General Flow Description 46
4.2.2.2 Flow Patterns in Drain Pan 47
4.2.2.3 Drain 2B Capacity with Weir Control 49
4.2.2.4 Drain 2B Capacity with Orifice Control and Piping Effects 56
4.2.2.5 Vortex Effects on Drain 2B Capacity 67
4.2.3 Summary of Large Model Test Results 73
4.3 Comparison of Results with Holley et al. (1992) Tests 74
4.4 Small Model Tests 74
4.4.1 Experimental Methods 74
4.4.2 Small Model Test Results 75
4.4.3 Summary of Small Model Test Results 79
4.5 Sources of Error 80
4.7 Calculation of Bridge Deck Drain Flows 81
4.6.1 Approach 81
4.6.2 Drains 82
4.6.3 Weir Flow 82
4.6.4 Orifice Flow 89
4.6.5 Comparison of Design Calculations and Measurement 92
4.6.7 Design Recommendations 97

CHAPTER 5. SUMMARY AND CONCLUSIONS 99
5.1 Summary of Work 99
5.2 Results and Conclusions 99

REFERENCES 103
APPENDIX A. LIST OF SYMBOLS 105
APPENDIX B. EXPERIMENTAL DATA 109
APPENDIX C. PHOTOGRAPHS 127

CHAPTER 1. INTRODUCTION

1.1 BACKGROUND

Removal of precipitation runoff from bridge decks is an important aspect of highway safety. Roadways are often equipped with curbs and stormwater inlets to remove the runoff quickly and efficiently from highways. If curbs and inlets are not in place, then ditches are adjacent to the roadways to provide for drainage of stormwater from the pavement surface. Due to their elevation above the ground surface, bridges are limited in the types of drainage structures which can be used. Ditches are not an option. Curb inlets would be difficult to construct and would interfere with the superstructure of the bridge. The option most often used to remove water from bridge decks is bridge deck drains.

Bridge deck drains vary in shape and dimension, but typically these drains consist of a drain pan and a drain grate. The drain pan is installed in the bridge deck with the top of the drain flush with the road surface. The grate is placed over the top of the drain pan to prevent clogging of the drain, and to provide safety for pedestrians, bicyclists, and vehicles. The drain pan catches the stormwater and routes the flow to the drain pan orifice. Piping underneath the drain receives the captured flow from the drain pan orifice and carries the runoff to the ground below.

In 1991-1992, a study was performed by Holley et al. (1992) on bridge deck drains used by the Texas Department of Transportation (TxDOT). That study was performed at full-scale using a model of a single lane roadway. One purpose of the study was to quantify the effects of various piping configurations on the capacity of the bridge deck drain. The piping was connected directly to the bottom of the drain pan with no gap or vent in the piping (see Section 1.3). The observed behavior of the drain for some of the piping configurations was not expected. There appeared to be a relationship between the drain capacity and the total vertical length of pipe, but this relationship was also impacted by the distance between the drain and the first piping elbow. The results from the experimentation were presented in a graphical form, but the drain and piping system behavior was not fully understood. The purpose of the research presented in this report was to continue the initial study on one of the drains used by Holley et al. in order to determine the drain behavior for various piping configurations.

1.2 OBJECTIVES

The specific objectives of this research were to

- study the hydraulic behavior of the bridge deck drain and piping systems,
- determine the relationship between the drain capacity and downspout piping length,
- determine the relationship between the drain capacity and the location of the first downspout piping elbow, and
- present design recommendations based on the results.

1.3 METHOD OF STUDY

To achieve these objectives, two major processes were implemented. One was a thorough literature search on bridge deck drains and piping systems and on the variables which can influence the drain and downspout piping behavior. The other was experimentation in the form of full-scale modeling of the drain and piping systems.

The same drain which was studied by Holley et al. was studied in the present research, but the drain was rotated 180° relative to the curb. The drain was rotated because that is how the drain is presently installed in the prototype by TxDOT. Also in the prototype, an air vent is located between the drain and the piping system. This vent acts as an overflow. In case the piping becomes clogged, stormwater will flow out of the vent rather than backing up into the roadway. The vent also allows for differential movement between the bridge deck and the drain piping. In the study by Holley et al. and in the present study, the piping was connected directly to the drain so that there was no vent. The vent was closed in order to determine the possible beneficial effects on the drain capacity.

The full-scale modeling was performed at the Center for Research in Water Resources (CRWR) at the University of Texas at Austin. This research was funded by the Texas Department of Transportation through the Center for Transportation Research (CTR), Project Number 705XXA4004-0-1409.

CHAPTER 2. LITERATURE REVIEW

2.1 INTRODUCTION

Various topics were studied in the literature to identify the general behavior of bridge deck drains and how their capacities may be affected by the piping system beneath the drain. In this chapter, the modified Manning's equation will be presented because that is the equation used to calculate normal depth at the curb. This calculated normal depth is the independent variable used in the design equations for bridge deck drains. The Federal Highway Administration (FHWA) has found that grate inlets in sags have both weir and orifice behavior depending on the gutter depth (Johnson and Chang, 1984). This behavior was also discovered in this research, and therefore, the general equations for weir and orifice flow will be presented. However, the orifice behavior in this research relates to the orifice leading to the drain piping whereas, the FHWA's orifice behavior refers to the grate acting as an orifice. A section of this chapter will cover how a piping configuration is expected to affect the drain capacity based on one-dimensional hydraulics. The findings from the previous study pertaining to the effects of a piping system on drain capacity will be given and will be compared with the behavior predicted by one-dimensional hydraulics. Finally, vortices will be discussed, with an explanation as to how their existence in the drain and in the piping system may influence the capacity of a bridge deck drain.

2.2 MODIFIED MANNING'S EQUATION

The usual form of Manning's equation in SI units for flow through a channel is

$$V = \frac{1}{n} R_h^{2/3} S^{1/2} \tag{2.1}$$

where V = flow velocity,

n = Manning's roughness coefficient,

R_h = hydraulic radius, and

S = slope of the energy grade line.

Equation 2.1 can be written for flow in a triangular channel, such as a street gutter. Assuming that the transverse slope of the road is uniform and that the wetted perimeter is equal

to the ponded width, or equivalently that the hydraulic radius is $y_n/2$, Manning's equation applied to the normal depth can be written as

$$Q = \frac{0.32 y_n^{8/3} S^{1/2}}{n S_x} \tag{2.2}$$

where Q = gutter flow rate (m^3/s),

y_n = normal depth (m),

S = longitudinal roadway slope, and

S_x = transverse slope.

Izzard (1946) used an alternative form of the equation. Rather than applying Manning's equation in an average sense, he applied it in a local sense. He assumed that the velocity at each distance, ζ, from the curb could be calculated using Manning's equation with the local depth, η, at that point being equal to the hydraulic radius. Thus, at each ζ where the depth is η, he had

$$V = \frac{1}{n} \eta^{2/3} S^{1/2} \tag{2.3}$$

For uniform flow, the flow through an incremental area, $\eta d\zeta$, at each ζ was then $(V\eta)d\zeta$. Using Equation 2.3, he integrated $(V\eta)d\zeta$ with respect to ζ across the flow area with a uniform transverse slope. The result was

$$Q = \frac{3}{8} \frac{y_n^{8/3} S^{1/2}}{n S_x} \tag{2.4}$$

The only difference between this form of Manning's equation and Equation 2.2 is the coefficient. For a given set of hydraulic conditions (Q, n, S, and S_x), y_n calculated from Equation 2.4 is 7% larger than when calculated using Equation 2.2. Equation 2.4 is the form of Manning's equation typically used for gutter flows. This equation was the form of Manning's equation used to calculate normal depth in the research presented in this report and in the study by Holley et al. (1992) (see Section 2.5).

2.3 GRATE INLETS

The FHWA (Johnson and Chang, 1984) reports that a grate inlet in a sag operates as a weir up to a certain gutter depth, at which point it begins operating as an orifice. The FHWA design equations for grate inlets on-grade are presented in terms of design charts. Johnson and Chang do not define the behavior of on-grade inlets in terms of weir or orifice flow regimes. Also, the equations for grate inlets presented by Johnson and Chang do not include the effects of a pan located under the grate. However, their results are still relevant because the weir and orifice behaviors were also observed in this research, even though the drain in this study was not located in a sag and even though the orifice behavior in this project is different from Johnson and Chang's, as stated previously.

The equation for a broad-crested weir is (Bos, 1989)

$$Q = C_{wd} C_{wv} \frac{2}{3}\left(\frac{2}{3}g\right)^{0.50} L_e h_w^{1.5} \tag{2.5}$$

where C_{wd} = weir discharge coefficient,

C_{wv} = velocity head correction coefficient,

g = acceleration due to gravity,

L_e = effective weir length, and

h_w = weir head.

An explanation of this equation will be given in Section 4.2.2.3, which discusses the behavior of Drain 2B with weir control.

The equation for an orifice is (Bos, 1989)

$$Q = C_{ov} C_{od} A_o \sqrt{2gh_o} \tag{2.6}$$

where C_{od} = orifice discharge coefficient,

C_{ov} = velocity head correction coefficient,

A_o = area of orifice, and

h_o = orifice head.

C_{ov} is a correction coefficient because the approach velocity head is often excluded from the orifice head term. When the approach velocity head is included in h_o, $C_{ov} = 1.0$, and h_o becomes H_o. Equation 2.6 is then

$$Q = C_{od} A_o \sqrt{2gH_o} \tag{2.7}$$

If piping were connected to the drain pan orifice, then the piping would increase the value of the orifice head as described in the next section.

2.4 ONE-DIMENSIONAL HYDRAULICS (Daugherty et al., 1985)

Consider a bridge deck drain and piping system as shown in Figure 2.1.

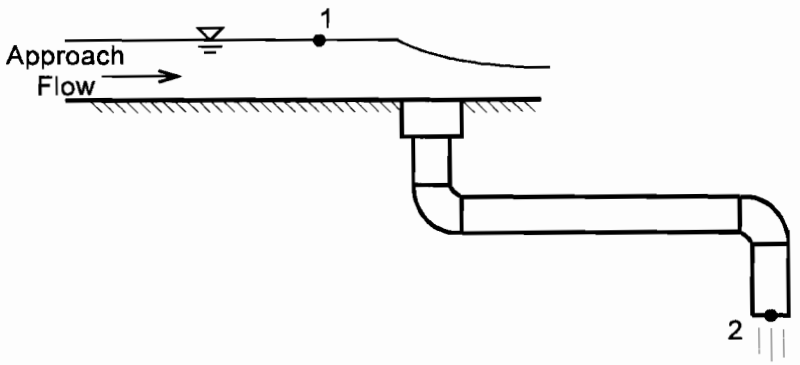

Figure 2.1 Elevation View of Bridge Deck Drain and Piping System

Assuming there is no air vent between the drain and the piping system, the energy equation from point 1 to point 2 for a pipe flowing full is

$$\frac{p_1}{\gamma} + z_1 + \frac{V_1^2}{2g} = \frac{p_2}{\gamma} + z_2 + \frac{V_2^2}{2g} + h_L \tag{2.8}$$

where p = pressure,

V = velocity,

z = elevation,

γ = specific weight, and

h_L = head loss through the system.

Atmospheric pressure exists at points 1 and 2. Therefore,

$$\frac{p_1}{\gamma} = \frac{p_2}{\gamma} = 0 \tag{2.9}$$

and Equation 2.8 reduces to

$$z_1 - z_2 = \frac{V_2^2}{2g} - \frac{V_1^2}{2g} + h_L \tag{2.10}$$

Since the capacity of Drain 2B was limited by orifice control for some of the tests (see Section 4.2.2.4), Equation 2.10 was combined with Equation 2.7 to determine the relationship between the piping configuration and the flow rate captured by the drain. Considering the piping system in Figure 2.1, Equation 2.10 gives the orifice head in Equation 2.7 as

$$H_o = z_1 - z_2 + \frac{V_1^2}{2g} - \frac{V_2^2}{2g} - h_L \tag{2.11}$$

In Equation 2.7, C_{od} is considered to account for all losses between point 1 and the drain piping. These losses include channel loss, drain loss, and orifice loss. Since these losses were accounted for in C_{od}, h_L in Equation 2.11 represents the remaining losses, which are the piping losses. For the piping system in Figure 2.1,

$$h_L = 2h_{EB} + h_P \tag{2.12}$$

The elbow losses are represented by h_{EB} and the straight pipe loss is represented by h_P.

Equation 2.11 reveals that as the value of the vertical pipe length, z_1-z_2, increases, the total head across the drain orifice will increase. An increase in the orifice head results in an increase in the captured flow rate, according to Equation 2.7.

This analysis of the drain and piping system considers only one-dimensional hydraulics, without consideration for the interaction between the various head loss terms and how they might influence each other. In other words, according to one-dimensional hydraulics, the distance from the drain to the first elbow should have no influence on the drain capacity, given a constant value

for z_1 - z_2. However, for Holley et al. (1992), the distance from the first elbow to the drain pan seemed to have a significant impact on the drain capacity for any given total vertical length of pipe.

2.5 PIPING EFFECTS ON DRAIN CAPACITY (Holley et al., 1992)

Holley et al. (1992) performed tests on Drain 2, the same drain discussed in this report (see Figure 3.1), to study the influence the downspout piping had on the drain capacity. In the study by Holley et al., the drain was oriented such that the deep portion of the drain was placed next to the curb. The orifice of the drain was located in the deep portion of the drain pan. (In the present research, the drain was rotated 180° so that the deep portion of the drain faced the center of the road. The shallow portion of the drain was placed next to the curb.) The results in the Holley et al. study were surprising. The reaction of the drain capacity to various piping configurations did not appear to correspond to one-dimensional hydraulics theory.

Holley et al. performed full-scale tests on the drain using a model of one lane of a roadway (see Section 3.3). Seven different piping configurations using 0.152 m diameter clear PVC pipe were studied, as shown in Figure 2.2. These configurations were named A - G. Configurations A - E in Figure 2.2 are looking normal to the flow direction on the model road surface. Configurations F and G are looking downstream. All the tests were performed at a longitudinal slope of 0.001 and transverse slopes of 0.06 and 0.08. These slopes were chosen because they were expected to produce the largest drain flows, and therefore, the largest influence by the piping on the drain capacity.

Figure 2.3 shows the results obtained from the tests on Drain 2. The captured flows, Q_2, for each of the piping configurations are plotted with respect to the calculated normal depths at the curb. These normal depths were computed using Equation 2.4. Some general trends were revealed from the results in Figure 2.3. For low approach flow rates, or similarly low approach normal depths, all drain piping configurations behaved essentially the same. At some point,

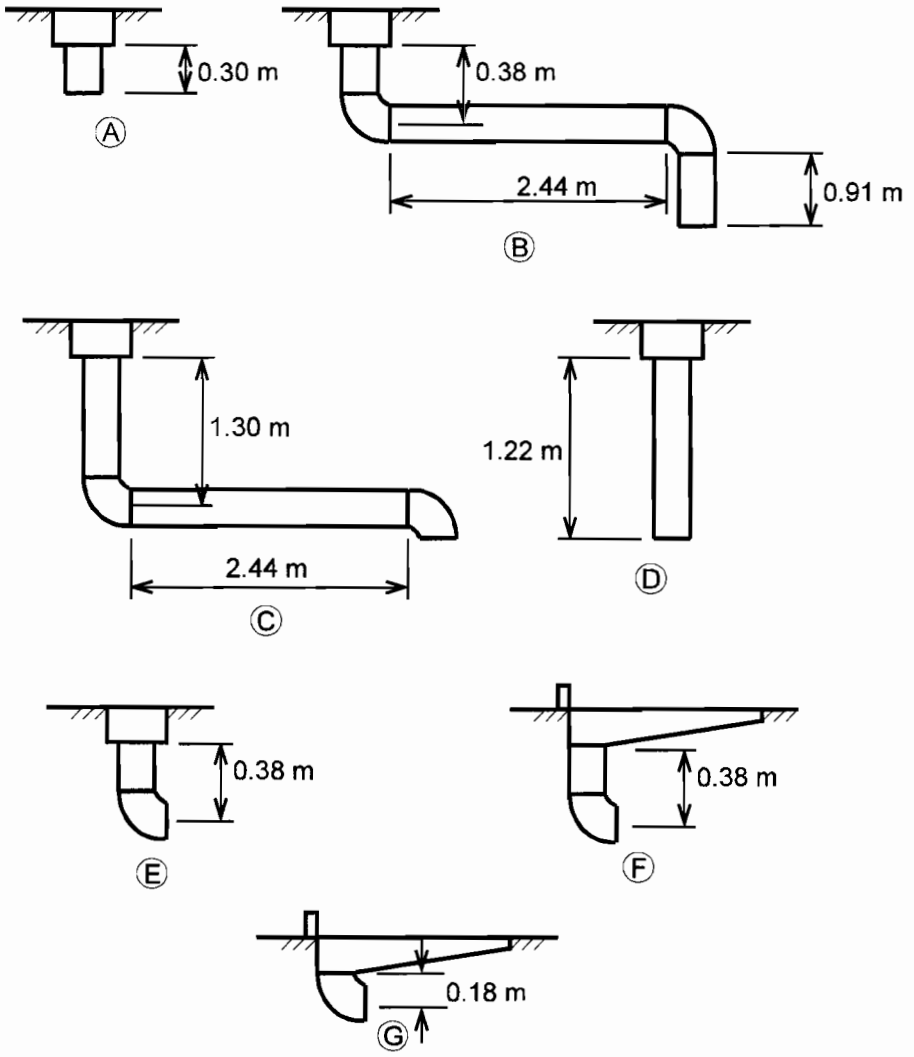

Figure 2.2 Piping Configurations for Tests by Holley et al. (1992) (not to scale)

depending on the piping configuration, the slope for each configuration deviated from the trend, and a different relationship was observed. The data points then shifted to a much steeper slope. The slope of the steep portions of the graph seemed similar in value for all the configurations, but the transition from the flatter slope to the steeper slope occurred at different normal depths, or different values of Q_2, for each configuration. It was presumed that the lower slope corresponded to weir control as the water flowed over the lip of the inlet, or orifice control, as water flowed

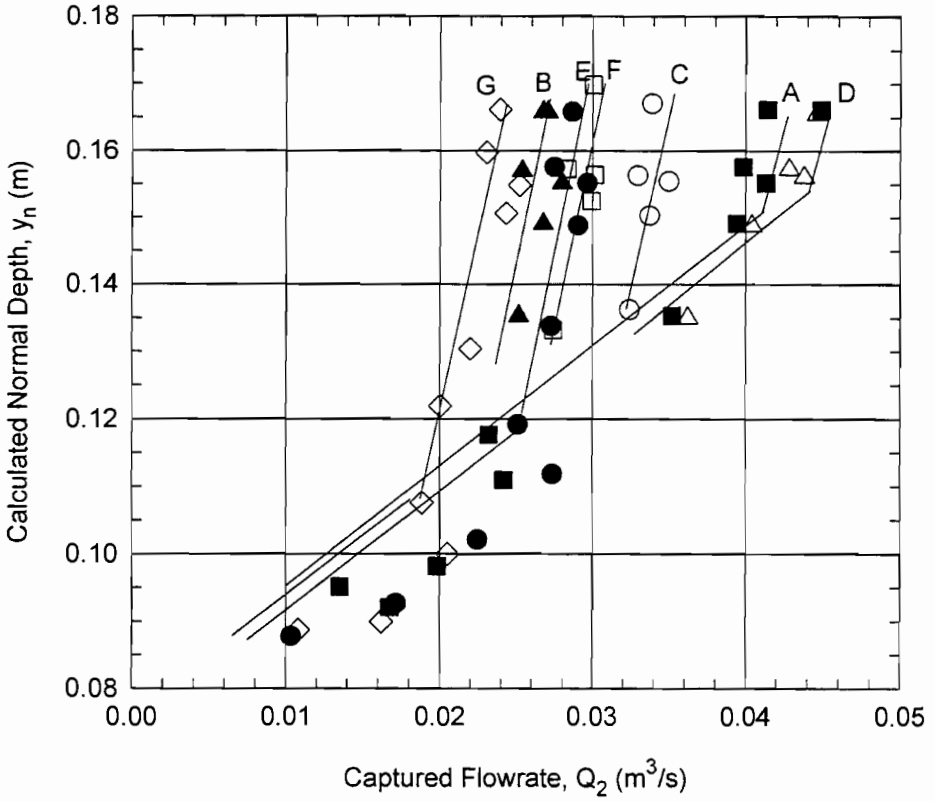

Figure 2.3 Effects of Piping Configurations on Drain 2 Capacity (Holley et al., 1992)

from the inlet box into the piping system. The steeper slopes presumably corresponded to back pressure effects from the piping system. The research presented in this report revealed that the flatter sloped portions correspond to weir control, and the steeper portions correspond to orifice control. This observed behavior will be discussed further in Chapter 4. For all of the points on the steeper slope in Figure 2.3, at least part of the piping systems was flowing full.

Other relationships and general conclusions were drawn from this data and are listed below. For orifice control conditions:

1) $Q_2(A) < Q_2(D)$, in accordance with one-dimensional hydraulic theory because there was a greater difference in head across the piping system as the vertical pipe length was increased, going from A to D.

2) $Q_2(B) < Q_2(C) < Q_2(D)$, with significant differences between the behaviors of each configuration. Configurations B, C and D all had essentially the same values of z_1-z_2. Configuration D captured the most flow, in accordance with theory because there were no losses from elbows, and it had the shortest total length of pipe. According to

one-dimensional hydraulic theory, there should have been no difference between B and C. They both had the same total length of pipe, the same number of elbows, and the same vertical head difference. The essential difference was the location of the first elbow.

3) $Q_2(B) < Q_2(E)$, but the difference was small. It was surprising that B was not significantly larger than E, since B had an extra 0.91 m of vertical pipe to create a larger head difference across the piping system. The total calculated head loss in B from the elbow and extra pipe length was only about 0.18 m. The essential feature which was similar between B and E was the location of the first elbow.

4) $Q_2(E) = Q_2(F)$, with the difference in piping being only the elbow orientation with respect to the drain.

5) $Q_2(G) < Q_2(F)$, and the outlet for G was 0.30 m higher than for F, so it was not determined if the reduction in flow for G was due to the decrease in head across the pipe, or due to the change in location of the elbow with respect to the drain.

Finally, conclusion 6 stated that the flow differences for the various piping configurations were determined to be much greater for back-pressure control than for what Holley et al. called weir or orifice control. Now knowing that the trends shown in Figure 2.3 are really weir and orifice control conditions, conclusion 6 could be reworded by saying that the drain capacity was essentially the same for all configurations under weir control, but the drain capacity was significantly different for each configuration under orifice control.

It was concluded by Holley et al. that the location of the first elbow had a strong influence on the amount of flow captured by the drain, when back-pressure existed. This back pressure region was actually the orifice control region. Orifice flow occurred because the piping configuration reached capacity such that the drain pan became full, preventing weir flow over the lip of the grate. When all other factors were equal, the captured flow decreased as the first elbow was placed closer to the bottom of the drain pan. The reason for this behavior was not determined by Holley et al., but it seemed that the distance between the drain pan and the first elbow was very crucial in establishing the flow pattern in the pipe. One hypothesis proposed to explain this behavior was that a vortex was created at the orifice of the drain and was interacting with the first elbow to affect the drain capacity. This hypothesis was pursued in the present study, but the observations during testing determined that the vortex had little or no influence on the drain capacity (see Section 4.2.2.5). The reason that the distance to the first elbow had such

an influence on the drain capacity, as will be thoroughly discussed in Chapter 4, is that the vertical pipe which was connected to the second elbow in Configuration B was never full. This pipe did not add to the total head across the drain. Since this conclusion was not determined until after most of the research was performed and after much of the literature search was done, the theory of the vortex affecting the drain capacity was pursued. It is also possible that at least the lower part of the vertical pipe in Configuration D was not full. If so, then the small differences in the results for A and D would not be surprising.

2.6 VORTICES

A vortex is defined as the rotating motion of a multitude of material particles around a common center (Lugt, 1983). Gordon (1970) studied vortex formation by observing vortices at existing hydroelectric intakes. He determined there were four factors influencing the formation of a vortex in those situations. The factors were the geometry of the approach flow relative to the intake, the flow velocity at the intake, the size of the intake and the submergence of the intake. Any of these factors can result in creating angular momentum in a flow. The angular momentum of a flowing particle is proportional to the vector cross-product of its velocity and its distance from the center about which it is rotating. As a particle having a small angular momentum is drawn toward an opening, the particle must increase its azimuthal velocity at a rate inversely proportional to the distance from the center of the opening. This increase in velocity makes the presence of a vortex more apparent.

A literature search was conducted to determine how a vortex might affect the capacity of the bridge deck drain studied in this research. As will be discussed in Chapter 4, a vortex was observed in the orifice of the bridge deck drain. It was thought that maybe the vortex was interacting with the elbow under the drain in such a way as to cause the behavior that was observed by Holley et al. (1992). The literature search was performed in order to determine if it was possible for the vortex to interact with the elbow in such a way as to increase the head loss through the piping system above that predicted by one-dimensional hydraulics.

Most of the literature on the topic of vortices discusses the study of vortices through hydraulic intakes at hydroelectric plants. There are many problems in transferring the results

obtained in those studies to useful information for this study. One reason is that vortices are highly complex, and thus many researchers contradict other researchers' conclusions in describing vortices. Also, vortex behavior is highly dependent upon the specific conditions present in each study. Third, much of the literature is highly mathematical and requires known boundary conditions and velocity profiles of the vortex. These parameters were not measured in this study. The fourth and most important reason that the results from other research are difficult to transfer to this study is that no study was found which directly relates to this one. The complexity of vortices and the limited scope of this research in terms of vortex study prevented detailed correlation between results of past research on vortices and the results found in the present study. Even though detailed correlation is not possible, some general conclusions can be drawn from past research. It was hoped that these general conclusions would shed light on the drain behavior seen in the study by Holley et al. (1992) and in the study detailed in this report.

According to Knauss (1987), vortices at intakes can cause a reduction in flow. This reduction in flow is caused by an increase in head loss, due to the hindered intake process (Knauss, 1987). Bennie (1962) also stated that the existence of a vortex reduces the intake pipe capacity. Another study performed by Jain et al. (1978) also found that swirling flow in a pipeline causes increased energy loss. It appears from these sources that the existence of a vortex in the drain orifice or the piping system can reduce the capacity of the drain.

In addition to decreasing the drain capacity by increasing the head loss through an orifice, vortices can decrease the drain capacity through air entrainment. If the vortex is strong enough, it can form an air-core that will reach the intake. The depth of submergence of an intake when the air-core first reaches the intake is called the critical submergence (Lugt, 1983). When the submergence of the intake is equal to or less than the critical submergence, air will be entrained into the intake and the connected piping. This air entrainment decreases the flow area within the pipe connected to the intake and can therefore decrease the capacity of the pipe. Bennie (1962) verified this conclusion when he studied swirling flows in a vertical pipe and bend. He found that greater discharges occurred when there was no air entrainment.

Vortices can also influence head loss through bends in pipes. Shimizu (1975), as referenced by Kitoh (1987), studied velocity measurements of swirling flow through multiple 90°

bends. Shimizu connected three 90° bends to study the influence of various connection configurations on the head loss through the piping. He found that the head loss had a "complicated form depending on the manner in which they (the three bends) were connected" (Kitoh, 1987). The total loss through the three bends was anywhere from two to five times the loss through one bend, depending upon the configuration of the connections. He also found that the swirling motion and the uneven axial velocity appearing in a bend were the primary effects on the bend loss. So Shimizu showed that losses in piping systems can interact in such a way that the total loss through the system is greater than what would be predicted if each loss were considered separately. So in the above example by Shimizu, one-dimensional hydraulics did not accurately describe the losses through the piping system.

Finally, through a study performed by Posey and Hsu (1950), vortices were found to change the discharge coefficient through an orifice. They discovered that as the vortex strength increased, the orifice discharge coefficient decreased for a given head over the orifice.

From this literature study on vortices, it is safe to predict that one-dimensional hydraulics is not detailed enough to describe the flow of fluid through complicated piping systems, especially in the case of swirling flow through the system. Thus, if a vortex exists upstream of an elbow, then that vortex may alter the head loss through the elbow. The true head loss value may be different from the value predicted by one-dimensional hydraulics. Also, the existence of a vortex at the orifice of the drain may decrease the capacity of the drain.

Although much of the literature on vortices is not directly applicable to this research, it is clear from this literature search that vortices *can* have an influence on the capacity of the drain and piping system. The vortex can decrease the orifice discharge coefficient, entrain air into the piping and cause a reduction in the flow area, interact with the first elbow to increase the head loss through the elbow, or all of these simultaneously. However, as will be discussed in Chapter 4, the vortices observed in this research did not appear to significantly influence the drain capacity.

CHAPTER 3. EXPERIMENTAL METHODS

3.1 INTRODUCTION

Two physical models were used in the study of the bridge deck drain. One model was designated the *large* model. The other model was called the *small* model. In order to make these models useful in the study of the bridge deck drain, other lab equipment was used. Some of this equipment included V-notch weirs, swirl meters, a venturi meter, manometers, point-gauges, and all equipment which moved water to and from the models.

The details of the drain which was studied will be discussed, then a description of the two models, followed by the flow measurement devices and their calibration data, will be given. Finally, the swirl meter and its use in this study will be described.

3.2 DRAIN 2B

The drain which was studied is designated Drain 2B in this report. Figure 3.1 shows the shape and size of Drain 2B. The drain consisted of a grate and a drain pan. The shallow portion of the pan sloped to a 0.152 m diameter outlet pipe, called the drain pan orifice. This pipe was located at the deepest portion of the pan. The pan had a 0.025 m wide shoulder 0.025 m below the top of the pan; the grate rested on this shoulder. The entire drain was made of plexiglass so that the flow behavior inside the drain could be observed.

Drain 2B was called Drain 2 when it was used in a previous study by Holley et al. (1992). At that time, the drain was aligned such that the deep side of the drain was placed next to the curb, with the shallower end extending transverse into the road. However, in this study the drain orientation was reversed. The deep portion of the pan was toward the center of the road, and the shallow portion was next to the curb. For this reason, the designation was changed from Drain 2 to Drain 2B.

The Texas Department of Transportation formerly installed these drains in the orientation modeled in the first study. However, due to structural and aesthetic considerations, the Department is now installing them in the orientation modeled in this research.

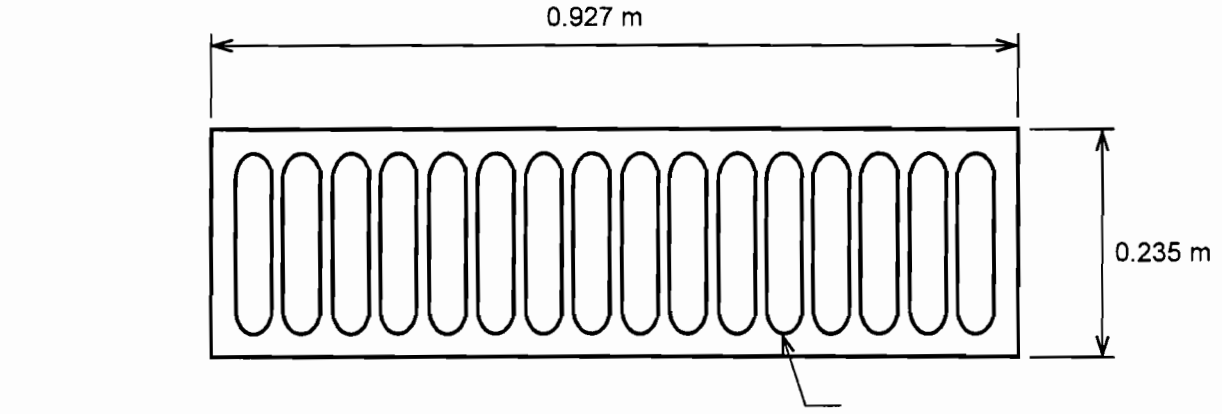

a) Plan View of Grate

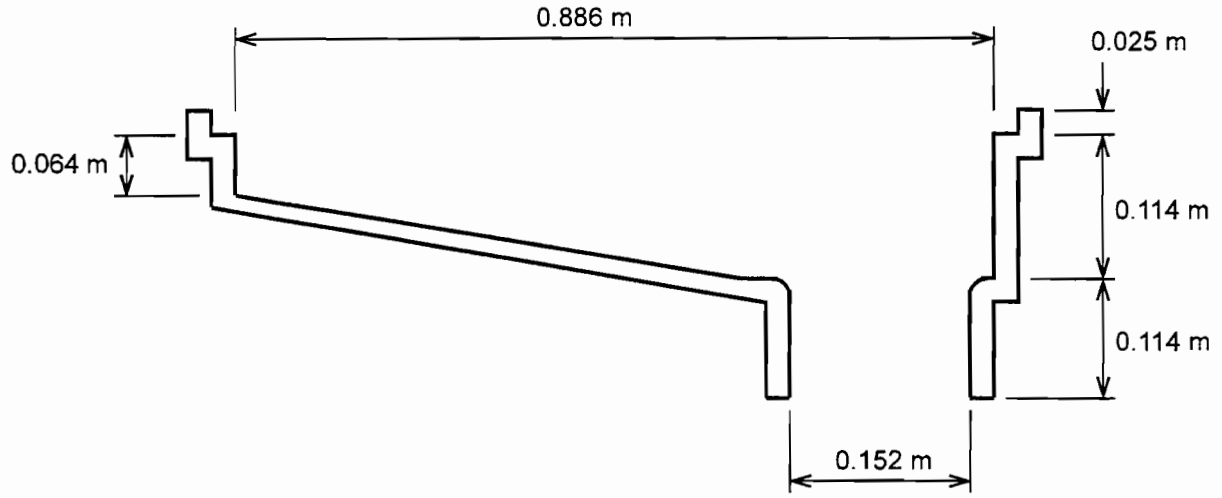

b) Cross- Section of Drain Pan

Figure 3.1 Drain 2B (not to scale)

3.3 LARGE MODEL

The large model was intended to simulate one lane of a roadway at 3/4 scale. It was used to study Drain 2B at full-scale, and other bridge deck drains and stormwater curb inlets at 3/4 scale in the previous study. The following sections describe the construction, dimensions, and layout of the large model.

3.3.1 Large Model Size and Construction

Figure 3.2 is a plan view of the large model. The 3.20 m width is 3/4 scale of a 4.27 m width. Walkways existed outside of both curbs to provide easy and dry access to any portion of the model. The model was supported at four points, as shown in Figure 3.3. One support was a rotating ball joint, while the other three supports consisted of hoist systems. This combination of hoists and ball joint supports allowed the model to be tilted in both longitudinal and transverse directions so that the roadway slope could be adjusted to observe the resulting effects on drain and curb-inlet capacities.

Two 18.3-m, wide-flanged beams provided the major structural support for the model. These beams were spaced six feet from center to center. Transverse joists, which were 2"x6" (0.051 m x 0.152 m) lumber, were spaced on 0.610 m centers in the longitudinal direction on top of the beams. The joists supported the deck which consisted of 3/4" (0.019 m) tongue-and-groove plywood.

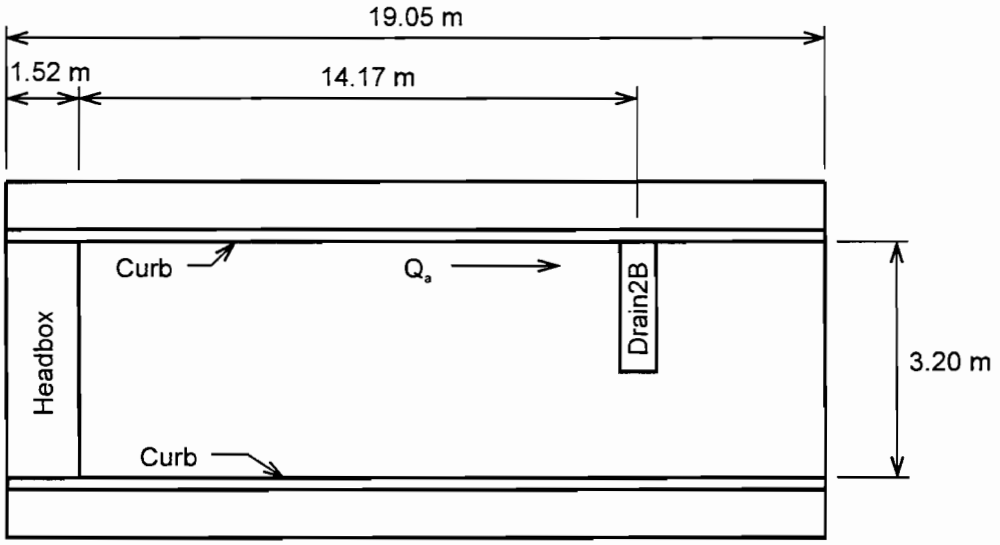

Figure 3.2 Plan View of Large Model (not to scale)

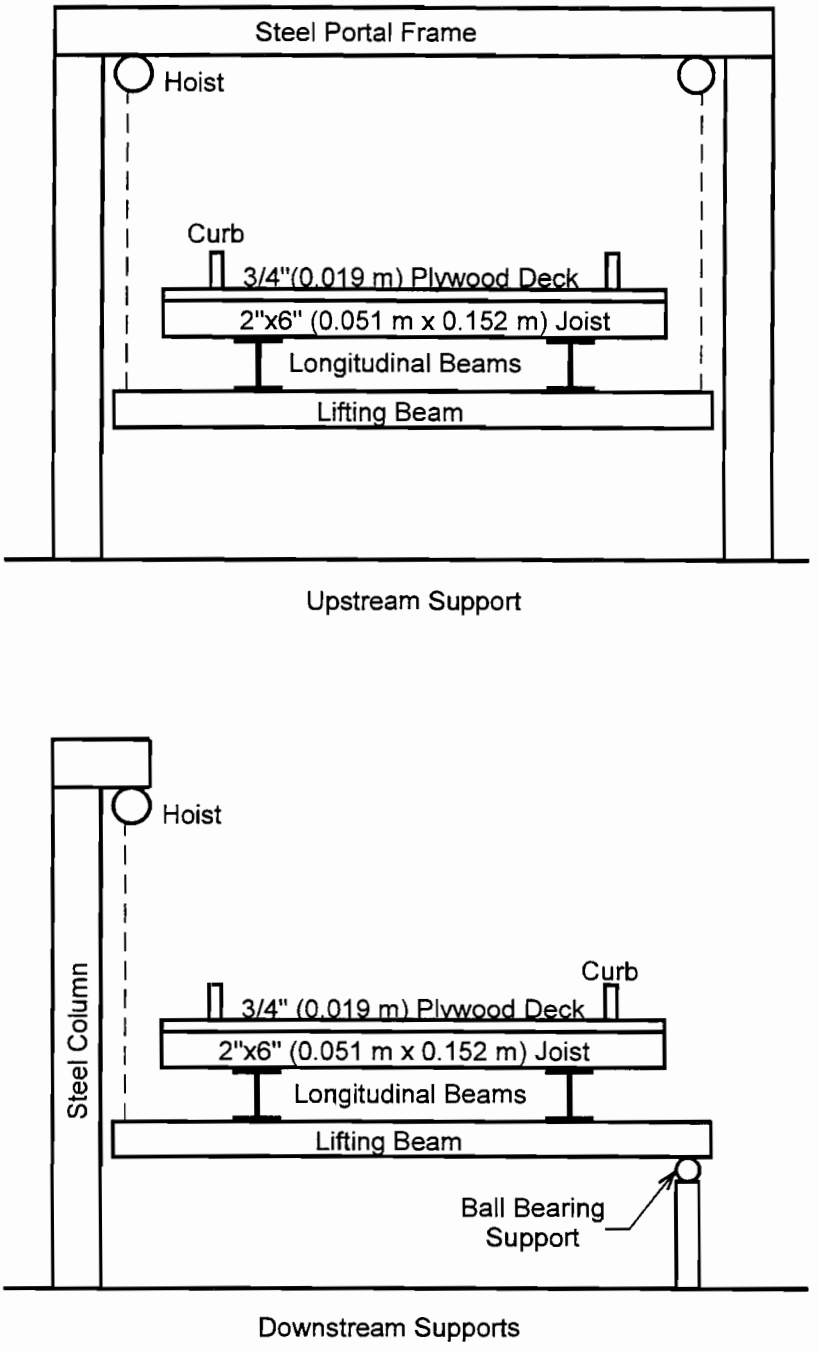

Figure 3.3 Elevation View of Support Structure for Large Model (not to scale)

The large model was initially constructed in 1990. Latex paint with imbedded sand grains was used to waterproof the model and provide the necessary texture. However, by 1993 when

this project began, the model surface had warped and deteriorated, as the paint was not sufficient to prevent rotting and warping of the structure. At the beginning of this project, all of the plywood deck, and most of the transverse joists were replaced.

During the reconstruction process, it was discovered that the wide-flanged beams were slightly curved. Because of this curvature, shims were placed between the beams and the transverse joists to provide a level surface on which to screw the plywood deck. A surveying level and rod were used throughout the reconstruction process to guarantee that the model surface was level, within a 0.002 m tolerance. After the plywood deck was in place, 2"x8" (0.051 m x 0.203 m) joists were secured to the deck to simulate the curbs. To complete the reconstruction, fiberglass was used to seal the surface and prevent water damage. Once the fiberglass had cured, one last layer of resin was placed on the model deck and sand grains were scattered in the wet resin to simulate a typical roadway hydraulic resistance.

Drain 2B was located on the left side, 15.70 m from the upstream end of the model. The right-hand side of the model was used for studying curb inlets. In hydraulics, left and right are defined by looking downstream, or in this case, looking from the headbox to the drain. The model was large enough to have a bridge deck drain and a curb inlet installed together. Also, another drain could be studied by simply removing Drain 2B and cutting a hole for the new drain, either slightly upstream or downstream of the location of Drain 2B.

3.3.2 Large Model Hydraulic System

A 1900 m^3 reservoir provided the water which was used in the study of Drain 2B. The water was pumped into the headbox of the large model through a 0.305 m diameter pipe. The flow into the headbox was controlled by a 0.305 m butterfly valve. In the headbox, water passed through baffles which adjusted and dampened the flow conditions in the model. Figure 3.4 shows the piping system for the large model. The water was pumped from the north pump, south pump, or both simultaneously. Either pump, when operating alone, was capable of discharging approximately 0.12 m^3/s of water into the model. Operating together, the two pumps had a maximum discharge of 0.20 m^3/s. (Higher flows are possible for models on the laboratory

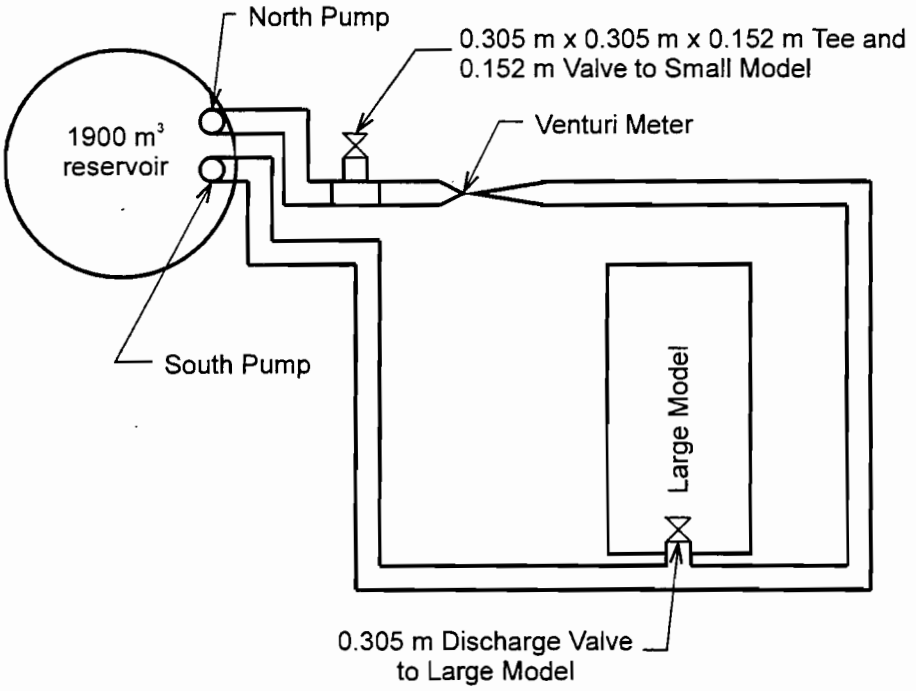

Figure 3.4 Piping System for Large Model (not to scale)

floor. The discharge point for flow into this model was about 3.7 m above the floor, thereby increasing the head on the pumps.) The north pump flow rate was measured using a venturi meter. The south pump flow rate was measured using a flow sensor attached to a Hewlett Packard data acquisition system. The data acquisition system was calibrated, but presented some problems early in the study and was not used. Flow from the south pump was never directly measured because the south pump was only used when the north pump was used. The total flow rate from both pumps was measured by summing the flow through two V-notch weirs as described further in this section.

Water traveled down the model, reached uniform flow upstream of the drain, and was either intercepted by the drain, flowed over it, or flowed around it. The captured flow entered the drain and flowed through the attached piping system, which consisted of 0.152 m PVC pipe. All straight pieces of PVC pipe were clear so that the flow conditions in the pipe could be observed. However, the elbows used in the piping systems were white PVC. Clear PVC elbows are not a

standard item for most PVC manufacturers. After flowing through the drain piping, the water discharged into a tank beneath the model and flowed from this tank over a V-notch weir, called the *captured flow weir*, as shown in Figure 3.5. Similarly, the carryover flow not captured by the drain flowed over the end of the model and into another tank which discharged over another V-notch weir, called the carryover weir. The two weirs discharged into a return channel which routed the flow back outside the lab and into the reservoir. The return channel held another V-notch weir, designated the outside weir.

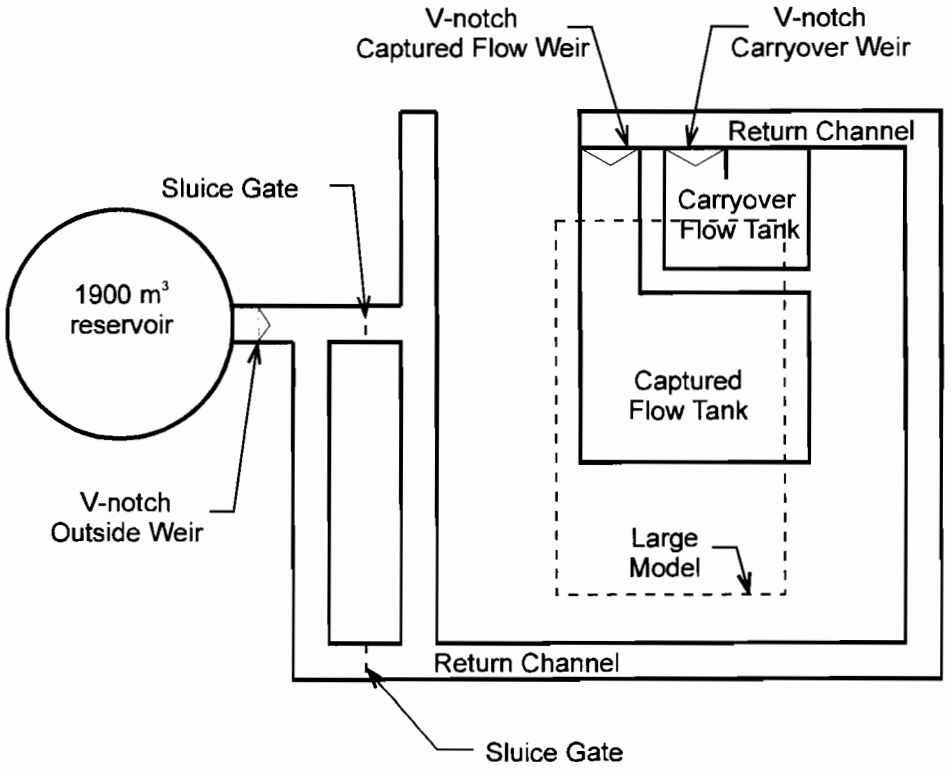

Figure 3.5 Plan View of Return Channel and Flow Measurement Instruments for Large Model (not to scale)

3.3.3 Large Model Instrumentation

Walkways straddled the simulated roadway surface and rested on the tops of the curbs. These walkways provided access across the model as tests were being run, and point-gauges on instrument carriages next to the walkways were used to measure the curb depths. Each point-

gauge was mounted on a linear bearing. The linear bearing was connected to a horizontal instrument bar on the instrument carriage which rested on the tops of the curbs.

Three stilling wells were located at 1.52 m, 3.05 m, and 4.57 m upstream of Drain 2B. The stilling wells were installed for other studies, and were necessary when flow conditions were supercritical. Under supercritical flow, the exact location of the water surface was difficult to pinpoint due to the waviness of the water surface. Therefore, the stilling wells provided a level water surface from which to measure the curb depths. All tests run on the large model for this study were subcritical, therefore, the stilling wells provided verification to the depths measured directly at the curb. The curb depths needed to be measured in order to determine whether uniform flow was obtained upstream of the drain. They were also used to calculate the roughness coefficient for the model.

3.3.4 Large Model Roughness

The typical Manning's roughness coefficient of a Portland cement concrete or asphaltic cement road is between 0.015 and 0.020. The drain was studied at full-scale and therefore, the roughness also needed to be within this range of values.

The roughness was achieved by scattering sand grains over the model deck which was coated with wet fiberglass resin. A relationship between sand grain size and Manning's roughness coefficient for a plane sand bed channel, as given by Henderson (1966), is

$$n = 0.041 d^{1/6} \tag{3.1}$$

where n = Manning's roughness coefficient and

d = median sand grain size (m).

The median sand grain size used was 0.0013 m. According to Equation 3.1, this sand grain size corresponded to a Manning's roughness of 0.014.

Although Equation 3.1 gives a relationship between the sand grain size and Manning's n, the true value of Manning's n for the model needed to be determined by experimentation. Manning's n was determined by using the standard-step method as described by Henderson (1966). Equations used in the standard-step method were input into a spreadsheet and a water surface profile was calculated for each test using various values of n. The calculated profile was

compared to the measured profile. The calculated profile which most closely matched the measured profile had the correct value for Manning's n.

Experiments were conducted on the model to determine the roughness before the drain was placed in the model. Manning's n tests were performed with various longitudinal slopes and flow rates, but with zero transverse slope. Both subcritical and supercritical flow regimes were used. In order to obtain the flow profiles, three depths were measured at each of three cross-sectional profiles along the length of the model using point-gauges. From these tests, the average value of Manning's n was 0.017.

Manning's n = 0.017 was verified during initial tests run on Drain 2B and during curb inlets tests being performed by Hammons and Holley (1995). Figure 3.6 shows a comparison of

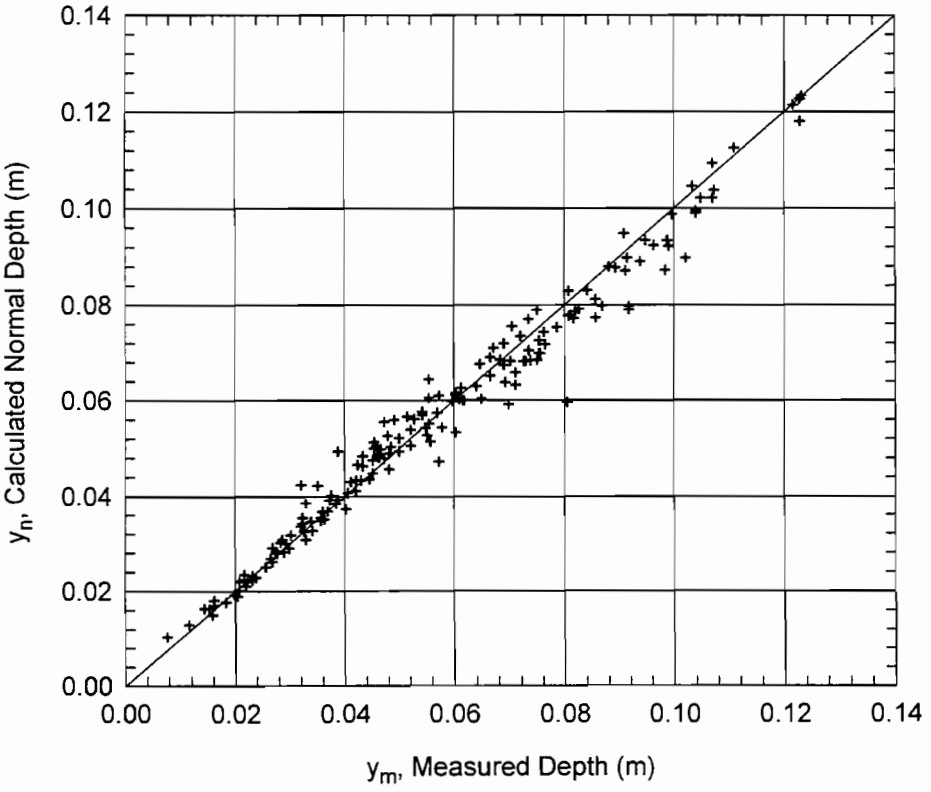

Figure 3.6 Comparison of Calculated Normal Depth and Measured Depth for Various Tests Run on the Large Model (Hammons and Holley, 1995)

the calculated normal depths and measured depths for various curb inlet and drain tests run on the large model. Normal depths for these drain and curb inlet tests were calculated using Equation 2.4 with a model Manning's n value of 0.017. Although there is some scatter in the data in Figure 3.6, the agreement between the calculated and measured depths is acceptable considering not all flows reached uniform flow. It was not known for certain why the model roughness value of 0.017 did not correspond to that value predicted by Equation 3.1. The most likely reason is that the sand grains scattered on the roadway surface had a greater grain-to-grain spacing than would exist for a plane sand bed channel for which Equation 3.1 was developed.

3.4 SMALL MODEL

The small model was built to represent a part of the large model due to the limitations on the large model. The large model had a clearance of 1.2 m from the bottom of the drain pan to the typical water surface in the captured flow tank. The small model was constructed 4.9 m above the ground. This increase in height allowed for greater variation in the pipe length under the drain.

The results obtained from the small model tests did not provide significant new information about the drain behavior for various piping configurations, but the small model results did provide reinforcement to the results shown in the large model. Section 4.3 details the problems with the small model and the results that were obtained using the small model.

3.4.1 Small Model Size and Construction

Figure 3.7 is a plan view of the small model. The deck was 3.66 m long with 1.52 m width between the curbs. Two 2"x8" (0.051 m x 0.203 m) longitudinal beams supported the deck on a scaffold type structure. Transverse 2"x6" (0.051 m x 0.152 m) joists were spaced on one foot intervals in the longitudinal direction, providing support to which the 0.019 m plywood deck was attached. Adjustable support winches (three "come-alongs"), which served the purpose of changing the longitudinal and transverse slopes, were located on three of the corners of the small model deck. There was a hinge on the fourth corner with a large pin connection creating a

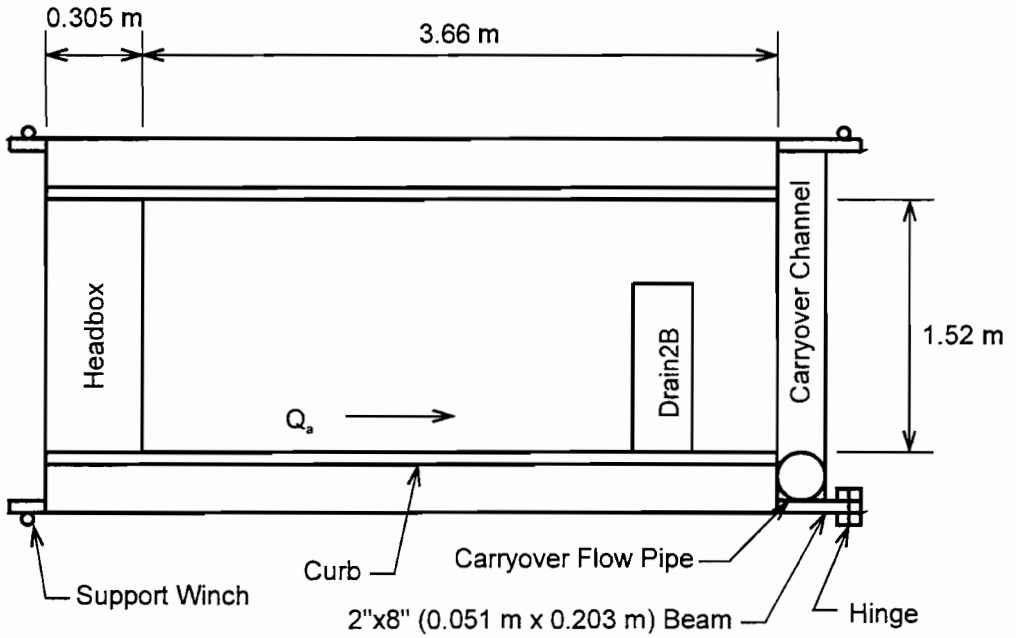

Figure 3.7 Plan View of Small Model (not to scale)

pivot point for the deck. The model was raised using the winches, and shims were placed between the 2"x8" (0.051 m x 0.203 m) longitudinal beams and the frame supporting the deck. Shim size varied depending upon the desired model slope. Curbs were created using 2"x6" (0.051 m x 0.152 m) boards attached to the plywood deck. Fiberglass was placed on the simulated road surface to prevent deterioration.

It was understood that this model was too small to accurately model the flow conditions in a typical highway lane due to its small size. It was also known that this small size would not allow uniform flow to be obtained upstream of the drain. The model was constructed mainly to provide extra height for extended vertical piping regimes. It was hoped that even if the limited size prevented recreation of data produced on the larger model, the data on the small model, for vertical piping lengths over 1.219 m, could be compared with the data obtained on the small model for piping lengths shorter than 1.219 m. This comparison would provide valuable information on the general behavior of the drain and piping system, even if they did not accurately recreate the behavior observed on the prototype roadway surface.

3.4.2 Small Model Hydraulic System

Water was pumped from the reservoir by either or both of the pumps into the headbox. Flow was routed through a 0.305 m x 0.305 m x 0.152 m tee, through a 0.152 m pipe and 0.152 m butterfly valve into the model headbox. This tee was located between the north pump and the venturi meter (see Figure 3.4). Due to this piping configuration, the approach flow rate for the small model could not be directly measured. Instead, the approach flow rate was calculated by summing the captured and carryover flow rates, which were measured as described in Section 3.6.

The headbox contained adjustable baffles which were used to stabilize the flow conditions upstream of the drain. The captured flow entered the drain and flowed through the attached piping system, which consisted of clear 0.152 m PVC pipe. A 0.254 m pipe was supported near the discharge of the 0.152 m PVC pipe to receive the captured flow. The 0.254 m pipe served the purpose of routing the captured flow from the drain piping system to the return channel. The discharge location of the 0.254 m pipe was between the sluice gate and the outside weir (see Figure 3.5). The sluice gates were closed during small model test runs, in order to decrease the time for the channel to stabilize so that the captured flow could be measured using the outside V-notch weir.

The carryover flow dropped into a carryover trough which discharged into a 0.152 m drain pipe dropping to the ground below. This pipe entered a 7.6-m-long flume containing a 90° weir which measured the carryover flow. The water then passed from the flume back into the reservoir.

3.4.3 Small Model Instrumentation

Just as in the large model, there was a walkway supported across the tops of the curbs to provide access to the flow and to both sides of the model during test runs. A point-gauge was also used to measure curb depths upstream of the drain. The point-gauge was mounted on a bracket which slipped over the curb top. The point-gauge and bracket assembly could be removed and placed at any location along the length of the model.

3.4.4 Small Model Roughness

The small model was too small to allow for an accurate determination of Manning's n. Comparison of the "feel" of the model surface with a table of Manning's n values for various materials seemed to show the roughness to be near 0.012. Also, comparison of a few of the subcritical tests on Drain 2B for low approach flow rates indicated an approximate value for Manning's n of 0.014. So the value of Manning's n for the model was probably between 0.012 and 0.014.

3.5 VENTURI METER

As stated earlier, flows from the north pump were measured using a venturi meter. The meter was connected to both a mercury-water manometer and an air-water manometer. For flow rates larger than 0.0425 m^3/s, the mercury-water manometer was used. The air-water manometer provided a more accurate measurement for flow rates less than 0.0425 m^3/s.

Twenty-four tests were run to calibrate the venturi meter, using the return channel as a volumetric tank. The total surface area of the tank was 191.8 m^2. Multiplying the surface area by the change in depth of water in the channel for each test gave the volume of flow. Dividing the volume of flow by the time the water was flowing gave the flow rate.

The calibrations of the venturi meter and the large model weirs (see Section 3.6) were verified with many tests. For approach flows less than 0.116 m^3/s, all of the flow measured by the two large model weirs flowed through the venturi meter. The sum of the carryover flow weir and the captured flow weir was never more than five percent different from the venturi meter flow rate.

The general equation for flow through a venturi meter is (Roberson and Crowe, 1985)

$$Q = \frac{C_d A_2 \sqrt{2g\Delta h}}{\sqrt{1-(A_2/A_1)^2}} \tag{3.2}$$

where Q = flow rate

C_d = discharge coefficient

A_1 = area of venturi entrance

A_2 = area of venturi throat

Δh = difference in piezometric head between the venturi entrance and the throat

g = acceleration of gravity.

For a given venturi meter, A_1 and A_2 are constant. This venturi meter had an approach diameter of 0.305 m with a throat diameter of 0.152 m.

Reynolds number for the venturi throat, Re_2, is defined as

$$Re_2 = \frac{V_2 D_2}{\nu} \tag{3.3}$$

where V_2 = the throat velocity,

D_2 = the throat diameter and

ν = kinematic viscosity.

For the venturi meter used, the discharge coefficient should be constant for Reynolds numbers greater than 2.0×10^5 (Daugherty et al., 1985), which corresponds to a throat velocity of 1.5 m/s, or a flow rate of 0.028 m^3/s.

Equation 3.2 can be rewritten as

$$Q = K\Delta h^{0.5} \tag{3.4}$$

where

$$K = C_d A_2 (2g)^{0.5} \left[1 - \left(\frac{A_2}{A_1} \right)^2 \right]^{-0.5} \tag{3.5}$$

K should be constant for any discharge greater than approximately 0.028 m^3/s.

The measured data was initially fit to Equation 3.4, but it was determined that the regression line was not a good fit. The flows for six of the calibration tests were less than 0.028 m^3/s, and these probably resulted in the bad fit of the regression. Therefore, the venturi meter was calibrated using

$$Q = K\Delta h^x \tag{3.6}$$

Taking the logarithm of both sides gives

$$\log Q = \log K + x \log \Delta h \tag{3.7}$$

A plot of Q versus Δh for the venturi meter is shown in Figure 3.8 with log-log scales. Performing a regression on log Q versus log Δh gave the resulting calibration equation

$$Q = 0.0684 \Delta h^{0.528} \tag{3.8}$$

The standard error for this equation was 0.0024 m^3/s, with a correlation coefficient of 0.998.

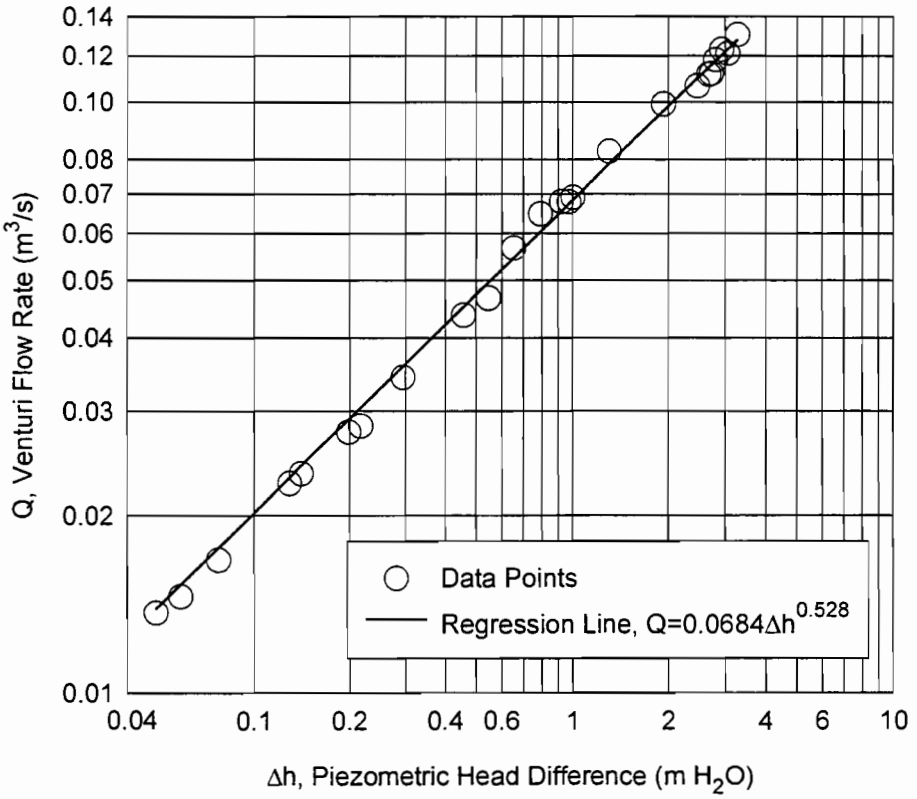

Figure 3.8 Venturi Meter Calibration Curve

Figure 3.9 is a plot of the resulting venturi discharge coefficients. The coefficients stabilized to an average value of 0.84 at a Reynolds number in the venturi throat of approximately 4×10^5. Typical venturi meter discharge coefficient values range between 0.94 and 0.99 (Streeter and Wylie, 1985). The difference between the expected values and the values obtained reveal that the venturi meter was not well streamlined at the contracting section.

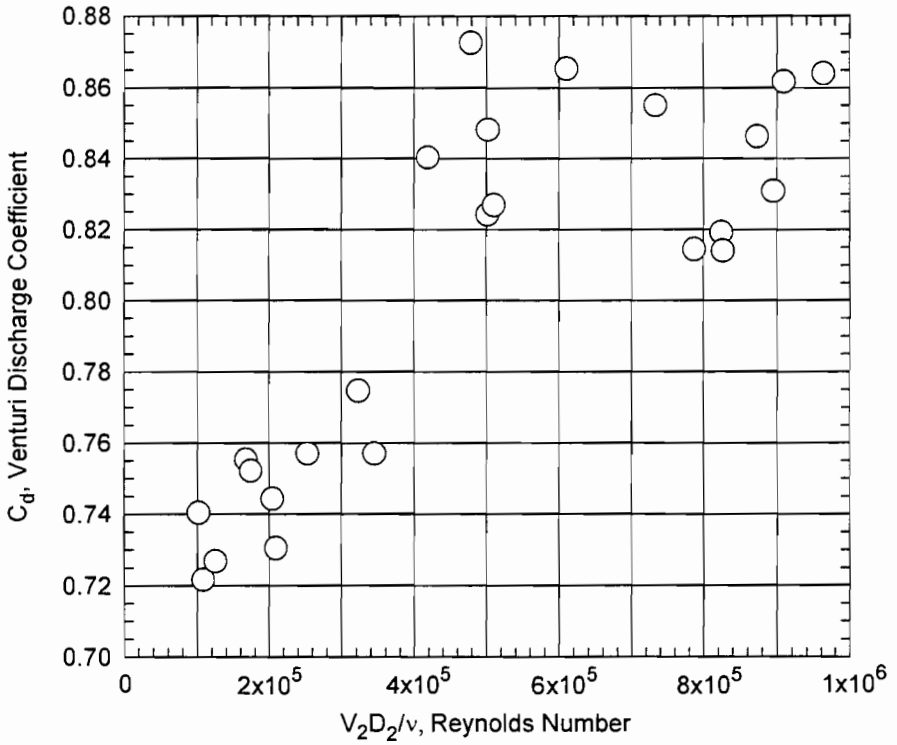

Figure 3.9 Discharge Coefficients for Venturi Meter

3.6 V-NOTCH WEIRS

V-notch weirs measured both the captured flow and the carryover flow for the large models. A 90° weir, located in the outside return channel, was used to measure captured flows for the small model. Another 90° weir, designated the *small model carryover weir*, was located in a flume near the small model. This weir measured the carryover flow from the small model.

The basic equation for a V-notch weir according to Bos (1989) is

$$Q = C_e\left(\frac{8}{15}\right)(2g)^{0.5}\tan\left(\frac{\theta}{2}\right)h_1^{2.5} \tag{3.9}$$

where C_e = effective discharge coefficient for a V-notch weir,

θ = angle of the weir notch and

h_1 = head on the weir.

In order to apply this equation to both fully and partially contracted sharp-crested weirs, it is modified to a form developed by Kindsvater and Carter (1957), expressed as

$$Q = C_e\left(\frac{8}{15}\right)(2g)^{0.5}\tan\left(\frac{\theta}{2}\right)h_e{}^{2.5} \tag{3.10}$$

The effective head, h_e, is $h_1 + K_h$, where K_h represents the effects of fluid properties such as surface tension and viscosity. The value of K_h for all three weirs was approximately 0.001 m (Bos, 1989).

To obtain values for h_e, depth measurements on all weirs except the small model carryover flow weir were taken with the use of a bubbler tube connected to a manometer. Oxygen was connected to 0.0064 m diameter flexible tubing which had a regulator valve on it. Downstream of this valve was a tee which branched to the manometer and to the weir tank or channel. The latter tube was fixed to the bottom of the tank, and was located upstream of the weir a distance of three to four times the maximum head on the weir. By regulating the discharge of oxygen to approximately one bubble per second, the depth of the water in the tank could be read on the manometer. The height of the crest of the weir, P, was subtracted from this measurement to obtain the value of h_1. Corrections were also made for the slope of the channel or tank and for the value of K_h to give the value for h_e on each weir.

Depths on the small model carryover flow weir were measured by the use of a 0.0127 m diameter piezometer tube. A hole was drilled into the side of the flume upstream of the weir a distance of approximately four times the maximum head on the weir. At the location of the hole, a nipple was welded to the outside of the flume and was connected to the piezometer tube with flexible tubing. The depths were read on a scale placed behind the piezometer tube. The scale and the piezometer tube were both attached to the side of the flume.

All of the weirs, except the small model carryover weir, were calibrated using the venturi meter as the flow rate measuring device. The small model carryover weir was calibrated volumetrically using part of the return channel as a volumetric tank.

For water temperatures between 5°C and 30°C, the discharge coefficient for a sharp-crested weir is a function of h_1/P, P/B_1, and θ, where P is the height of the weir crest from the

channel floor, and B is the width of the approach channel (Bos, 1989). P, B, and θ were constant for each of the four weirs; therefore, C_{ev} was only a function of h_1/P.

3.6.1 Large Model Carryover Weir

The large model carryover flow weir had a notch angle of 134.9°. Twenty calibration tests were run to determine Q as a function of h_e, and C_e as a function of h_1/P. For this weir, P = 0.311 m and B = 1.68 m. The measured data and the resulting calibration line are plotted in Figure 3.10.

The resulting equation for the calibration of the V-notch carryover weir was

$$Q = 3.04h_e^{2.5} \tag{3.11}$$

The correlation coefficient for this regression line was 0.99 with a standard error of 0.0013 m^3/s.

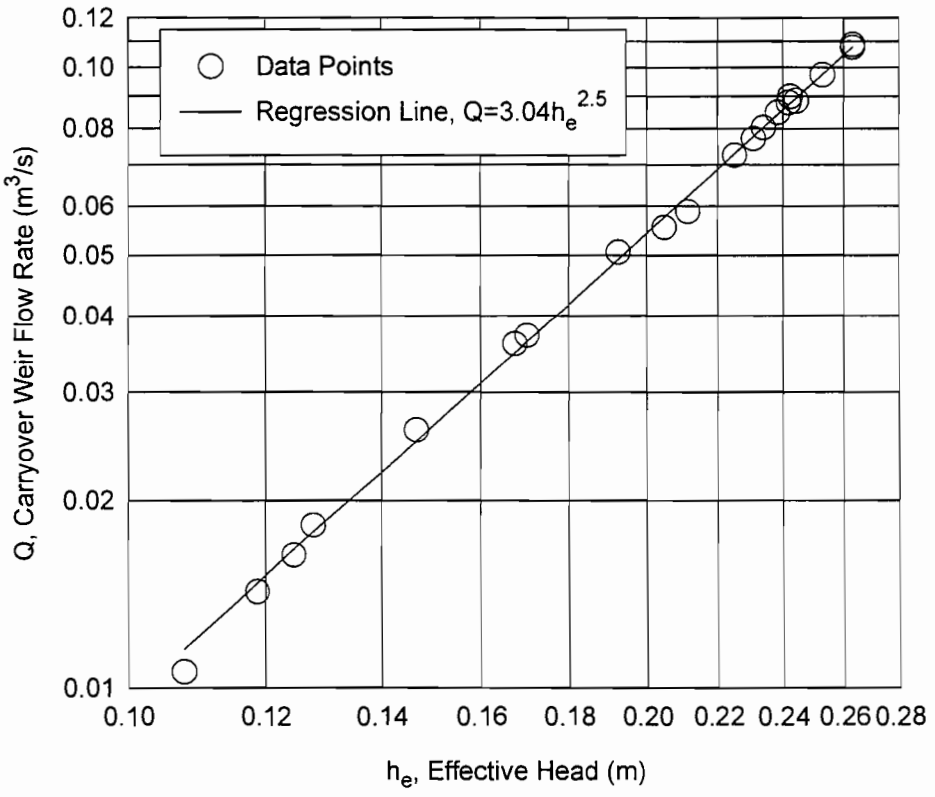

Figure 3.10 Large Model Carryover Weir Calibration Curve

The discharge coefficients for the large model carryover weir are plotted in Figure 3.11. These values were calculated using Equation 3.10. The average value of C_e was 0.53, with a standard deviation 0.016. Even after a thorough literature search, no data was found for a 135° V-notch weir to provide a comparison for the discharge coefficient values.

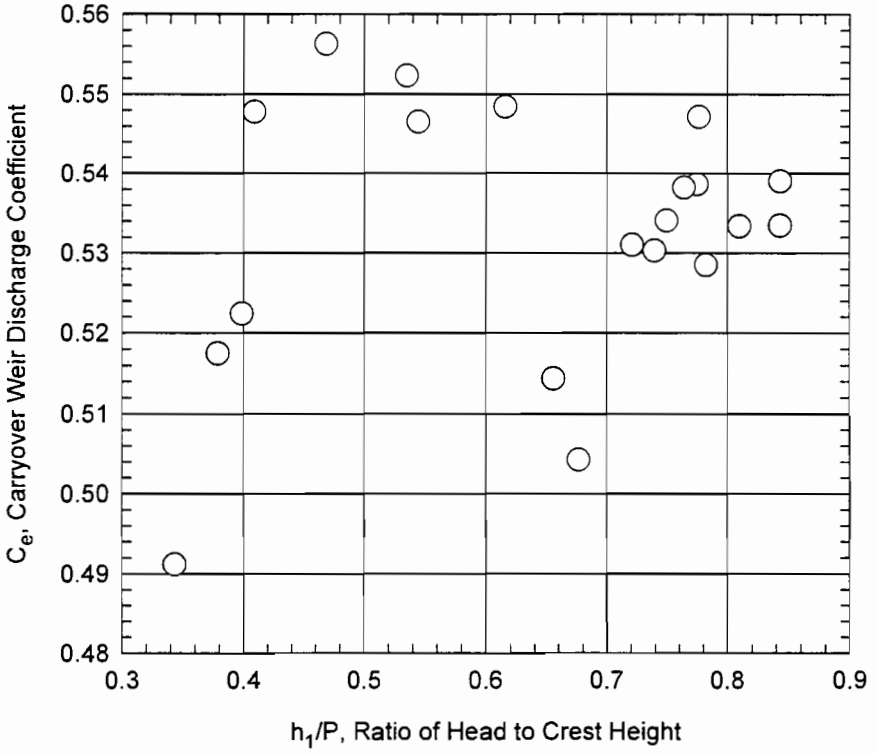

Figure 3.11 Discharge Coefficients for Large Model Carryover Weir

3.6.2 Large Model Captured Flow Weir

The captured flow weir had a notch angle of 138.8°. Nine calibration tests were run to determine the calibration line and the discharge coefficients. For the captured flow weir, P = 0.302 m and B = 1.83 m. The data for the captured flow weir did not fit Equation 3.10 well. Therefore, a regression was performed on the logarithms of the data, similar to the process used to calibrate the venturi meter. The data and regression line are plotted in Figure 3.12.

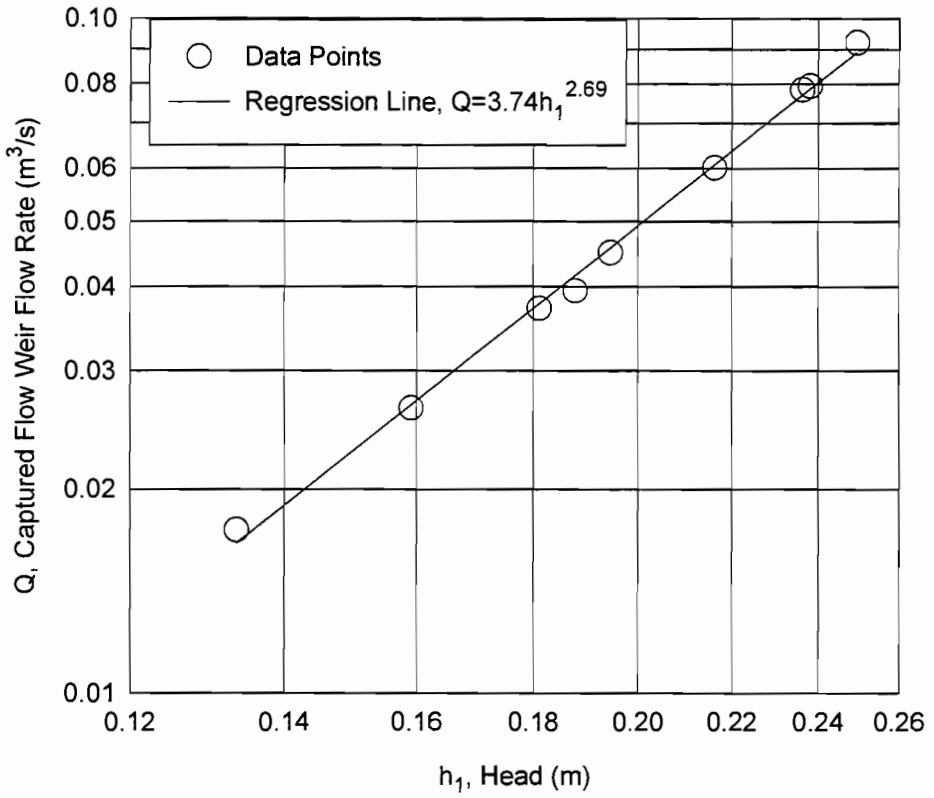

Figure 3.12 Large Model Captured Flow Weir Calibration Curve

The calibration equation for the captured flow weir was

$$Q = 3.74h_1^{2.69} \tag{3.12}$$

This equation had a standard error of 0.0015 m^3/s and a correlation coefficient of 0.99.

The discharge coefficients for the captured flow weir were calculated using Equation 3.10. They are shown in Figure 3.13. There is a fairly consistent trend of increasing C_e with increasing h_1/P.

One possible reason for the increasing discharge coefficients is that the weir was not well aerated. In a weir that is not well aerated, the flow will cling to the face of the weir and create a vacuum under the weir nappe. This vacuum will increase the discharge of the weir and therefore, the discharge coefficients will also increase (Bos, 1989).

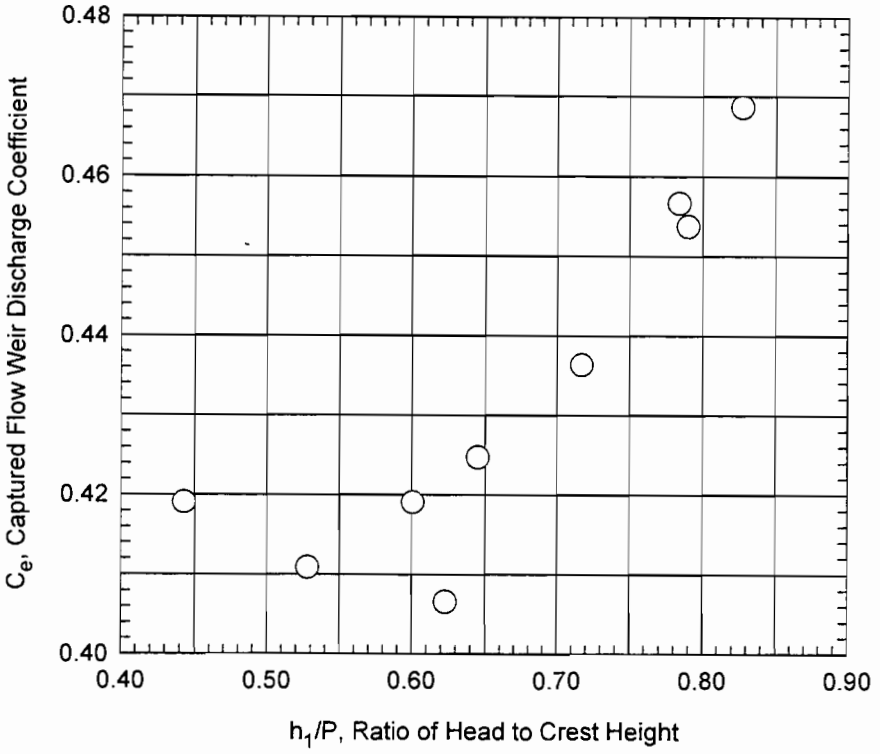

Figure 3.13 Discharge Coefficients for Large Model Captured Flow Weir

3.6.3 Outside Weir

Fourteen calibration tests were run on the outside weir. For the outside weir, P = 0.305 m, B = 1.52 m, and $\theta = 89.9°$. Figure 3.14 is a plot of the measured data with the calibration line. Similar to the captured flow weir calibration, a calibration equation was calculated by using a regression of log Q versus log h_e. The calibration equation for the outside weir was

$$Q = 1.28h_e^{2.53} \tag{3.13}$$

The standard error was 0.0014 m^3/s and the correlation coefficient for Equation 3.13 was 0.998.

Figure 3.15 is a plot of the discharge coefficients for the outside weir. These coefficients were calculated from Equation 3.10. The average value was 0.526 with a standard deviation for the coefficients of 0.012. These discharge coefficients were less than the typical 0.58 suggested

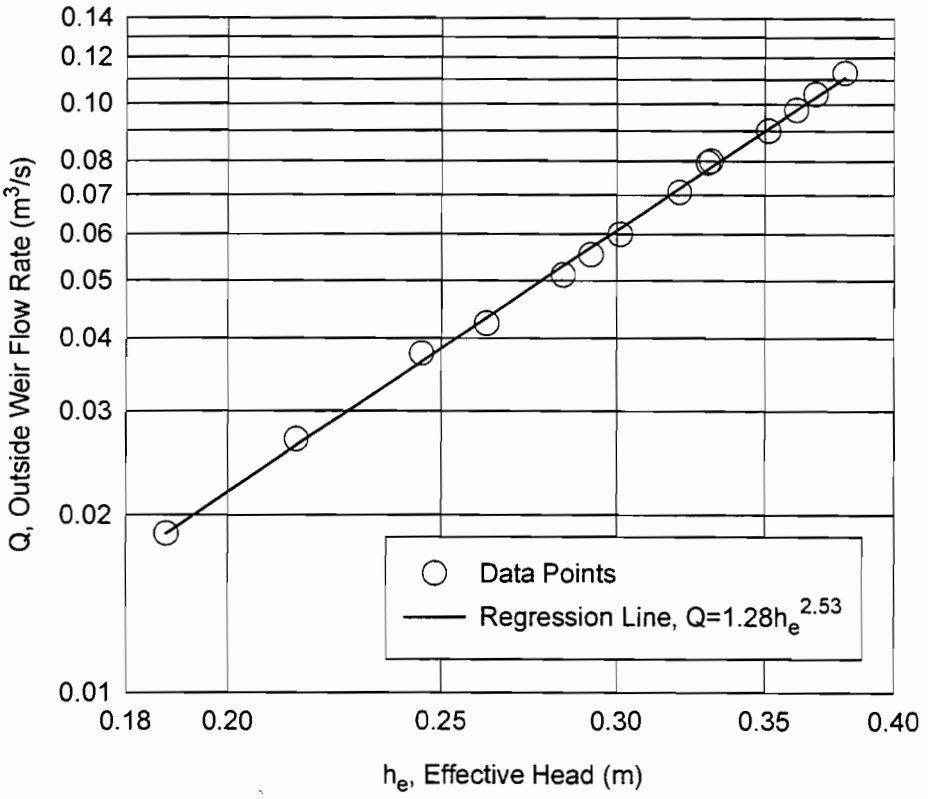

Figure 3.14 Outside Weir Calibration Curve

by Grant (1992) for a 90° V-notch weir. However, this value is for comparison to a supposedly standard weir, and the calibration itself was much more accurate that the comparison with a standard weir.

3.6.4 Small Model Carryover Weir

Six calibration tests were run on the small model carryover flow weir. The weir was calibrated volumetrically by bolting a plate over the outside weir and closing the sluice gates in the return channel (see Figure 3.5). Blocking off the return channel created a volumetric tank having a surface area of 59.52 m^2.

The crest height, P, for the small model carryover weir was 0.178 m and the width, B, was 0.905 m. The angle for the weir was 89.4°.

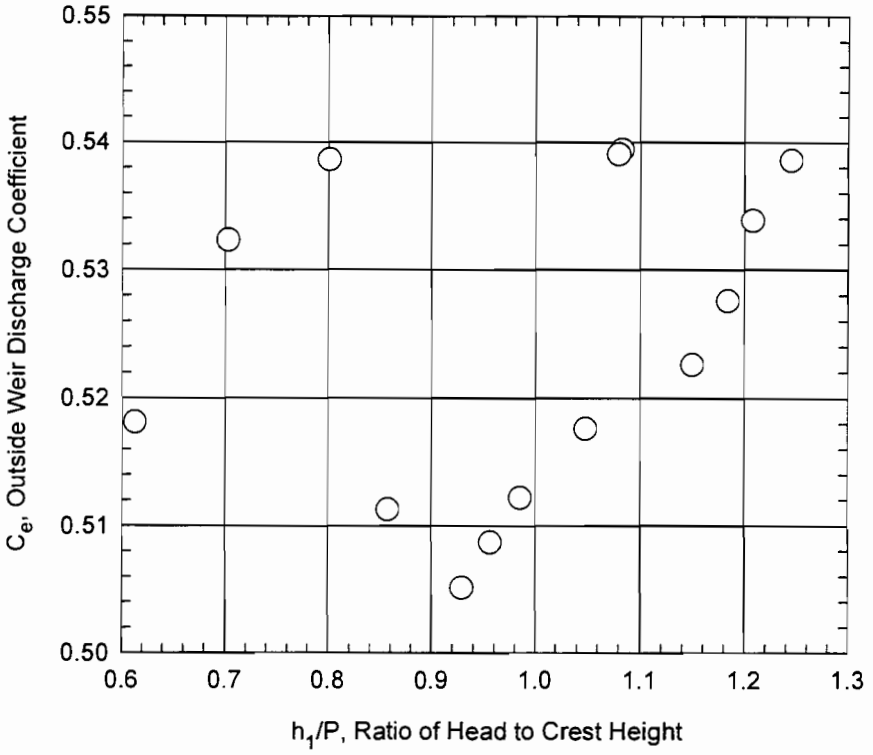

Figure 3.15 Discharge Coefficients for Outside Weir

Figure 3.16 shows the measured data with the calibration line. The calibration equation for the small model carryover weir was

$$Q = 1.34 h_e^{2.5} \tag{3.14}$$

Equation 3.14 has a standard error of 0.0002 m^3/s and a correlation coefficient of 0.999.

Figure 3.17 shows the discharge coefficients for this weir, as calculated from Equation 3.10. The average value for C_e was 0.572 with a standard deviation of 0.004.

3.7 SWIRL METER

A swirl meter was installed in the drain pan orifice in order to measure the vortex strength exiting the drain. It was hoped that quantifying the vortex strength in the pipe downstream of the drain would provide an explanation for why the drain capacity decreased as the first elbow underneath the drain was moved closer to the drain. The swirl meter consists of four vanes

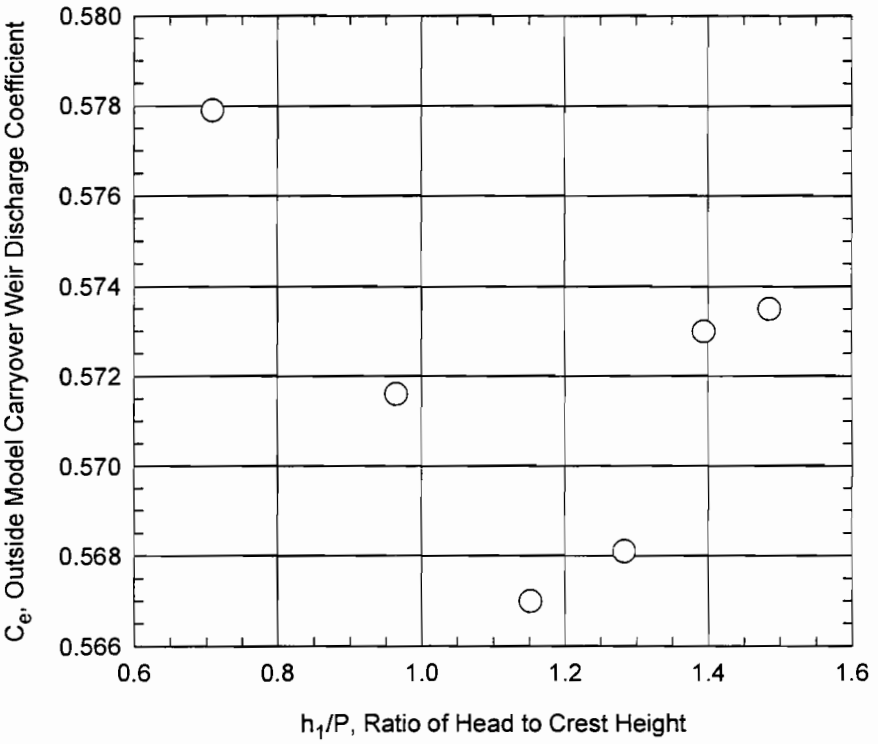

Figure 3.16 Small Model Carryover Weir Calibration Curve

mounted on a tube which rotates around a rod located in the axial direction of the pipe. The swirl meter is mounted in the axial direction of a pipe and simply rotates under swirling flow conditions in the pipe. The speed of rotation indicates the strength of the vortex.

3.7.1 Swirl Meter Dimensions

Four swirl meters were constructed from plexiglass with the dimensions shown in Figure 3.18. The general design of the swirl meters was based on a previous design developed by Alden Research Laboratory, Inc. (Knauss, 1987). One vane was painted so that the revolutions could be counted. A stopwatch was used to obtain the revolutions per minute. The rotations were used to calculate the swirl angle.

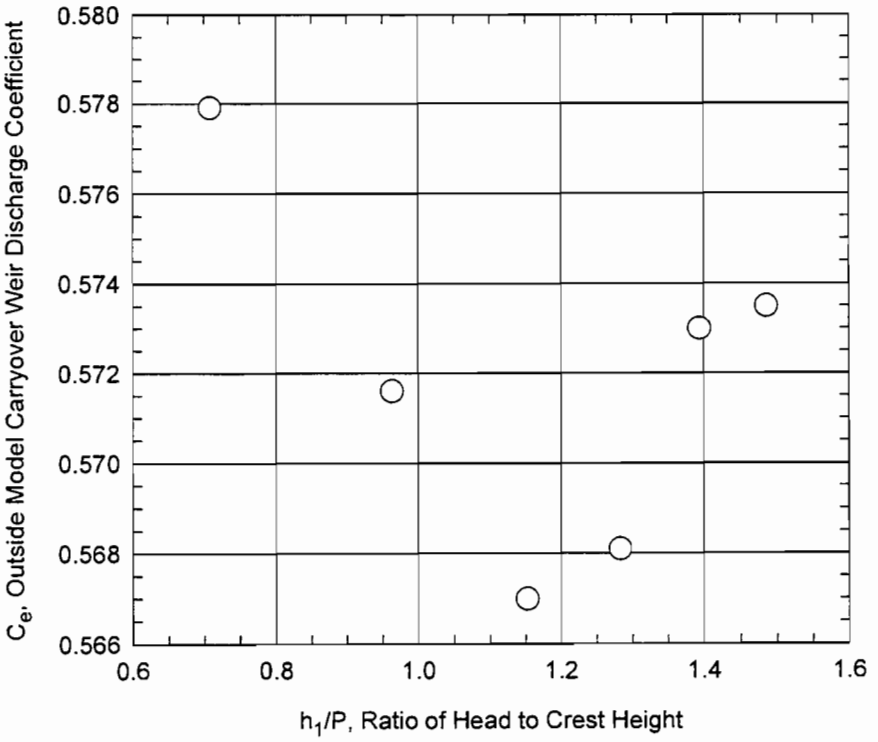

Figure 3.17 Discharge Coefficients for Small Model Carryover Weir

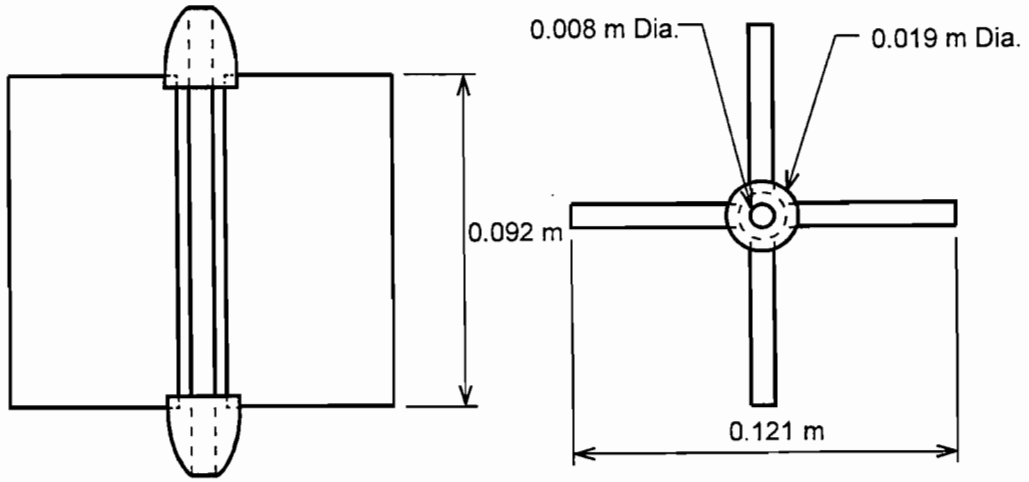

Figure 3.18 Swirl Meter (not to scale)

3.7.2 Swirl Angle

The swirl angle, α, is a dimensionless parameter which relates the tangential velocity to the axial velocity. The swirl angle is defined as (Knauss, 1987)

$$\alpha = \arctan\frac{v_t}{v_a} \tag{3.15}$$

where v_t = tangential velocity and

v_a = axial velocity.

The actual value of the swirl angle was calculated using (Knauss, 1987)

$$\alpha = \arctan\frac{\pi Dn}{V} \tag{3.16}$$

where D = pipe diameter

n = swirl meter revolutions per time

V = axial flow velocity in pipe.

Equation 3.16 implies that v_t is taken as $2\pi n(D/2)$.

In general swirl meters and swirl angles are useful only for comparing various flow conditions in a given model. They normally should not be used for comparing studies at different institutions since there are no standard dimensions and mountings for the meters.

CHAPTER 4. EXPERIMENTAL RESULTS

4.1 INTRODUCTION

One-hundred-twelve tests were performed on Drain 2B for various piping configurations using the large and small models. As stated in the introduction of this report, the downspout piping was always connected to the drain in these tests. In the prototype, the downspout piping is installed with an air vent between the piping and a short nipple immediately below the orifice of the drain. These tests were performed in order to determine the hydraulic behavior of the drain with the vent closed. This research included studying the hydraulic flow behavior of the bridge deck drain and connected downspout piping, determining the relationship between drain capacity and downspout piping length, determining the relationship between drain capacity and the location of the first downspout piping elbow, and presenting design recommendations based on the results of these tests. This chapter presents the methods of experimentation using each model, the results from the experimentation on the drain and piping systems, comparison of the results of this research with the results from Holley et al. (1992) for Drain 2, possible sources of error in the results, and conclusions and design recommendations. Data from all of the tests are given in Appendix B.

4.2 LARGE MODEL TESTS

4.2.1 Experimental Methods

The large model was used to perform 94 tests on Drain 2B. All tests were performed at a longitudinal slope of 0.004 and a transverse slope of 0.0417. The longitudinal slope of 0.004 is the minimum allowable slope used by the Texas Department of Transportation in bridge design. The transverse slope of 0.0417 is the maximum transverse slope used in bridge design. These slopes were chosen because they should provide the greatest variability in the captured flow rates for the various piping configurations. These slopes were also chosen because the minimum longitudinal slope and the maximum transverse slope were used by Holley et al. (1992).

The piping configurations studied using the large model are shown in Figure 4.1. These piping configurations are named Configurations H-P. All configurations shown in Figure 4.1 are looking normal to the flow direction. Also, in Figure 4.1, the horizontal piping is pointed in the downstream direction, so that the flow direction in the horizontal pipe is the same as the flow direction on the model surface. All vertical piping dimensions shown in Figure 4.1 are from the inside bottom of the drain pan.

Four swirl meters were constructed in the middle of the experimental program. Tests on Configurations H-K had been performed before the swirl meters were ready for installation. Later, more tests were done with the swirl meter installed in Configuration I. Three swirl meters were initially installed in Configuration L as shown in Figure 4.2. Tests were performed with various combinations of the swirl meters installed in the piping to determine if the swirl meters would have an impact on the drain capacity. The captured flow rate, Q_{2B}, decreased by approximately 5% when all three were installed in Configuration L. When any two of the swirl meters were installed, Q_{2B} was still approximately 4% less than without any swirl meters. It was determined that the most important swirl meter was swirl meter 1, installed in the drain orifice. The drain capacity was decreased by approximately 2% when only swirl meter 1 was installed. The exact location of swirl meter 1 in the drain pan orifice is shown in Figure 4.3. This location was chosen in order to quantify the strength of the swirl directly leaving the drain pan. The swirl meter was not installed lower in the drain orifice due to concern that the meter might interfere with the flow regime in any configuration where the first elbow was mounted directly underneath the pan. All piping configurations which contained the swirl meter had it installed in the location as shown in Figure 4.3. Tests on Configurations I, L and M were done both with and without the swirl meter. All tests on Configurations N, O, and P were done with the swirl meter installed. Configurations containing the swirl meter will be specified with an asterisk next to the piping configuration designation, such as L* or O*.

All tests on Drain 2B using the large model were done using the following procedure. The longitudinal and transverse slopes were set. The approach flow rate was obtained by using either the north pump or both pumps and by adjusting the valve discharging to the headbox of the

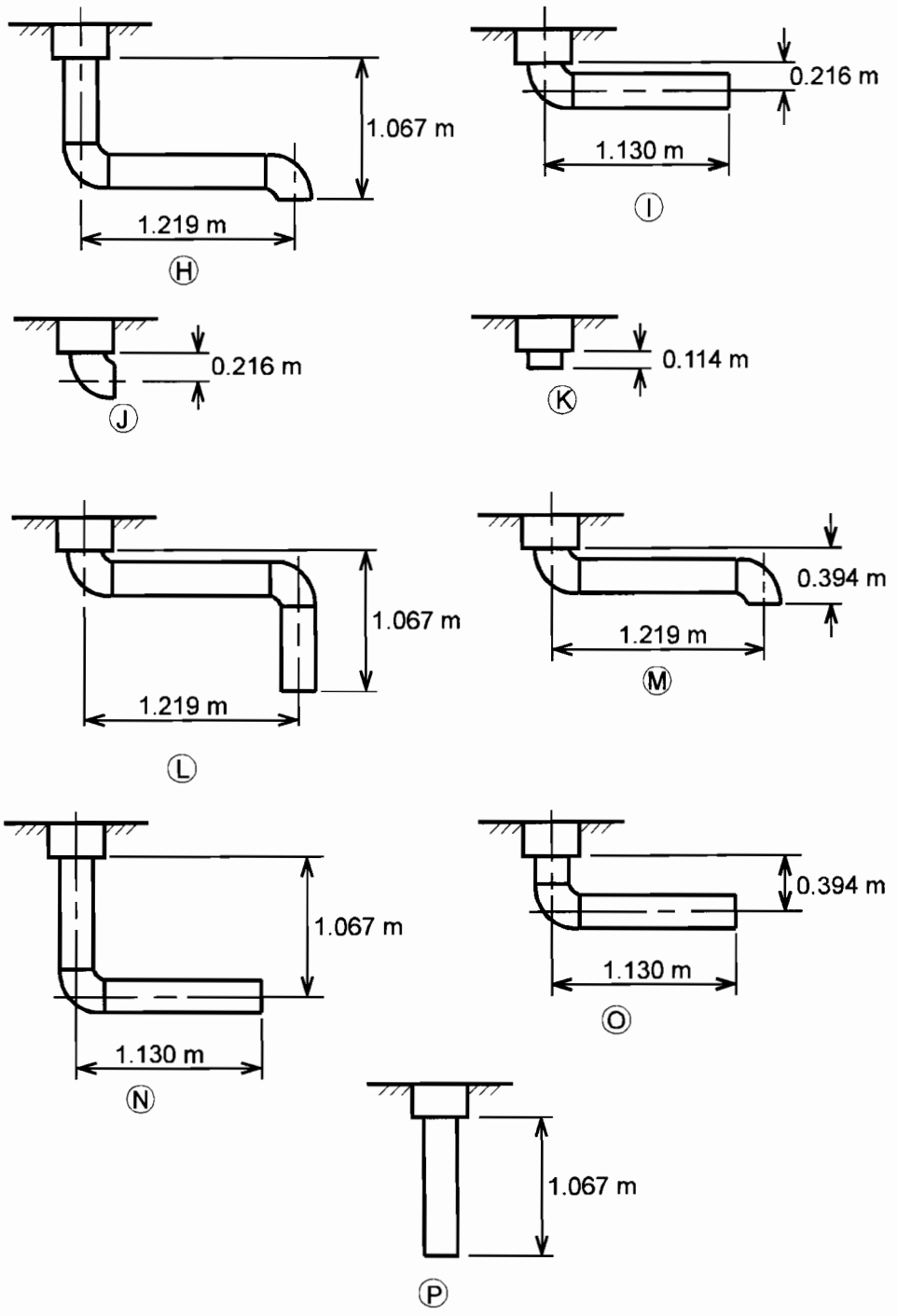

Figure 4.1 Piping Configurations for Tests on Drain 2B in the Large Model (not to scale)

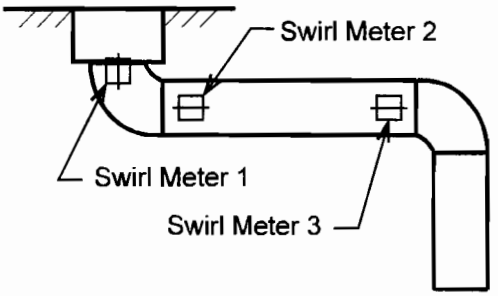

Figure 4.2 Swirl Meter Locations in Piping Configuration L (not to scale)

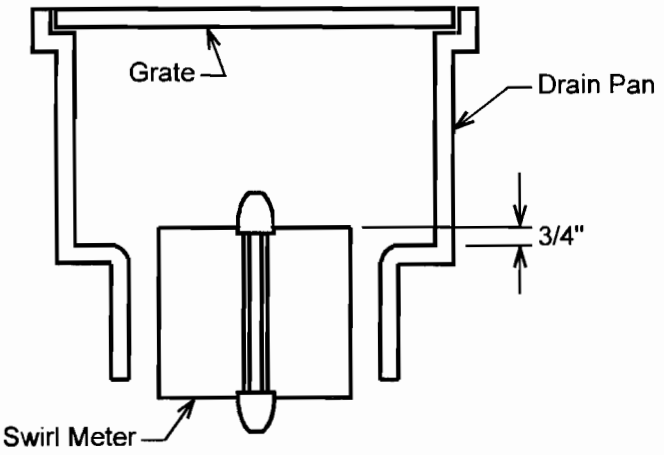

Figure 4.3 Swirl Meter 1 Location in Drain 2B Orifice (not to scale)

model. Once the approach flow had become steady-state, the curb depths were measured using the point-gauge. Curb depths were measured at 3.05 m and 4.57 m upstream of the drain. For configurations containing the swirl meter, the swirl meter rotations were counted for approximately one minute. The counting was done by visual observation of the swirl meter which had one colored vane. Counting of the swirl meter rotations was done three times for each approach flow rate in order to obtain an average swirl strength. The average difference between any set of three countings of the swirl meter was approximately 3%. For flows using only the north pump, the manometer connected to the venturi meter was read to determine the approach flow. The captured and carryover flow rates were determined by measuring the depths on the

captured flow weir and the carryover flow weir. Approach flow rates which required the use of both pumps were calculated by summing the carryover flow rate and the captured flow rate. After all data were recorded, the approach flow rate was changed and the above procedure was repeated. From 3 to 15 tests were run using various approach flow rates for each piping configuration. Once the desired tests were performed for a given configuration, the piping configuration was changed and the above process was repeated.

4.2.2 Large Model Test Results

Figure 4.4 shows the test results on Drain 2B for most of the piping configurations using the large model. Results for all tests will be presented in this chapter, but inclusion of all data in Figure 4.4 would make the figure difficult to read due to the plethora of data.

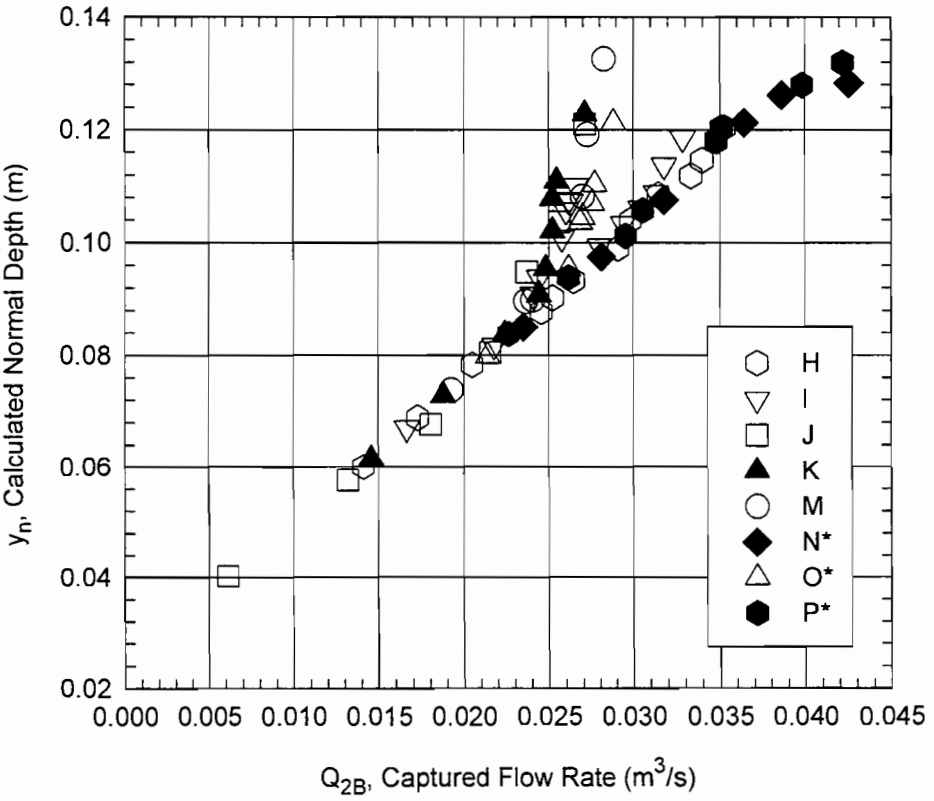

Figure 4.4 Drain 2B Piping Configuration Test Results Using Large Model

4.2.2.1 General Flow Description

The full description of the behavior of the drain and downspout piping configurations will start with a discussion of the limiting drain configuration. Configuration K had no piping attached to it (see Figure 4.1). The 0.114 m pipe is what was permanently attached to the drain. For low approach normal depths, $y_n \leq 0.06$ m, the majority of the approach flow basically flowed over the edge of the drain grate and fell into the drain pan. Some of the flow also passed over the solid portions of the drain grate, or passed between the first grate slot and the curb. Once in the drain pan, the captured water flowed freely toward the drain pan orifice and exited the drain. The flow over the upstream edge of the grate and into the drain pan appeared to be weir flow.

As the normal depth increased from 0.06 m to 0.085 m for Configuration K, the shallow portion of the drain pan next to the curb began to fill up due to the shallowness of the drain. The majority of the approach flow next to the curb flowed over the submerged portion of the grate and past the drain. Yet weir flow was still occurring over the deeper portion of the drain, where the pan was not full. Dye was injected upstream of the drain near the curb and revealed that a small amount of the approach flow upstream of the shallow portion of the drain pan was being captured by the drain, but a significant portion of that flow was not being captured. This behavior corresponded to the flatter sloped data in Figure 4.4, for $0.06 \text{ m} < y_n < 0.085$ m Increasing the normal depth toward 0.085 m increased the amount of the drain that was full, but weir flow still occurred over the deepest portion of the drain.

When the normal depth reached approximately 0.085 m for Configuration K, the drain pan became full and another flow regime was visible in the drain. Weir flow was no longer occurring because the drain was completely full. The drain was now under orifice control; in other words, the orifice at the bottom of the drain pan was controlling the amount of captured flow. The orifice behavior corresponded to the steeper sloped portion of Figure 4.4. As the normal depth increased further, the drain continued to behave under orifice control.

When a new piping configuration was installed, Configuration P* for example, the drain behavior was initially similar to that of Configuration K. The drain grate behaved as a weir for very low flows. Increasing the approach flow rate caused the drain pan to gradually fill in the shallower portion of the drain, but at normal depths of 0.085 m and greater, the pan never

became completely full as it did in Configuration K. The extra head created by the 1.07 m of vertical pipe in Configuration P* increased the drain capacity such that the drain did not become full. In essence, the piping added extra head across the drain, as described by one-dimensional hydraulics (see Section 2.4), and increased the drain capacity. Since the drain pan never filled up, the drain capacity continued to be controlled by weir behavior.

Regardless of the piping configuration, the drain experienced weir control for $y_n \leq$ 0.085 m. Only three configurations remained in weir control for all approach flow rates tested. Configurations N* and P* were tested for approach normal depths up to 0.132 m, or approach flows up to 0.152 m^3/s. Configuration H was tested up to a normal depth of 0.120 m, equivalent to an approach flow rate of 0.119 m^3/s. All three of these configurations had approximately 0.76 m to 1.07 m of vertical pipe connected directly to the drain pan orifice. The only other configuration tested with any vertical pipe connected directly to the drain pan orifice was Configuration O*. Configuration O* had only 0.216 m of vertical pipe between the bottom of the drain pan and the first elbow. Configuration O* still transitioned to orifice control at a normal depth of nearly 0.095 m, whereas all other configurations experiencing orifice control transitioned to orifice control at normal depths less than 0.095 m.

Effects of the downspout piping on the drain capacity are discussed further in Section 4.2.2.4 which also deals with the behavior of the drain under orifice control. Variations in the piping configuration altered the drain capacity because different configurations created different heads on the drain piping. The head on the piping influenced the fullness of the drain for any given approach flow rate. The fullness of the drain determined the control regime for the drain and piping system. Also, the fullness of the drain determined the flow pattern within the drain pan.

4.2.2.2 Flow Patterns in Drain Pan

Dye was injected at various points in the approach flow stream and in various locations in the drain pan during some of the tests. The dye tests were done to observe the flow behavior in the drain.

Figure 4.5 shows the flow pattern in the drain pan for very low approach flows. This pattern is designated the β flow pattern. For this flow pattern, the approach flow traveled down the curb and dropped through the grate slots into the drain pan. β occurred only in the portion of the drain that was not full. For the lowest approach flows, β occurred across the entire width of the drain (perpendicular to the curls) because no portion of the drain was full. For flow pattern β, the captured flow fell freely to the bottom of the drain pan and then to the downstream edge of the pan (downstream with respect to flow in the gutter). The flow then struck the downstream edge of the pan and rose up the side. This pattern of flow created a swirl in the drain pan. In addition to the general swirl shown in Figure 4.5, the captured flow was also moving toward the drain pan orifice. So the β flow pattern existed in the flow traveling toward the orifice. As the flow entered the orifice, this swirl was entrained in the orifice and the swirl pattern continued into the piping system. For low approach flows, the direction of rotation of the swirl meter was consistent with the β flow pattern (see Section 4.2.2.5). The free fall of water over the grate lip and into the drain pan resulting in the β flow pattern was essentially weir flow over the grate lip. However, the above type of flow in the drain pan will not be called weir behavior in this report because it was found that the flow pattern in the pan did not determine the control on the drain capacity. The control regime on the drain capacity will be called weir or orifice control. The flow patterns in the drain will be called β or δ.

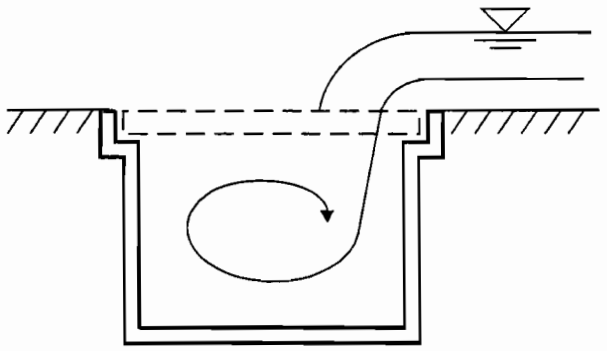

Figure 4.5 Cross-Section of Drain 2B with Flow Pattern β in Drain Pan (not to scale)

As the approach flow rate increased above the smallest approach flows, the portion of the drain next to the curb became full, so there was no free-fall to the bottom of the pan as in β flow. The δ flow pattern occurred in the region of the drain near the curb where the drain was full. δ flow occurred by water striking the downstream edge of the drain first. This flow continued downward along the edge of the drain until striking the bottom of the drain. The flow then turned back upstream toward the upstream edge of the pan. This flow behavior resulted in the swirl depicted in Figure 4.6b. Although δ occurred in the full portion of the drain, the drain pan was not necessarily full all of the way across the drain width. When the drain was partially full, approach flow upstream of the deep portion of the drain experienced free-fall into the drain pan. Figure 4.6 shows a plan view and cross-sectional views of Drain 2B when the drain was partially full. A combination flow pattern occurred in the transition region of the drain. In this transition region, the drain pan was full at the upstream edge of the drain, yet not full at the downstream edge. The δ flow from the shallow portion of the drain continued its flow pattern on the upstream side of the pan as it flowed toward the drain orifice, while the flow coming from the top of the drain pan created the flow pattern β on the downstream side of the pan. The flow pattern near the drain pan orifice was difficult to observe due to the turbulence of the flow in that region. Even with a combination flow pattern occurring in a partially submerged drain, the swirl meter showed that the δ flow pattern was entrained into the drain orifice. So the δ flow pattern dominated when the drain was partially full.

Once the calculated normal depth obtained a value of approximately 0.085 m, the piping configuration became a significant factor in the drain capacity. When the head in the connected piping was not sufficient to keep the drain pan from becoming entirely full, the drain completely filled and flow pattern δ occurred across the entire width of the drain.

4.2.2.3 Drain 2B Capacity with Weir Control

As stated earlier, weir control regulated the drain capacity when a piping configuration created enough head on the drain to prevent the drain pan from filling up. Figure 4.7 is a plot of

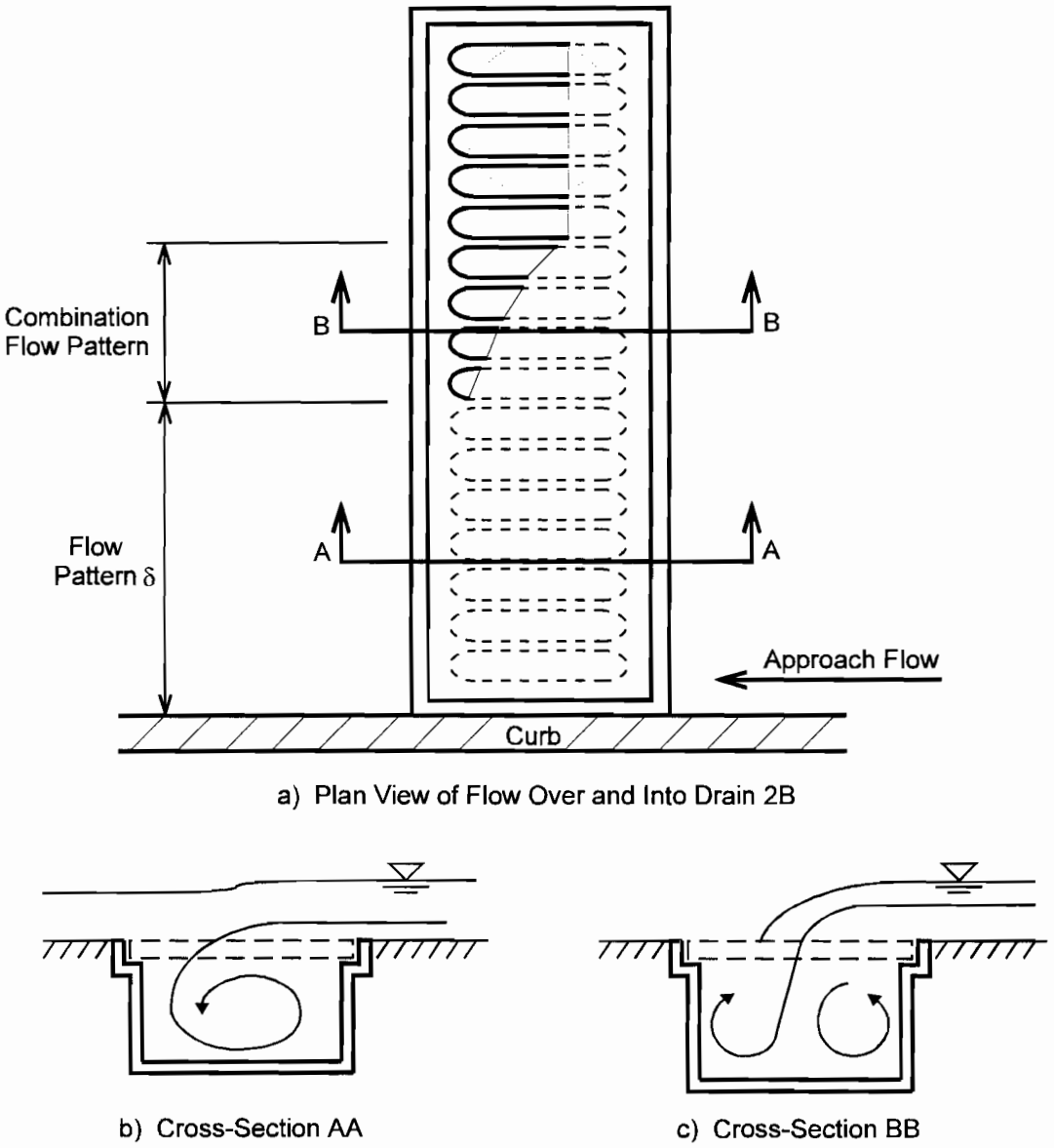

Figure 4.6 Flow Patterns for Drain 2B When Partially Full (not to scale)

all of the data representing weir control for Drain 2B. Some of this data was presented earlier in Figure 4.4, and was called the flatter sloped data.

Visual observation during many of the tests in Figure 4.7 revealed that weir behavior was controlling the drain capacity. It also appeared that the effective weir length decreased as the approach flow rate increased. That is, as the approach flow rate increased, more of the drain pan

filled up so that the length of the grate acting as a weir decreased. In order to verify that the observed weir behavior was truly the limiting factor on the drain capacity for tests in Figure 4.7, the effective weir length for each test was determined. Comparison of the effective weir length values for each test would help determine if weir control was the true limiting factor on the drain capacity, or if other behavior was having influence in controlling the drain capacity.

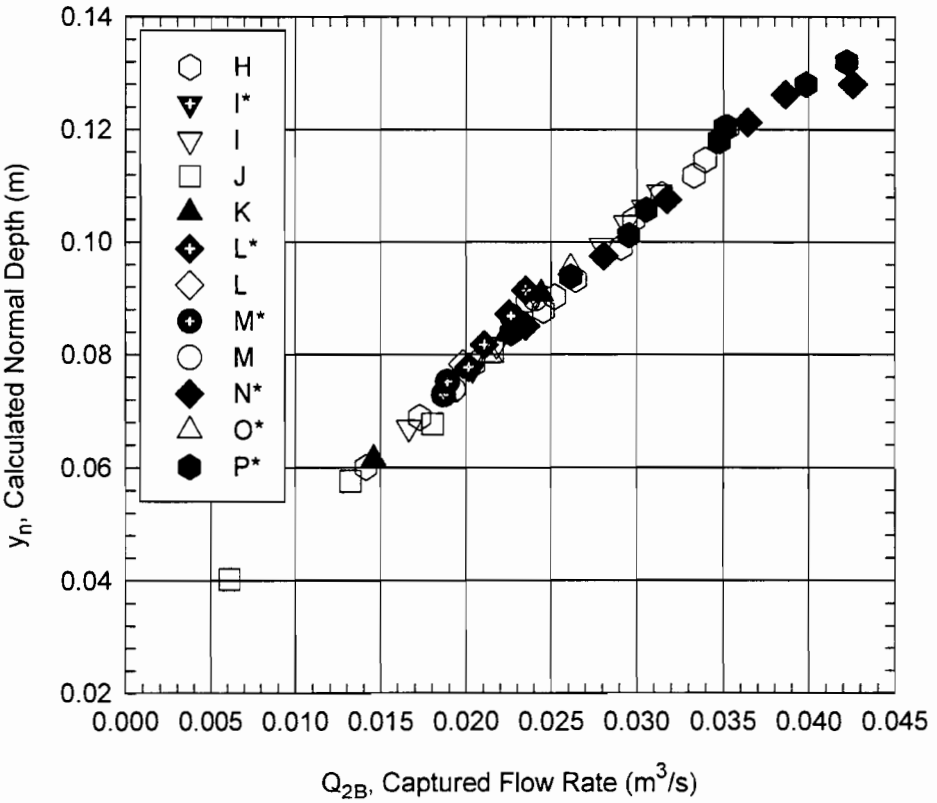

Figure 4.7 Test Results for Drain 2B with Weir Control

The general equation for a broad-crested weir, presented earlier as Equation 2.4, is (Bos, 1989)

$$Q = C_{wd} C_{wv} \frac{2}{3}\left(\frac{2}{3}g\right)^{0.50} L_e h_w^{1.5} \tag{4.1}$$

where C_{wd} = weir discharge coefficient,

C_{wv} = velocity head correction coefficient,

g = acceleration due to gravity,

L_e = effective weir length and

h_w = weir head.

The velocity coefficient corrects for the exclusion of the approach channel velocity head from the weir head term. It was decided that the approach channel velocity head would be included in the weir head term so that $C_{wv} = 1.0$ and h_w became H_w, the total weir head. Because all of the weir flow was captured flow, Q is equal to Q_{2B} so Equation 4.1 was rewritten as

$$Q_{2B} = C_{wd}\frac{2}{3}\left(\frac{2}{3}g\right)^{0.50} L_e H_w^{1.5} \tag{4.2}$$

A new variable, a, was defined to include all of the known constants in Equation 4.2 so that

$$a = C_{wd}\frac{2}{3}\left(\frac{2}{3}g\right)^{0.50} \tag{4.3}$$

where C_{wd} was set equal to 1.0. Equation 4.2 then became

$$Q_{2B} = aL_eH_w^{1.5} \tag{4.4}$$

Because the value for H_w varied across the weir length, the best approach to apply Equation 4.4 to the data was to take an incremental weir length, dL, and integrate Equation 4.4 from 0 to L_e. Figure 4.8 is a view looking downstream at Drain 2B. In this figure, dL is the incremental weir length, L is the distance to dL, and L = 0 at the edge of the drain.

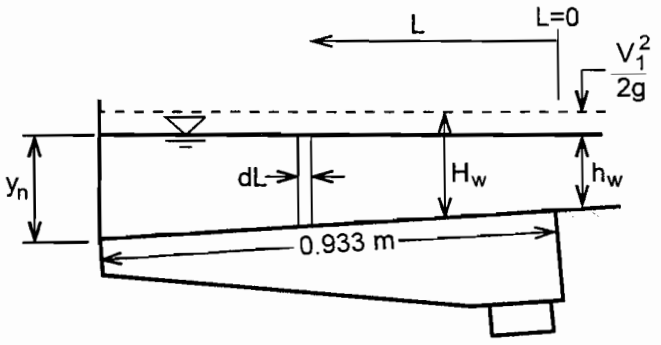

Figure 4.8 Upstream View of Drain 2B with Incremental Weir Length (not to scale)

Equation 4.4 was written for flow through the incremental weir length as

$$dQ_{2B} = aH_w^{1.5}dL \tag{4.5}$$

The velocity head in the approach flow was calculated as the average velocity head in the approach channel. That is

$$\frac{V_1^2}{2g} = \frac{(Q_a/A)^2}{2g} \tag{4.6}$$

where Q_a was the approach flow rate and A was the area of the approach flow. The weir head, h_w, at L was

$$h_w = y_n - 0.933\sin\phi + L\tan\phi = y_n - 0.0389 + 0.0417L \tag{4.7}$$

where ϕ was 2.39°, the angle equivalent to the transverse slope. The value of 0.933 m was the distance from the curb to the outer edge of the last grate slot. The total weir head at any L then became

$$H_w = \frac{V_1^2}{2g} + y_n - 0.0389 + 0.0417L \tag{4.8}$$

Substitution of variables and integration of Equation 4.5 gave

$$Q_{2B} = \int_0^{L_e} a\left(\frac{V_1^2}{g2} + y_n - 0.0389 + 0.0417L\right)^{1.5} dL \tag{4.9}$$

Assuming C_{wd} and a to be constant, Equation 4.9 was

$$Q_{2B} = 9.59a\left(\frac{V_1^2}{2g} + y_n - 0.0389 + 0.0417L\right)^{2.5}\Bigg|_0^{L_e} \tag{4.10}$$

Solving for L_e in Equation 4.10,

$$L_e = 24.0\left\{\left[\frac{Q_{2B}}{9.59a} + \left(\frac{V_1^2}{2g} + y_n - 0.0389\right)^{2.5}\right]^{0.4} - \left(\frac{V_1^2}{2g} + y_n - 0.0389\right)\right\} \tag{4.11}$$

The values for effective weir length were calculated for each Drain 2B test with weir control using Equation 4.11 and are shown in Figure 4.9 based on an assumed value of 1.0 for

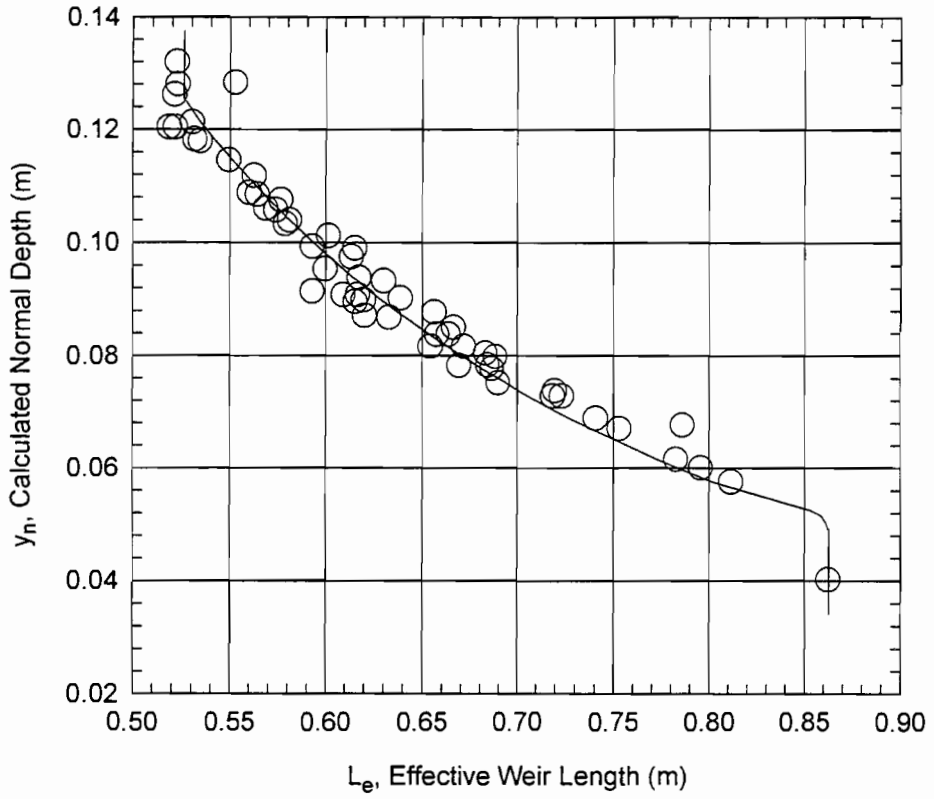

Figure 4.9 Effective Weir Lengths for Drain 2B Tests Under Weir Control

C_{wd}. However, 1.0 was not the true value for C_{wd}. The actual value for C_{wd} for each test was unknown, but was certainly less than 1.0 due to losses between the location where normal depth occurred in the channel and the location of the drain.

The values of L_e for y_n less than approximately 0.1 m seem reasonable because these L_e values are less than 0.9 m, which was approximately the maximum weir length, and because L_e decreased for increasing y_n. However, the values of L_e for the higher normal depths are too large to correspond to simple weir flow over L_e along the upstream edge of the grate. Visual observation during these tests revealed that the large majority of the drain pan was full, so that free fall into the drain pan was occurring over less than one-third of the total grate width.

A combination of two things helps to explain the magnitude of L_e for the higher normal depths. One is that weir flow was occurring not only over the unsubmerged portion of the grate, but also over the submerged portion of the grate. This behavior can be explained by the

schematic shown in Figure 4.10. The solid line in Figure 4.10 represents the assumed variation of C_{wd} used in calculating L_e. By visual observation, the values for L_e for the larger normal depths were too large to correspond to weir flow over only the unsubmerged portion of the grate. Therefore, it was concluded that the total grate length, L_t, acting as a weir included not only the unsubmerged portion of the grate, but also the submerged portion. Also, due to submergence effects, the discharge coefficient had to be changing across the total length of the weir. A schematic of the probable actual variation of C_{wd} is shown by the dashed line in Figure 4.10. So the actual values for L_e in Figure 4.9 could be described as the area under the dashed line in Figure 4.10, where each test in Figure 4.9 would have a different C_{wd} versus weir length curve based on the normal depth and on the amount of submergence of the grate for each test.

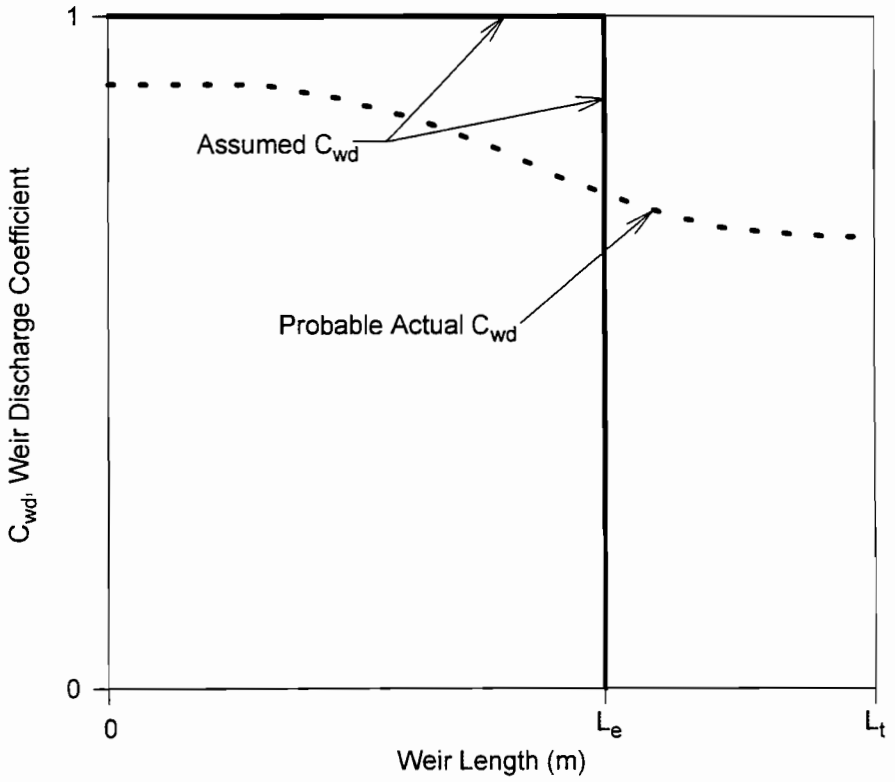

Figure 4.10 Schematic of the Weir Length and the Variable Discharge Coefficient (not to scale)

Besides the behavior described above, the magnitude of L_e for the higher normal depths can also be attributed to the fact that the length of the grate acting as a weir was really a portion of the perimeter of the grate slots, not just the width of the grate slots. That is, the total weir length was larger than 16 grate slots times the slot width of 0.038 m.

The general trend shown in Figure 4.9 is that L_e decreased for increasing values of y_n. One data point, y_n = 0.040 m, appeared to show that the effective weir length reached a maximum somewhere between y_n = 0.055 m and y_n = 0.040 m. As long as the ponded width of the approach flow was at least as large as the width of the grate normal to the curb, the weir length would reach a maximum value when all of the grate acted as an unsubmerged weir. So it was reasonable that L_e obtained a maximum value for low approach normal depths. At the highest normal depths, L_e again reached a constant value. L_e obtained a minimum value at high normal depths because the drain grate was completely submerged except for the area directly over the drain pan orifice. The weir length could not decrease any more, since increasing the approach flow rate even more would have put the drain into orifice control.

So it appears that the piping configuration influenced the drain capacity in such a way as to prevent the drain from filling up and having orifice control. As long as a portion of the drain pan was not full, the drain capacity was restricted by weir control. This weir behavior was characterized by a changing weir discharge coefficient due to the filling up of part of the drain with the result that part of the grate had smaller C_{wd} values due to submerged weir behavior. When the drain pan became full, the drain and downspout piping operated under orifice control.

4.2.2.4 Drain 2B Capacity with Orifice Control and Piping Effects

The analysis of the orifice control data for Drain 2B will center around determining the factors affecting the captured flow rate for each configuration. Comparison of the head losses for each configuration will help determine if one-dimensional hydraulics accurately predicts the flow behavior in the drain and piping systems.

Figure 4.11 shows the results from all of the tests where Q_{2B} was limited by orifice control, with a line representing the weir control data. One-dimensional hydraulics was used to

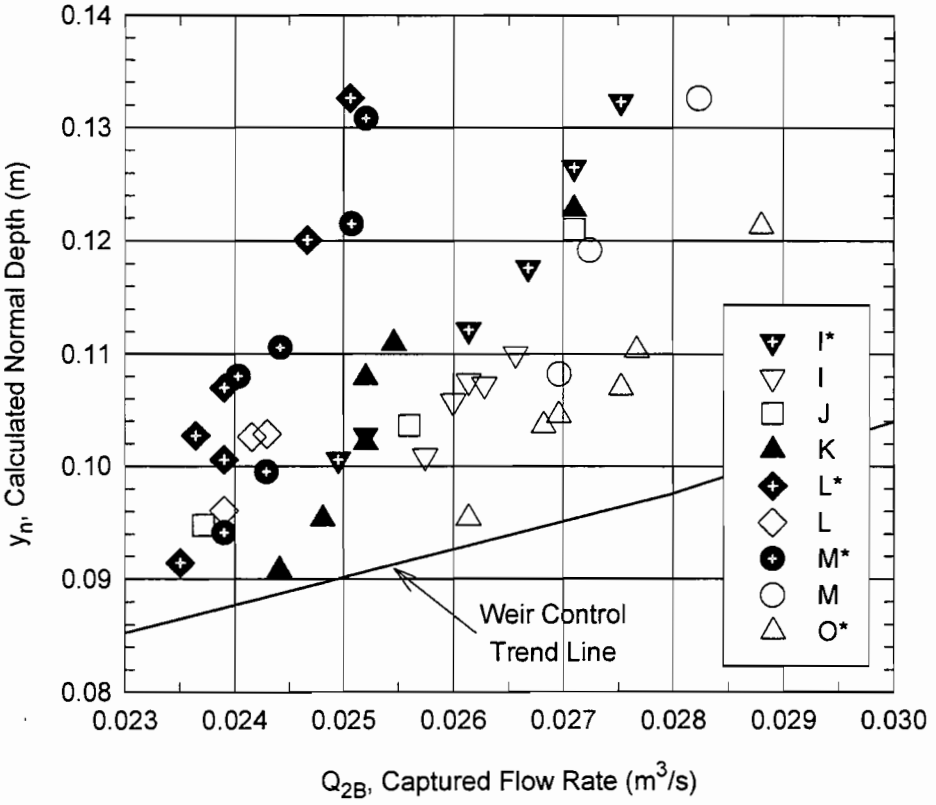

Figure 4.11 Test Results for Drain 2B Under Orifice Control

calculate the head loss through the various piping systems and then the orifice equation was used to analyze the drain behavior shown in Figure 4.11.

The general equation for orifice flow, stated earlier as Equation 2.7, is

$$Q = C_{od} A_o \sqrt{2gH_o} \tag{4.12}$$

where C_{od} = orifice discharge coefficient,

A_o = area of orifice and

H_o = total orifice head.

H_o represents the total head across the orifice, given by Equation 2.11 as

$$H_o = z_1 - z_2 + \frac{V_1^2}{2g} - \frac{V_2^2}{2g} - h_L \tag{4.13}$$

where h_L represents the losses through the piping system. Point 1 was a distance y_n above the roadway surface at the drain. Point 2 was the location where atmospheric pressure occurred in the piping system. Atmospheric pressure in the piping system did not always occur at the end of the pipe. It sometimes occurred inside the pipe for certain piping configurations. The elevation difference between the approach flow surface and the location of atmospheric pressure, $z_1 - z_2$, was calculated by computing y_n upstream of the drain pan orifice location, adding the depth of the drain, and adding the distance from the pan bottom to the location of atmospheric pressure. The location where normal depth occurred for each test was not calculated, so $z_1 - z_2$ did not include the difference in elevation between points 1 and 2 due to the longitudinal slope of the model. Also, the head loss between the location of y_n and the drain was not included in the calculation of H_o. Instead, this loss was included in the value of C_{od}.

There were two possible locations where orifice control could have occurred in the drain. One was the grate slots and the other was the drain pan orifice. The total area of the grate slots was too large to be the controlling orifice area. Also, if the grate were acting as the orifice control, then the drain would not have filled as the transition from weir to orifice control occurred. Therefore, A_o was chosen to be the drain pan orifice area 0.0182 m^2.

The piping head loss term in Equation 4.13 was separated into two parts, the straight pipe loss, h_P, and the elbow loss, h_{EB}. Both of these losses were determined using the Hazen-Williams equation. The Hazen-Williams equation for head loss in a pipe is (Daugherty et al., 1985)

$$S = \frac{1.35V^{1.852}}{C^{1.852}R_h^{1.167}} \tag{4.14}$$

where S = energy gradient,

C = Hazen-Williams coefficient of roughness,

V = velocity of pipe flow (m/s), and

R_h = hydraulic radius (m).

Eslon Thermoplastics (1993), a PVC manufacturer, lists the head loss through a standard 90° elbow as being equivalent to the loss for 5.5 m of straight pipe. Eslon also uses a value of 150 for the Hazen-Williams coefficient for extruded smooth wall thermoplastic pipe. These

values were used in the calculation of losses for each piping configuration. Equation 4.14 was used to calculate S for straight pipe for a given Q_{2B}. Multiplying S by 5.5 m gave the head loss for an elbow, h_{EB}, experiencing the same flow rate. This elbow head loss was then converted to a loss coefficient, K_{EB}, where (Daugherty et al., 1985)

$$K_{EB} = \frac{h_{EB}}{V_2^2/2g} \tag{4.15}$$

The values for the elbow loss coefficient, K_{EB}, as a function of captured flow rate (flow in the pipe) are shown in Figure 4.12. In the subsequent discussion of the various piping configurations, it is pointed out that sometimes the elbows flowed full and sometimes they did not. However, the elbow loss from Equation 4.15 was used only for cases where the elbow was either observed to be full or assumed to be full.

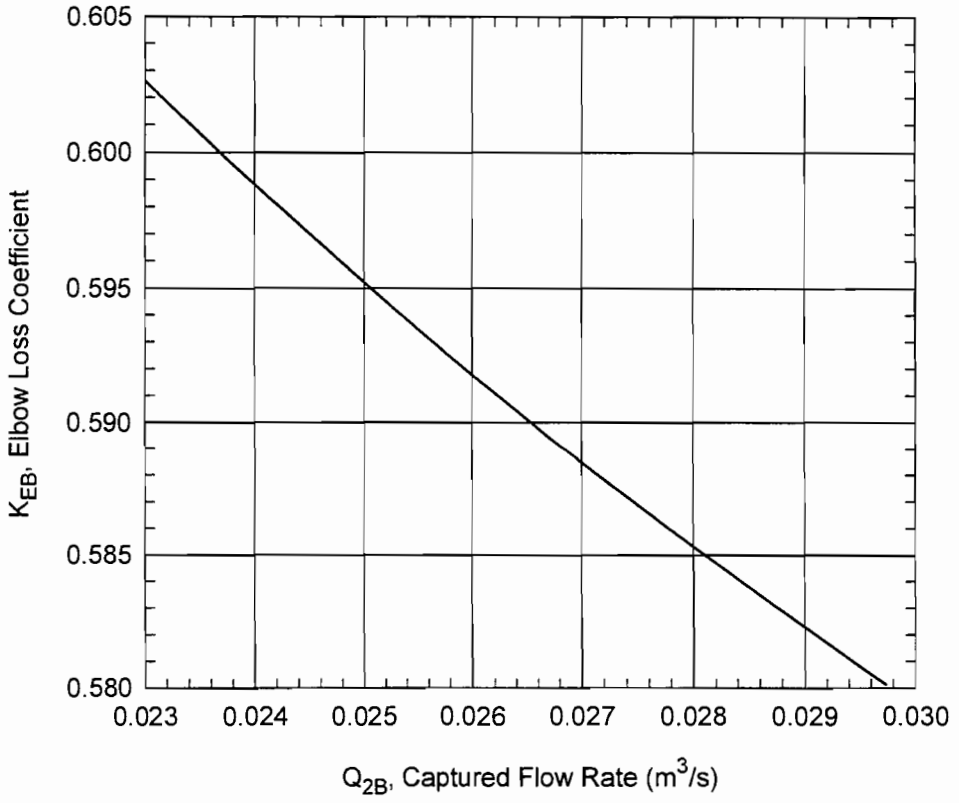

Figure 4.12 Elbow Loss Coefficient Using the Hazen-Williams Equation

The values shown in Figure 4.12 for K_{EB} were used in calculation of elbow losses for each piping configuration in this study. Substitution of the calculated elbow and straight pipe losses into Equation 4.13 resulted in the total head, H_o, across the drain orifice. Equation 4.12 was then used to calculate the values for C_{od}. The calculation of losses for each piping configuration did not include loss due to the swirl meter. Therefore, any loss from the swirl meter would have resulted in a decreased value for C_{od}.

The orifice discharge coefficient, C_{od}, was converted to an equivalent channel and drain loss coefficient, K_d. The relationship between C_{od} and K_d was derived from the general orifice equation and from the energy equation. In Equation 4.12, Q_{2B} was the orifice area, A_o, multiplied by the pipe flow velocity, V_2. Equation 4.12 was solved for H_o in terms of the pipe flow velocity as

$$H_o = \frac{V_2^2}{C_{od}^2 2g} \tag{4.17}$$

Point 3 was defined as the location of the drain and piping connection. Point 1 was defined earlier as the distance y_n above the roadway surface at the drain. The relationship between the head at points 1 and 3 was

$$H_1 = H_3 - h_{L,1-3} \tag{4.18}$$

where $h_{L,1-3}$ was the head loss between points 1 and 3. The head loss term was written in terms of the channel and drain loss coefficient multiplied by the pipe velocity head,

$$h_{L,1-3} = K_d \frac{V_2^2}{2g} \tag{4.19}$$

In Equation 4.18, the difference between the head at points 1 and 3 was the orifice head, so

$$H_o = H_1 - H_3 = h_{L,1-3} \tag{4.20}$$

Substitution of Equation 4.19 into Equation 4.17 resulted in

$$K_d = \frac{1}{C_{od}^2} \tag{4.21}$$

Assuming one-dimensional hydraulics accurately described the behavior occurring in the drain and piping systems, K_d should have been similar for all piping configurations, because K_d

represented the losses from flow through the approach channel, flow through the drain grate, flow in the drain and flow through the drain pan orifice. For one-dimensional hydraulics, the losses represented by K_d would be independent of the piping configuration. Figure 4.13 shows the channel and drain loss coefficient values for Drain 2B tests under orifice control.

The following analysis of Figure 4.11 and Figure 4.13 will first present any relevant details pertaining to the calculation of the piping losses for each configuration. Each configuration will then be compared to the other configurations and an explanation will be given as to the possible reasons for the observed behavior. Figure 4.13 will be used to support conclusions drawn on the test results shown in Figure 4.11. Reference to Figure 4.1 will be beneficial during this discussion.

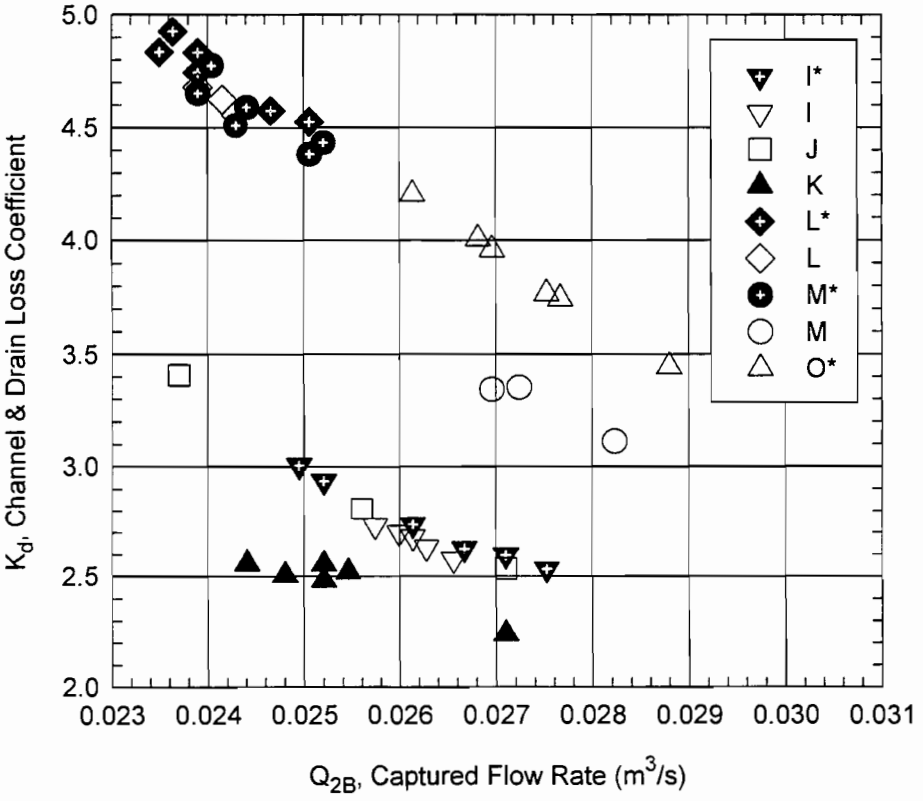

Figure 4.13 Channel and Drain Loss Coefficient Values for Drain 2B Tests Under Orifice Control

Configuration K had no piping connected to it, so there were no piping losses included in the calculation of H_o. Configuration K was chosen as the reference configuration because it had no connected piping.

Configuration J included one elbow connected directly under the drain pan. This elbow was assumed to be flowing full. Therefore the elbow added to the total head due to the lower discharge point, and subtracted from the total head due to the head loss in the elbow. In Figure 4.11, the data point having a captured flow rate of 0.024 m^3/s for Configuration J may have been in transition between weir control and orifice control. Based on the other two data points for Configuration J, $Q_{2B}(J)$ was anywhere from 2% to 5% larger than $Q_{2B}(K)$. This comparison of Q_{2B} seemed to show that the increase in head due to the extra 0.102 m of vertical pipe was slightly larger than the decrease in head due to the loss through the elbow. In Figure 4.13, $K_d(J)$ should have been similar to $K_d(K)$ assuming one-dimensional hydraulics correctly predicted the losses through the system. However, Figure 4.13 appears to show that either the elbow loss was incorrectly calculated, or one-dimensional hydraulics did not accurately describe the flow behavior. It was assumed that one-dimensional hydraulics was accurate in predicting the flow behavior, so K_{EB} was recalculated. K_{EB} was chosen to be 0.9 because this value caused $K_d(J)$ to be equivalent to $K_d(K)$. Daugherty et al. (1985) show the typical loss coefficient value for a short radius elbow to be 0.9, while Gupta (1989) shows 0.9 to be the maximum loss coefficient value for a screwed elbow. Although $K_{EB} = 0.9$ was probably high, this value was used because it still provided opportunity for comparison of the magnitude of K_d values for each piping configuration. K_d was then recalculated by the procedure described earlier. Figure 4.14 shows the recalculated values for K_d using $K_{EB} = 0.9$. The remaining discussion of the results will use Figure 4.14 in the analysis of the orifice control data rather than Figure 4.13.

Configuration I included an elbow and 1.13 m of horizontal pipe. During orifice control, the horizontal pipe never filled up so the head loss for full pipe flow included only the elbow. Figure 4.11 shows that $Q_{2B}(I)$ was nearly equivalent to $Q_{2B}(J)$. The head across the drain due to the piping was equal for both configurations, so the results for Configuration I were expected. Also, $K_d(I)$ was similar to $K_d(J)$.

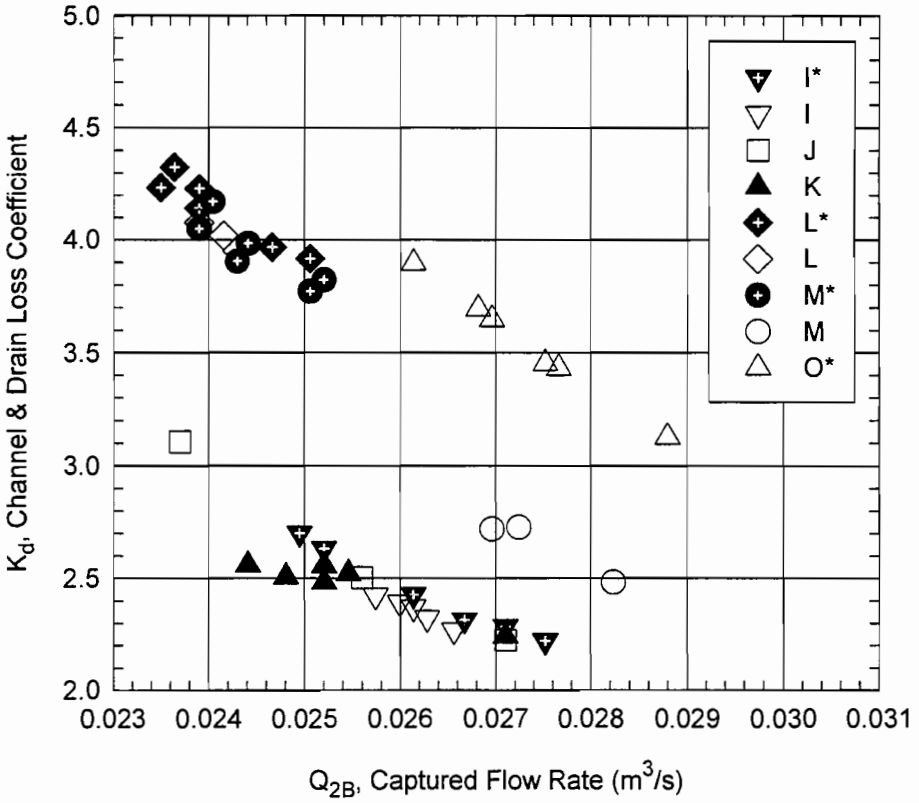

Figure 4.14 Recalculated Channel and Drain Loss Coefficient with $K_{EB} = 0.9$

Configuration I* included the swirl meter in the drain pan orifice. The horizontal pipe never filled up during orifice flow for Configuration I*. Figure 4.11 shows a slight decrease in $Q_{2B}(I^*)$ versus $Q_{2B}(I)$. This behavior was expected because the swirl meter was known to cause at least a small head loss. This small loss appeared in Figure 4.14 as a slight increase in K_d going from Configuration I to Configuration I*. These results seem to show that the swirl meter had negligible effects on the hydraulics of the flow.

Configuration M had a full flowing horizontal pipe while under orifice control, so losses in the calculation of H_o included two elbows and the horizontal pipe. $Q_{2B}(M)$ was slightly larger than $Q_{2B}(I)$. This behavior would again suggest that the increase in head due to the lower discharge point in the second elbow was larger than the head loss due to the second elbow. Figure 4.14 shows that $K_d(M)$ was larger than K_d for Configurations K, J, I, and I*. The increase

in K_d for Configuration M seemed to suggest that there was an interaction between the two elbows that created a greater total loss than was calculated by treating them as separate losses. This explanation for the behavior is supported by Shimizu (1975) as discussed in Section 2.6. These results seemed to show that one-dimensional hydraulics may not totally describe the hydraulics of the flow which occurred in the drain and piping system of Configuration M.

Configuration M* included the swirl meter in the drain pan orifice. This configuration also had a full flowing pipe while under orifice control. Inclusion of the swirl meter in Configuration M* appeared to cause a dramatic decrease in Q_{2B} from Configuration M. Figure 4.14 shows an increase of approximately 25% in K_d values going from Configuration M to M*. It is difficult to justify this large increase in K_d simply because of the existence of the swirl meter, based on a one-dimensional hydraulics viewpoint. So again, one-dimensional hydraulics may not fully describe the flow behavior through Configuration M*. Regardless of the reason, the swirl meter greatly decreased the drain capacity for this configuration. The question of why the swirl meter had such a significant impact on Configuration M* when it had minimal impact on Configurations I* and L* will be discussed later in this section.

Configuration L added an extra vertical pipe onto the elbow of Configuration M. The horizontal pipe in Configuration L was full during orifice control. However, the vertical pipe was not flowing full. Observation of the flow in the vertical pipe during Configuration L tests showed that the discharge was clinging to the sides of the vertical pipe, and that there was an air core through the center of the flow in the vertical pipe. Therefore, in the calculation of $K_d(L)$, z_2 was taken at the top of the vertical pipe and piping losses in Configuration L were equivalent to piping losses in Configuration M. The fact that the vertical pipe was not full explained much about the results obtained in both this research and the study by Holley et al. (1992). As stated earlier, z_1-z_2 in Equation 4.13 was the distance from the water surface in the approach channel to the location of atmospheric pressure in the pipe. Holley et al. assumed the location of atmospheric pressure occurred at the end of the piping system. The realization that the second vertical pipe was not full explains the unexpected behavior seen by Holley et al. The distance from the drain pan to the first elbow determined the total vertical piping head, not the distance from the drain pan to the end of the discharge pipe.

Since the vertical pipe in Configuration L was not full, the behavior of this configuration should have been equivalent to Configuration M, according to one-dimensional hydraulics. However, $Q_{2B}(L)$ was considerably less than $Q_{2B}(M)$, as shown in Figure 4.11. Also, $K_d(L)$ was much larger than $K_d(M)$. It is unclear why Configuration L behaved as it did, but possible explanations are presented later in this section. It is clear that, assuming there were no errors in the experimental process, one-dimensional hydraulics did not accurately predict the drain behavior for Configuration L. More data for Configuration L would be needed in order to fully understand the observed behavior. Only three tests were performed for Configuration L because construction of the swirl meters was completed by the end of the third test. The difference in Q_{2B} between Configurations L and L* was minimal, as shown in Figure 4.11. This minimal difference seemed to show that the swirl meter had little effect on the drain capacity. Therefore, no more tests were performed for Configuration L. It was only later that results showed the swirl meter seemed to have significant influence on the drain capacity for certain configurations. By then, little time remained to perform more tests on Configuration L.

Configuration L* included the swirl meter in the drain pan orifice. $Q_{2B}(L^*)$ was slightly less than Q_{2B} for Configurations L and M*. The channel and drain loss coefficients were comparable for Configuration L*, L and M*. The behavior of Configuration L* in comparison with M* was expected because the only difference was the addition of the vertical pipe which was never full. This behavior will be further discussed after a presentation of Configuration O* data.

Configuration O* was similar to Configuration I* except that the top of the elbow in Configuration O* was dropped 0.178 m below the drain. The vertical pipe was assumed to be full, but the horizontal pipe in Configuration O* never filled up. For the highest captured flow rates, the flow was clinging to the top of the horizontal pipe for approximately 0.3 m past the elbow, but the horizontal pipe never completely filled up. Thus, the losses for Configuration O* included the short vertical pipe and the elbow. $Q_{2B}(O^*)$ was greater than Q_{2B} for any other configuration under orifice control. This behavior was expected because the elbow was lower in Configuration O* than in any other configuration experiencing orifice control. (Larger values of Q_{2B} were obtained for other piping configurations, but only for weir control). $Q_{2B}(O^*)$ was

larger than $Q_{2B}(M)$ because Configuration O* had the same piezometric head as Configuration M but it did not have the loss from a second elbow. Since no tests were performed on Configuration O* without the swirl meter, it is difficult to quantify the influence the swirl meter had on Configuration O*.

Further Discussion of Results

As mentioned in the previous discussion, the drain behavior under certain piping configurations was unexpected. Depending upon the perspective taken in analyzing the data, various patterns emerge in the data for Configurations I, I*, L, L*, M and M*. There is more than one possible explanation for the behavior.

One possible explanation is that the general trend is revealed between Configurations I and I*, and L and L* and that the deviant configuration is Configuration M. In Figure 4.11, $Q_{2B}(I)$ is similar to $Q_{2B}(I^*)$, and $Q_{2B}(L)$ is similar to $Q_{2B}(L^*)$, while $Q_{2B}(M)$ is larger than $Q_{2B}(M^*)$. Also, $K_d(I)$ is similar to $K_d(I^*)$, and $K_d(L)$ is similar to $K_d(L^*)$, while $K_d(M)$ is much less than $K_d(M^*)$. The relationship between $K_d(M)$ and $K_d(M^*)$ is expected because of the behavior of the flow rates of these same configurations. $K_d(M^*)$ is nearly equal to $K_d(L^*)$, which is expected since the vertical pipe in Configuration L* was not full flowing, but it is unclear why $Q_{2B}(M)$ was so much larger than $Q_{2B}(L)$. Thus, the deviation in the trend may be in Configuration M. To explain the data in the manner just presented, it must be assumed that the swirl meter had little influence on the drain capacity for Configurations I*, L* and M*. Based on the data obtained, it cannot be explained why Q_{2B} increased when the vertical pipe on Configuration L was removed to create Configuration M.

A second possibility to explain the observed behavior is that Configuration L is the deviant configuration. The support for this view can be found by assuming that the swirl meter did have significant impact on Q_{2B} for a full flowing piping configurations and that the elbow in Configurations I and I* was not full flowing. Q_{2B} for Configurations L* and M* was less than for Configuration I*, and K_d for L* and M* was greater than for I*, due to the influence the swirl meter had on the captured flow under the full flowing piping conditions in L* and M*. The only unexplained behavior using this approach is the behavior seen in Configuration L. $Q_{2B}(L)$ and $K_d(L)$ were similar to $Q_{2B}(L^*)$ and $K_d(L^*)$, while there were significant differences in these same

parameters between Configurations M and M*. The difference in these parameters for Configurations M and M* is explained by the influence of the swirl meter. The reason Configurations L and L* did not show a similar pattern is unknown.

Any hypothesis used to explain the behavior leaves some unanswered questions. Some of the results in Figure 4.11 cannot be fully explained using the data gathered in this study. However, the behavior in Figure 4.14 could be at least partially explained by assuming that the location of atmospheric pressure in the piping system was incorrectly assumed. Using Configurations M and M* for example, the location of atmospheric pressure was assumed to be the same for both of these piping systems, but a difference of only 0.09 m (which is approximately 1/2 the depth of the elbow) would result in a K_d change of approximately 1.0. This value of $K_d = 1.0$ is nearly the difference between $K_d(M)$ and $K_d(M^*)$. It is known that the horizontal pipes were flowing full in Configurations L, L*, M and M*, yet the exact location of atmospheric pressure inside the elbow is unknown.

General Conclusions

The following points summarize the analysis of the results for Drain 2B under orifice control.

- It was uncertain what influence the swirl meter had on the drain capacity. It may have had negligible influence on all configurations, or it may have had significant influence on the configurations with full flowing pipes.
- In all configurations having two elbows, the vertical pipe below the second elbow was never full, so this pipe did not contribute to the total head across the drain.
- Configuration O* had the greatest distance from the drain pan to the first elbow and had the greatest captured flow rates. Thus, increasing the distance from the drain pan to the first piping elbow increased the captured flow rate.
- One-dimensional hydraulics was insufficient in describing the drain behavior for at least some of the piping configurations.
- There is not enough data to fully explain the behavior of Drain 2B under certain piping configurations.

4.2.2.5 Vortex Effects on Drain 2B Capacity

The previous two sections described the results from the tests on Drain 2B with weir and orifice control. Under orifice control, the drain behavior for some of the piping configurations

was not fully explained by one-dimensional hydraulics. The idea that the vortex or swirl in the drain was somehow interacting with the first piping elbow in such a way as to decrease the drain capacity was initially discussed in Section 2.6. The swirl meter was used in order to quantify the swirl strength and correlate this swirl strength with the captured flow rate. The use of the swirl meter would hopefully provide enough information about the swirl behavior to determine if the swirl was influencing the drain capacity. The measure of the swirl strength was called the swirl angle and was calculated according to the equations in Section 3.7.2. Figure 4.15 shows the calculated swirl angle, α, for all of the piping configurations which contained the swirl meter. Drain 2B experienced weir control for some configurations in Figure 4.15 and orifice control for other configurations shown in the same figure.

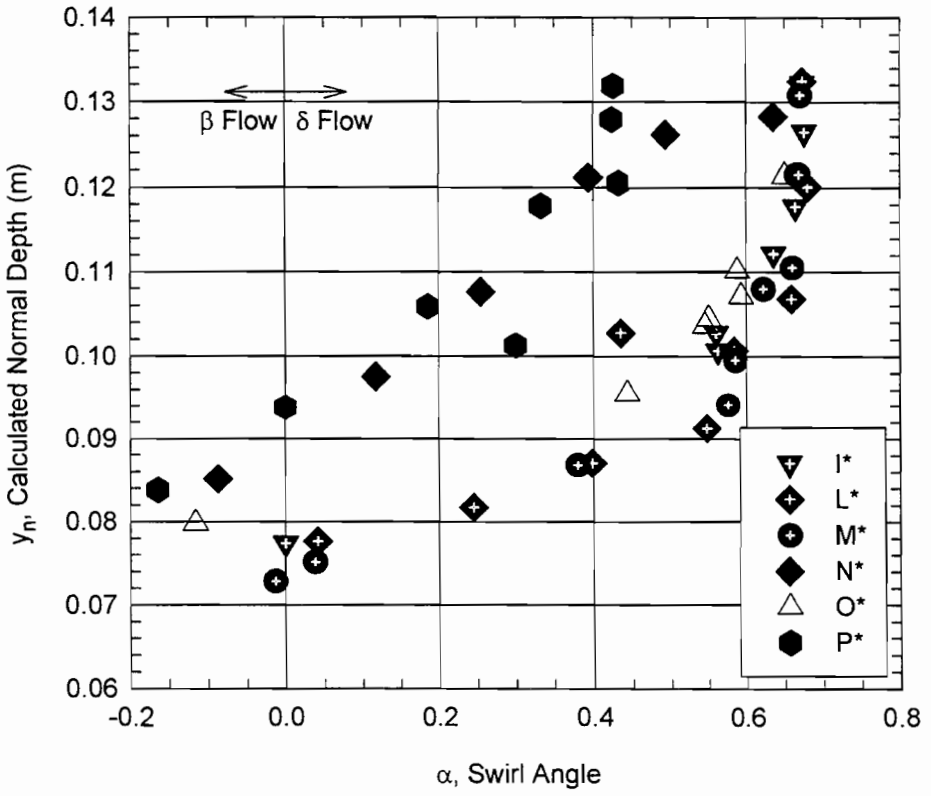

Figure 4.15 Swirl Angle for Piping Configurations Containing the Swirl Meter

Transition from negative to positive values for the swirl angle was the transition from the β flow pattern to the δ flow pattern in the drain pan orifice. In order to effectively analyze the results in Figure 4.15, the captured flow rates for each piping configuration containing the swirl meter are necessary. Figure 4.16 shows the captured flows for the piping configurations containing the swirl meter.

The most noticeable element in Figure 4.15 is that the data seemed to conglomerate in two sets, the configurations which stayed in weir control for all normal depths and the configurations which transitioned to orifice control. Transition from the β flow pattern to the δ

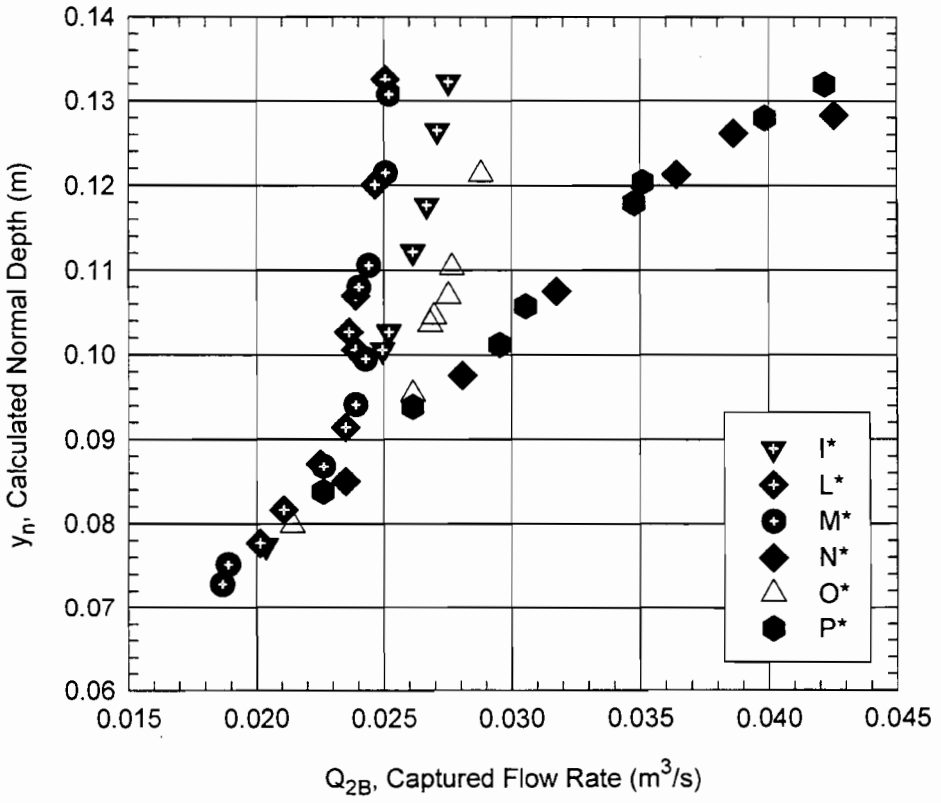

Figure 4.16 Test Results for Drain 2B Containing the Swirl Meter

flow pattern occurred at different normal depths for the two sets of data. Also, for a given normal depth, the swirl angle decreased as the total vertical pipe length increased. One possible explanation for these results is related to the flow pattern. Since the flow pattern depended on the depth of flow in the drain pan, then it is probable that the strength of the swirl in the drain pan was also dependent on the depth of flow in the drain pan. The swirl angle depended on the strength of swirl in the drain pan. Therefore, the magnitude of the swirl angle was also dependent on the fullness of the drain pan. Another possibility is that the influence of gravity due to the increased vertical piping straightened out the flow coming through the orifice. That is, the swirl strength was less for the piping systems with longer vertical pipe due to the increased "pull" by the longer pipe.

Making certain assumptions about the hydraulics of the drain flow, another possibility exists to explain the behavior in Figure 4.15. Assuming the drain pan in Configuration N* was 1/2 full and the drain pan in Configuration L* was 3/4 full, it could also be assumed that the swirl strength in the *drain pan* was the same for both. Since the pan depths were different, the swirl angle in the drain pan *orifice* for the configuration with the shallower drain pan depth (Configuration N*) would be smaller than the swirl angle for the configuration with the deeper drain pan depth (Configuration L*). This difference in α would occur because the swirl in the shallower pan had less change in the swirl area as the swirl traveled from the drain pan into the drain pan orifice. The swirl in the deeper pan had a larger change in the swirl area which would result in a larger swirl angle due to the necessary increase in angular velocity.

So any of these three possibilities exist to describe the general behavior shown in Figure 4.15. Without further data to describe the hydraulics of the flow in the drain pan, the specific reason or reasons for the behavior cannot be determined.

It is clear from Figure 4.15 that the hydraulics of the flow in the drain pan were dependent upon the piping configuration. Even when under weir control, the piping still appeared to influence the hydraulics of the flow in the drain pan. Configurations P* and M* had similar captured flow rates and were both under weir control for $y_n = 0.084$ m. Yet the swirl angles were significantly different. This difference was caused by a difference in the hydraulics of the flow in the drain pan for the two configurations.

Figure 4.15 shows that the data for Drain 2B with orifice control collapsed into a small range of swirl angles as compared to the somewhat larger range in the captured flow rates for the same data in Figure 4.16. This comparison seems to indicate that the swirl strength had little or no influence in the drain capacity. Otherwise, the data in Figure 4.15 should be more spread out according to the various configurations.

Comparison of Figure 4.15 with Figure 4.14 gives no more insight into the drain behavior. Again, Figure 4.15 data seems to conglomerate for orifice control tests, yet Configuration I* in Figure 4.14 shows significant differences in behavior from Configurations L* and M*. So the most reasonable explanation for behavior in Configurations I*, L*, and M* is still that the swirl meter influenced the captured flow rate only for full-flowing piping configurations.

Another trend in Figure 4.15 for the configurations which experienced orifice control is that the swirl angle approached a constant value for $y_n > 0.107$ m. This behavior occurred because as y_n increased past 0.107 m most of the increase in captured flow entered the drain from immediately upstream of the drain orifice, not from the drain pan. The flow pattern in the drain pan apparently had the primary influence on the swirl angle, not the flow entering from directly upstream of the drain orifice.

So use of the swirl meter provided little insight into the explanation of the drain behavior for various piping configurations. Yet the meter did reveal that the piping configuration influenced the hydraulics of the flow in the drain, even when the drain capacity was determined by weir control. The swirl meter also seemed to show that the swirl had little influence on the drain capacity.

Despite the fact that the vortex appeared to have minimal impact on the drain capacity, one benefit from the vortex was found from the Configuration I tests. All of the Configuration I data has not been presented in any of the figures provided thus far. Figure 4.17 shows all of the Drain 2B test results for Configuration I.

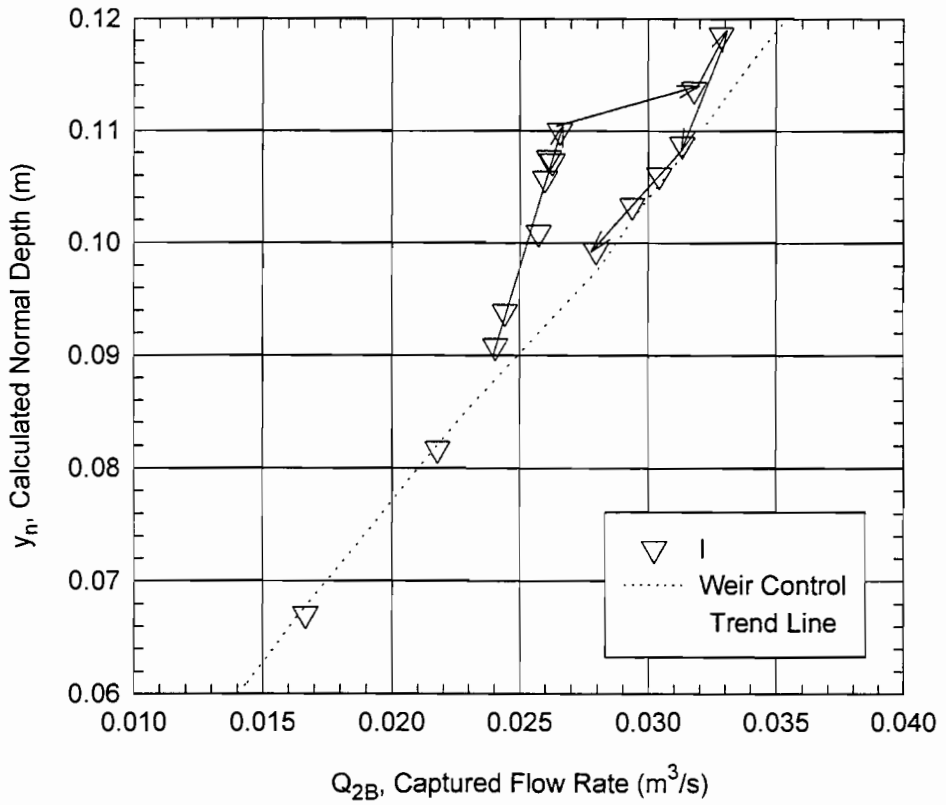

Figure 4.17 Test Results for Piping Configuration I

The arrows in Figure 4.17 show the trend in the behavior of the drain as y_n was increased up to 0.12 m and then decreased. The drain capacity was controlled by weir flow for $y_n <$ 0.085 m. As y_n increased above 0.085 m, the drain transitioned to orifice control. The drain continued to be controlled by orifice behavior up to y_n = 0.11 m. Q_{2B}(I) increased dramatically when y_n increased above 0.11 m. Further increasing the approach y_n increased the drain capacity along another trend that appeared to be orifice control, but the drain capacity was much greater than in the initial orifice control regime. Decreasing the approach y_n, the drain capacity was again controlled by weir control, but at a much higher flow rate than what the drain had obtained earlier in weir control. The drain behavior continued in weir control as y_n decreased. The hysteresis effect shown by Figure 4.17 was explained once the piping was observed during these tests. Approaching y_n = 0.11 m from a low flow rate, the drain behaved as expected and the

horizontal pipe was not full. As y_n increased above 0.11 m, the swirl exiting from the elbow and flowing into the horizontal pipe flowed to the top of the pipe and actually caused the pipe to fill up. From a one-dimensional hydraulics standpoint, gravity would want to pull the flow from the top of the pipe and prevent it from remaining full. Yet the pipe remained full. Since the pipe capacity was not exceeded, flow in the pipe had to be under negative pressure. Otherwise, gravity would have pulled the flow off the top of the pipe. The negative pressure acted as a suction and increased the drain capacity. Because the drain had a greater capacity when the pipe was full, the water level in the drain pan fell below the drain grate and weir flow was able to occur in the drain. So for Configuration I, the swirl was actually beneficial for some flow conditions. Nevertheless, the worst case, or the left part of the hysteresis curve in Figure 4.17, should be used for design.

4.2.3 Summary of Large Model Test Results

Ninety-four tests performed on Drain 2B using the large model provided significant results in determining the flow behavior of Drain 2B for various piping configurations. For normal depths less than 0.085 m, the drain capacity was determined by weir control. This weir control was characterized by a weir discharge coefficient which varied along the weir length due to submergence effects. The shallow portion of the drain filled up for $y_n < 0.085$ m simply due to the shallowness of the drain pan. Above $y_n = 0.085$ m, the piping influenced the drain capacity. An elbow directly under the drain pan resulted in transition to orifice control at a normal depth of approximately 0.085 m. Increased distance between the drain pan and the first piping elbow resulted in increased captured flow rates because the transition from weir to orifice control occurred at a higher normal depth. Vertical pipe directly underneath the drain increased the capacity of the drain such that the drain remained in weir control up to the capacity of the piping system. Vertical piping which followed a second elbow in the piping system never flowed full, so the vertical piping did not help increase the drain capacity.

The swirl meter showed that the piping system influenced the hydraulics of the flow in the drain pan, even when the drain was under weir control. The swirl meter also showed that the vortex had little or no influence on the capacity of the drain.

Even though these results are significant in providing information about the behavior of Drain 2B for various piping configurations, the behavior was not completely understood. It was obvious however, that one-dimensional hydraulics did not accurately describe the drain behavior for all of the piping configurations. In general, the more complex the piping system, the less accurate one-dimensional hydraulics was in predicting the drain behavior.

4.3 COMPARISON OF RESULTS WITH HOLLEY ET AL. (1992) TESTS

The differences in the drain behavior between various piping configurations were not as noticeable in this research as in the study by Holley et al. (1992) (see Section 2.5). This fact was most likely due to the differences between the piping configurations studied in the two projects. All conclusions found in this research explain the behavior seen in the research by Holley et al. The fact that the second vertical pipe in Configuration B was not full explains why Q_2(C) was larger than Q_2(B), and why Q_2(B) was nearly equal to Q_2(E). The fact that the vortex had no influence on Q_2 suggests that Q_2(G) was less than Q_2(F) simply due to the difference in 0.305 m of head across the drain.

4.4 SMALL MODEL TESTS

4.4.1 Experimental Methods

The small model was used to perform 18 tests on Drain 2B. Two sets of slopes were employed in the study of Drain 2B on the small model. Initially, the model was set at a longitudinal slope of 0.004 and a transverse slope of 0.0417 just as in the large model. Since flow at this model slope was subcritical, downstream effects affected the flow profile along the model length because of the short length of the small model. The profile generated on the small model was significantly different than the profile on the large model because of the differences in size and geometry of the two models. Therefore, the drain behavior for the small model was significantly different than the drain behavior for the large model. The small model was too small to recreate the large model conditions under subcritical flows. The second set of slopes was a longitudinal slope of 0.02 and a transverse slope of 0.0417. These slopes provided

supercritical flow conditions on the model. It was understood that the drain behavior would be different for subcritical and supercritical flows, but it was hoped that comparisons could be made between small model test results for different piping configurations rather than trying to compare small model test results with large model test results.

Two piping configurations were studied using the small model. The first configuration was Configuration K, which was the same Configuration K studied in the large model. Tests for Configuration K were performed under both subcritical and supercritical flow conditions. The second configuration studied was called Configuration R. Configuration R had 3.72 m of vertical pipe connected directly to the drain pan orifice. There were no elbows in this configuration, only straight pipe. All tests on Configuration R were under supercritical flow conditions. The swirl meter was not installed in any of the piping configurations for the small model tests.

All tests performed on the small model were done using the following procedure. First, the model slopes were set. The north pump or both pumps supplied water to the model, and the 0.152 m valve was used to control the flow rate into the headbox. The point-gauge was used to measure the curb depth at various locations upstream of the drain. Once the flows in the carryover weir flume and in the return channel had become steady state, the depths were measured on the carryover flow weir and the outside weir. The approach flow rate was changed and the procedure was repeated. Once the desired number of tests was performed for a given configuration, the piping configuration was changed and the process was repeated.

4.4.2 Small Model Test Results

Figure 4.18 shows a comparison of the results for Configuration K tested on the large and small models under subcritical flow conditions. That is, all tests in Figure 4.18 were for a longitudinal slope of 0.004 and a transverse slope of 0.0417.

The bars on the small model data points are the range of normal depth values corresponding to a Manning's n between 0.012 and 0.014 (see Section 3.4.4). Figure 4.18 shows

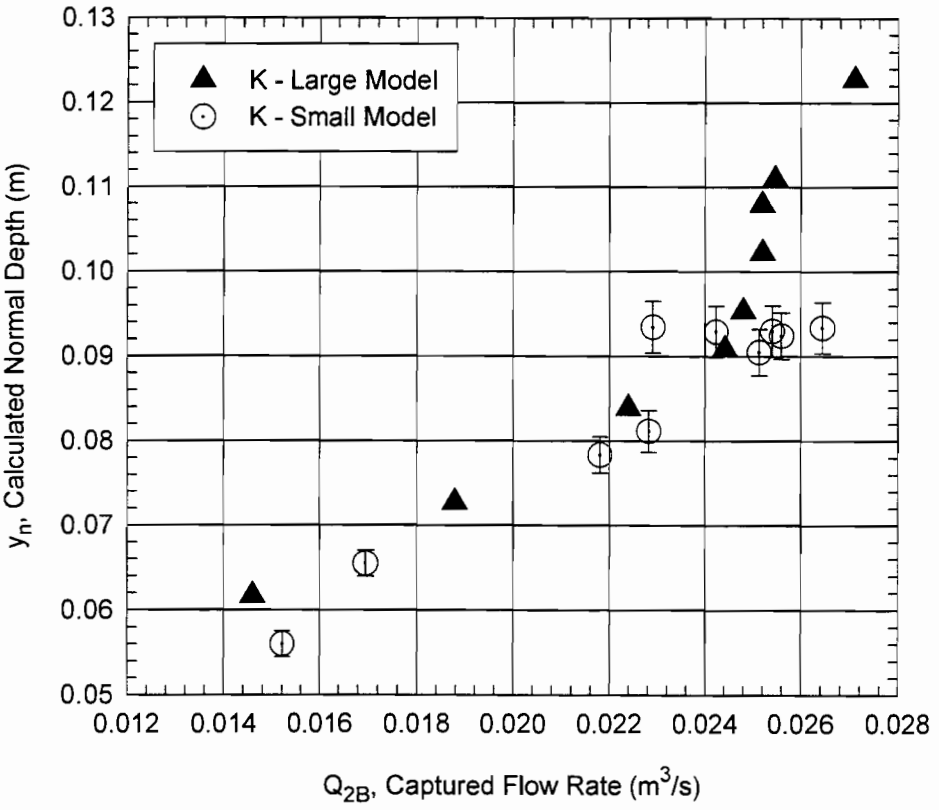

Figure 4.18 Drain 2B Tests Results Using Both Models for Configuration K Under Subcritical Flow Conditions

that the trend in drain behavior in the small model was somewhat similar to the drain behavior in the large model. Yet there were significant problems in the small model which are revealed in the data in Figure 4.18.

One problem with the small model is that the calculated normal depth was never greater than 0.098 m. The maximum approach flow rate achievable in the small model was approximately 0.068 m^3/s. This flow rate was obtained by using both pumps. The fact that the inflow point for the small model was approximately 2.4 m higher than the inflow point for the large model was one reason for the limitation in the maximum flow rate. Thus, the difference in elevation from the water surface in the reservoir to the headbox was greater for the small model than for the large model. The pumps therefore had to lift the water across a larger head difference in order to get the water up to the small model. Another contributing factor in the

limitation on the small model flow rate was the 0.152 m pipe which routed the water to the small model. The large model had a 0.305 m pipe discharging into the headbox. For any given large model approach flow rate, the pump head required to obtain the same flow rate in the small model was much greater. There were also significant losses due to the 0.305 m x 0.305 m x 0.152 m tee and due to the fittings in the 0.152 m piping. However, the limitation in the maximum approach flow rate was not the only problem in the small model.

In Figure 4.18, the scatter in the small model data can be attributed to the fact that uniform flow was not obtained upstream of the drain. The average difference between the calculated normal depths and the measured depths was 7%, with a maximum difference of 11%. Also, the surface of the approach flow was not stable during tests. No matter how the baffles were adjusted, a standing wave existed from the headbox all the way to the drain. The headbox was too small to adequately control the flow it received. The water was coming out of the headbox at different velocities across the width of the model. The intersection of the varying approach velocities created the standing wave. Not only did standing waves occur in the small model, but moving waves also occurred. Moving waves regularly traveled from the headbox to the end of the model. These waves were especially large for the smaller approach flow rates. The water rushed into the headbox and out through the baffles in pulses for low flows.

The reason that the small model tests appeared to capture more flow than the large model tests was at least partially due to the subcritical flow conditions. In the small model, the distance from the downstream edge of the drain to the carryover trough was approximately 0.3 m. For large approach flow rates, the trough was nearly full. It is probable that backwater effects from the trough caused an increase in the flow depth in the small model and thus also an increase in the captured flow rate for the small model compared to the captured flow rate in the large model.

The small model was modified many times during testing to adjust for all of the problems that appeared. The baffles were adjusted and modified. The carryover trough was enlarged. The size of the pipe which removed the carryover flow from the trough was increased. Many modifications were made, yet the problems still occurred. Despite all of the problems using the small model, one significant trend did appear in Figure 4.18. The slope of the data appeared to

be very similar for both the large and the small model. Even considering the scatter in the data for the small model tests, the drain appeared to behave under weir control.

Since the small model test results were influenced by subcritical flow conditions, tests were run on Configuration K and Configuration R under supercritical conditions to see if the results would prove useful. The model was set at a 0.02 longitudinal slope and a 0.0417 transverse slope. Figure 4.19 shows the results for all tests performed on Drain 2B using the small model. The depths shown in Figure 4.19 are measured depths instead of calculated normal depths since normal depth never occurred in the model. The data shown include the results for

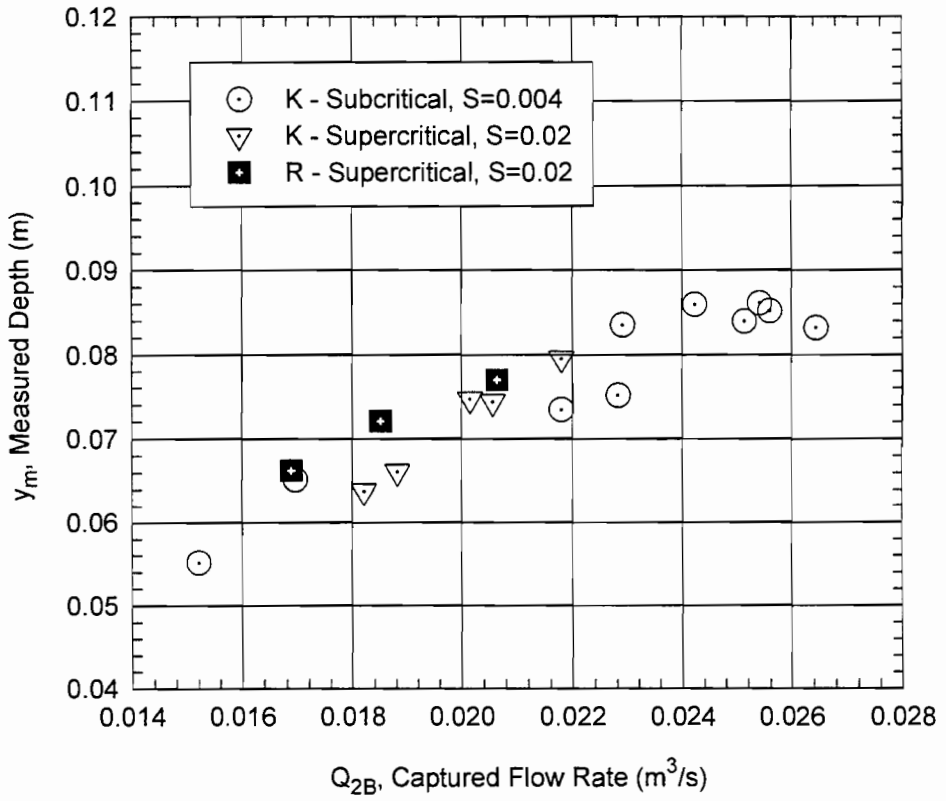

Figure 4.19 Drain 2B Test Results Using Small Model for Configurations K and R

Configuration K under both subcritical and supercritical flow conditions and the results for Configuration R under supercritical flow conditions. Depths on the subcritical tests were

measured 0.37 m upstream of the upstream edge of the drain. Depths on the supercritical tests were measured at the upstream edge of the drain.

For all of the tests on the small model, the drain never became completely full due to the limited approach flow rate. The approach flow was never large enough to cause the drain to fill up and transition to orifice control. For Configuration K data in Figure 4.19, Q_{2B} for S = 0.004 was approximately 9% greater than Q_{2B} for S = 0.02 at a measured depth of 0.064 m. For higher measured depths, Q_{2B} for S = 0.02 became slightly greater than Q_{2B} for S = 0.004. This behavior is inconclusive however, due to the problems already discussed in using the small model. The standing wave and the moving waves were even larger for the supercritical tests than for the subcritical tests. Due to the surface disturbances, the curb depths were difficult to accurately measure.

For S = 0.02, $Q_{2B}(R)$ was less than for $Q_{2B}(K)$. Since both configurations were under weir control and neither reached orifice control, the drain was expected to behave similarly for both configurations. This difference in captured flow rate was probably due to an adjustment which was made on the baffles between the two sets of tests. The baffle adjustment probably resulted in a change in the measured curb depths. Just as in Figure 4.18, the only result which is significant for Figure 4.19 is that the trend for all of the tests is similar. That is, the results show that the drain capacity was determined by weir control for all tests performed on the small model.

4.4.3 Summary of Small Model Test Results

Many problems were encountered in using the small model to analyze the effects of the piping configurations on Drain 2B capacity. Most of the problems were caused by the small model being too small. The size of the model prevented uniform flow from occurring upstream of the drain. The small model size caused effects from the downstream end of the model to be propagated onto the roadway surface; this condition was not experienced on the large model. Therefore, results from the two models for the same piping configuration were not comparable. Drain 2B never transitioned from weir control to orifice control due to the limited approach flow. The approach flow was limited because of the height of the model and the size of the pipe leading to the headbox. These problems create doubt about the accuracy of the data. The only

significant results obtained from the small model tests were that the drain capacity was controlled by weir behavior, which reinforced results shown in the large model tests.

4.5 SOURCES OF ERROR

Regardless of the caution taken in experimentation, errors still occur in the research process. There were three major sources for possible error in this study. All of these errors could lead to scatter in the data or simply incorrect data. One was the bubbler tubes used to measure the depths on the flow measurement weirs. These tubes sometimes had condensation built up in them such that water cut off the free flow of oxygen between the tube at the bottom of the weir channel and the manometer measuring the weir head. The weight of the water in any sags in the tube would have caused an imbalance of pressure across the section of the tube containing the water. This imbalance in pressure would have thrown off the depth measurements on the weirs. In order to prevent condensation from causing errors in the weir head measurements, by-pass valves were installed in each of the bubbler tubes. These valves were regularly opened and condensation was forced out of the lines. Even though this procedure was done quite frequently and great care was taken to check for condensation, the possibility remains that all condensation may not have been removed for every test.

Another possible source of error was in the venturi meter manometer. Many connections and valves existed in the venturi manometers because two manometers were used to measure the venturi flow rate (see Section 3.5). These connections provided opportunity for air to leak in and remain during testing. Air in any of the connections would have thrown off the manometer readings. These manometers were cleared of air each day before tests were run, and sometimes more than once per day. Even with this care, the possibility still exists that air was stuck between fittings and did not clear out of the manometers, or that air leaked in during a test. The probability that air in the venturi manometer caused errors was minimal however, because all venturi flow rates were checked by comparison with the other flow measurement devices.

The third possible source of error was human error. Numerous tests were performed over a two year period. There could have been errors in reading the captured flow weir, the carryover flow weir, the venturi meter, the point-gauge, or even the scales used to set the model slopes.

Deliberate care was taken to set the model slopes and verify them before tests were performed each day. All of the data were carefully read and recorded for each test. Yet it is possible that a researcher could have either misread or just incorrectly recorded data. All of the data were compared with other data to see if any reading was unreasonable, so the chances of human error having significant impact on the results were very minor.

4.6 CALCULATION OF BRIDGE DECK DRAIN FLOWS

4.6.1 Approach

An approach sometimes used for calculating the flow captured by a drain when hydraulic calibration data for that drain are not available is to take the smaller of the flows based on the capacity of the grate using HEC-12 (Johnson and Chang, 1984) and based on the capacity of the entrance into the drain piping. The calculation based on Johnson and Chang will be called the HEC-12 method or weir control and the later calculation will be called orifice control. Although HEC-12 does not include all of the types of grates which are used, the flow can be estimated by identifying a grate in HEC-12 with similar geometric and hydraulic characteristics to the grate being used. The data that have been reported by Holley et al. (1992) and Hammons and Holley (1995) plus the data in this report provide an opportunity to evaluate this approach, as presented below. The results are summarized in Tables B.3 through B.7 and Figure 4.23.

In order to check this calculation approach against the measured flows, it is helpful to first consider the flows with weir and orifice controls separately. Thus, it is necessary to know which tests were in which regime. This determination was made from the plots of y_n (normal depth for the approach flow) versus Q (captured flow). See for example, Figures. 2.3, 4.4, 4.7, and 4.11 and the related discussions. In most of the other discussion in this report, it has been assumed that there are two regimes, namely weir control and orifice control. However, for present purposes, three regimes were identified, namely weir control, orifice control, and a transition region or region of uncertainty between weir and orifice control. Flows in the third regime were not used in Section 4.6.3 for weir flow nor in Section 4.6.4 for orifice control to be certain that the flows for which calculations were being made for weir and orifice control were

actually in the assumed regime. However, all data were used in Section 4.6.5 to evaluate the approach of using the smaller of weir or orifice controlled flows for design.

4.6.2 Drains

Drain 2 (Holley et al., 1992) is described in Section 2.5 of this report, and Drain 2B is described in Section 3.2. Drain 3 (Holley et al., 1992) had a grate which was 0.610 m wide (normal to the flow) and 0.915 m long (in the flow direction). It had 11 longitudinal bars with 12 open slots. The bars were 0.013 m wide and were placed on 0.051 m centers. It also had 5 transverse bars which were 0.010 m wide and placed on 0.152 m centers. All bars were rectangular and vertical. The outlet from the drain pan was a rectangular conduit which exited the side of the drain pan away from the curb. At the side of the drain pan, the conduit was 0.102 m high and 0.775 m wide. Over a distance of 0.915 m, the sides of the rectangular conduit tapered linearly to a cross section which was still 0.102 m high but only 0.305 m wide. In the model, there was an additional 0.610 m of the conduit at this smaller cross sectional size. The conduit had a downward slope of 0.089 relative to the plane of the top of the grate. Drain 4 (Hammons and Holley, 1995) had a grate which was 1.051 wide and 0.349 m long with one longitudinal, vertical, rectangular bar which was 0.019 m thick and 3 tilted transverse bars which were also 0.019 m thick. The cross sections of the tilted bars were parallelograms which were created by cutting inclined rectangular bars so that the top and bottom surfaces of the tilted bars were flush with the top and bottom surfaces of the grate. Due to the inclination and thickness of the bars and the similarly inclined fillets on the upstream and downstream sides on the grate, the total open length of the grate in the flow direction was only 0.228 m equally distributed between four transverse slots between the tilted surfaces of the bars and fillets. The outlet from the drain pan was a 0.203 m diameter pipe which had a rounded entrance with a radius of curvature of 0.025 m. The geometric parameters used in the calculations are given at the top of each table for each of the grates.

4.6.3 Weir Flow

Even though the terminology "weir flow" is used, the flows are not really weir flows in the normal sense. This terminology has come to be used for drain flow conditions which perhaps

more properly should be called "free flow" conditions to indicate the absence of controlling effects from filling of the drain pan. In the normal sense, "weir flow" refers to subcritical approach flows which pass through a control on the crest of broad-crested weirs or in the vicinity of the crest for sharp-crested weirs. However, the majority of the gutter flows in these experiments were supercritical and thus could not pass through a control (e.g., critical depth) near the edge of the grates. Thus, there is no reason to expect the relationship between Q and the "head on the weir," e.g., y_n (the normal depth for the approach flow), to follow the usual weir relationship for y_n vs. Q.

For the analysis in this section, it was desired to use only flows which were clearly in the weir control regime. Since it was not possible to identify these flows from a quantitative relationship between y_n vs. Q, they had to be identified by the general character of graphs of y_n vs. Q graphs. This identification began with the recognition that the lowest flow-capture rates were in the weir control regime so that these low flows give an indication of the behavior to be expected between y_n and Q for weir flows. In particular, the tests which were selected were the ones which (a) had Q values low enough to clearly be in the weir regime, (b) had at least two tests in the weir regime for a given combination of S and S_x so that the y_n-Q slope could be determined, or (c) had other tests with different S and/or S_x values so that the adjacent points of a y_n-Q graph could be used to determine the flow regime. The flows which were selected as being in the weir regime are indicated with a W in the Regime column in Tables B.3 through B.7 and are shown in Figure 4.20. The letters used as plotting symbols in Figure 4.20 are shown in the last column of Tables B.3 - B.7. The plotting symbols were selected as follows:

S_x	0.01	0.02/0.0208	0.04/0.0417	0.06	0.08
S					
0.001	A	B	C	D	E
0.004/0.005	F	G	H	I	J
0.01	K	L	M	N	O
0.02	P	Q	R	S	T
0.04	U	V	W	X	Y
0.06	Z	a	b	c	d
0.08	e	f	g	h	i

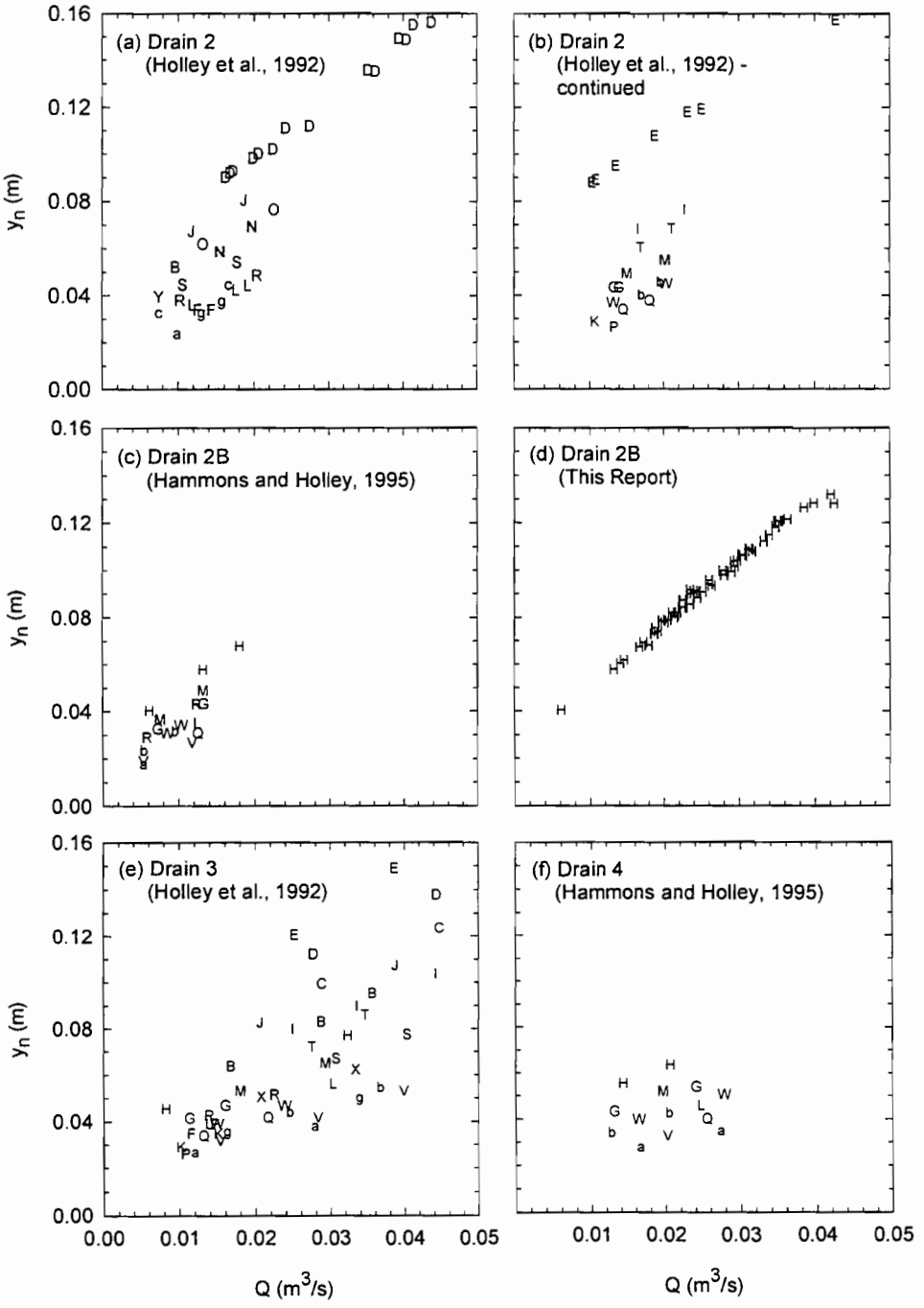

Figure 4.20 Experimental Results for Weir Flow Conditions

For calculation of the captured flow rates using HEC-12, Equations 9 and 10 in HEC-12 were converted to metric units to give

$$R_f = 1 - 0.30(V - V_o) \tag{4.22}$$

and

$$R_s = \frac{1}{1 + \frac{0.083V^{1.8}}{S_x L^{2.3}}} \tag{4.23}$$

where R_f = fraction of Q_w that is captured by the drain, Q_w = frontal flow = $[1 - (1 - W/T)^{2.67}]Q_a$ if $T > W$ or $Q_w = Q_a$ if $T \leq W$, W = width of the grate normal to the flow direction, T = ponded width for the approach flow, Q_a = approach gutter flow rate, V = average flow velocity in m/s for the approach gutter flow, V_o = splashover velocity in m/s, R_s = fraction of the side flow (Q_s) that is intercepted, $Q_s = Q_a - Q_w$, S_x = pavement cross slope, and L = length of the grate in m in the flow direction. The equivalent HEC-12 grates were chosen as follows:

Drain	Grate
2/2B	P-1-7/8-4
3	P-1-7/8-4
4	45° Tilt Bar

The values of W, L, and V_o are given in tables B.3 - B.7. At first, a P-1-7/8 grate was chosen to represent Drains 2 and 2B since these drains do not have transverse bars, but this grate gives V_o = 1.4 m/s for a grate length of 0.197 m. This value of V_o seems too large for this grate based both on intuition and on observation of the experiments. Thus, a P-1-7/8-4 grate was selected. This grate gives V_o = 0.67 m/s for Drain 2 and 2B. Even though this value of V_o is smaller, it still gives R_f = 1.0 for most cases for Drains 2 and 2B (Tables B.3 - B.5). Having R_f values which are almost all 1.0 for weir flow conditions seems unreasonable since splashover was observed to occur for many of the experiments for weir flow conditions.

The results of the HEC-12 calculations are given in Tables B.3 - B.7 and in Figures 4.21a and 4.21b. These figures give $Q_{HEC\text{-}12}/Q$ (the ratio of the captured flow rate calculated from HEC-12 to the measured captured flow rate) and are just for the flows identified as being weir flows. For Q/Q_a greater than about 0.8, $Q_{HEC\text{-}12}$ is within about 20% of the measured Q values.

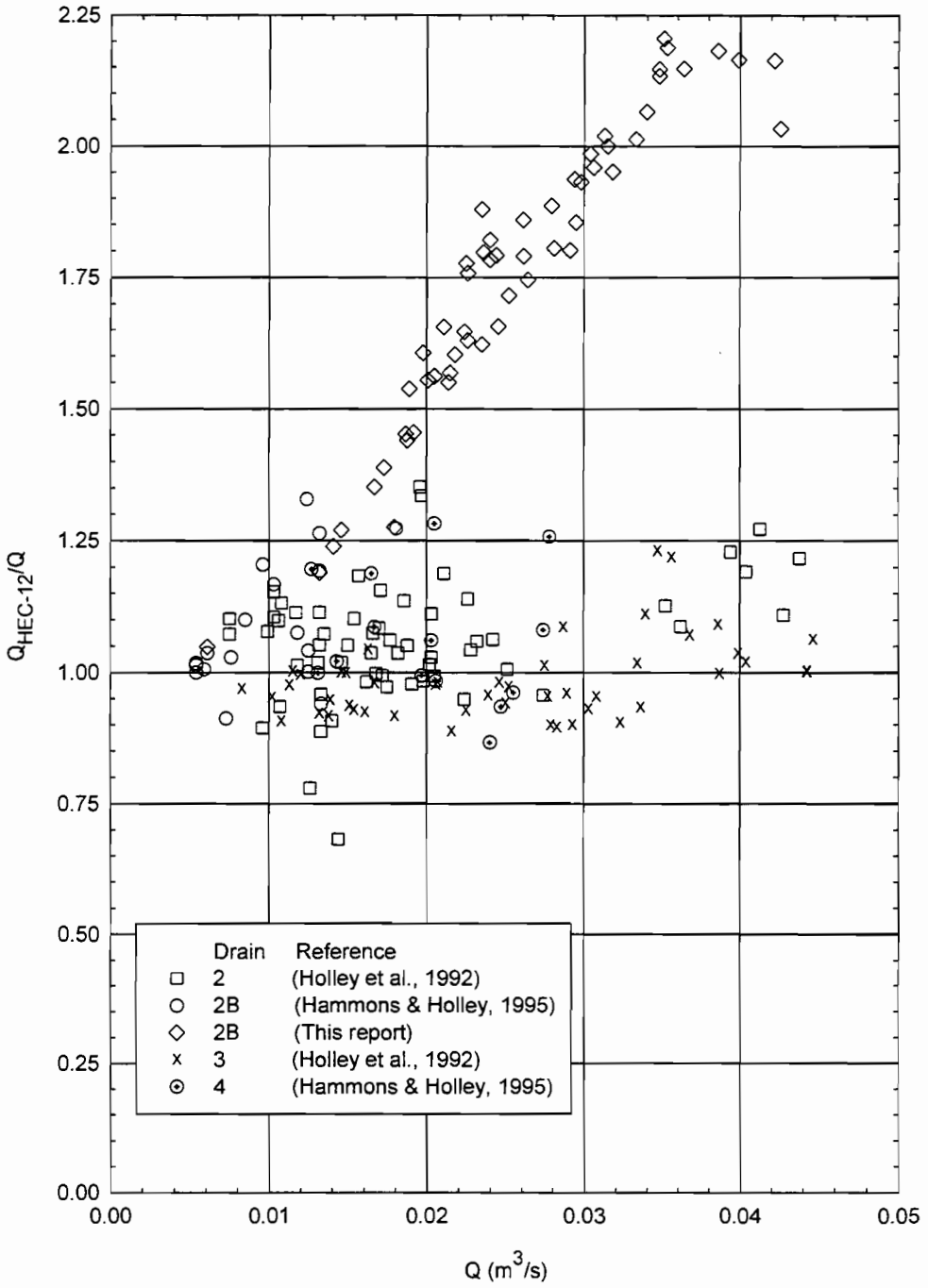

Figure 4.21 Ratios of Calculated and Measured Captured Flows for Weir Conditions (a) Plotted versus Captured Flow

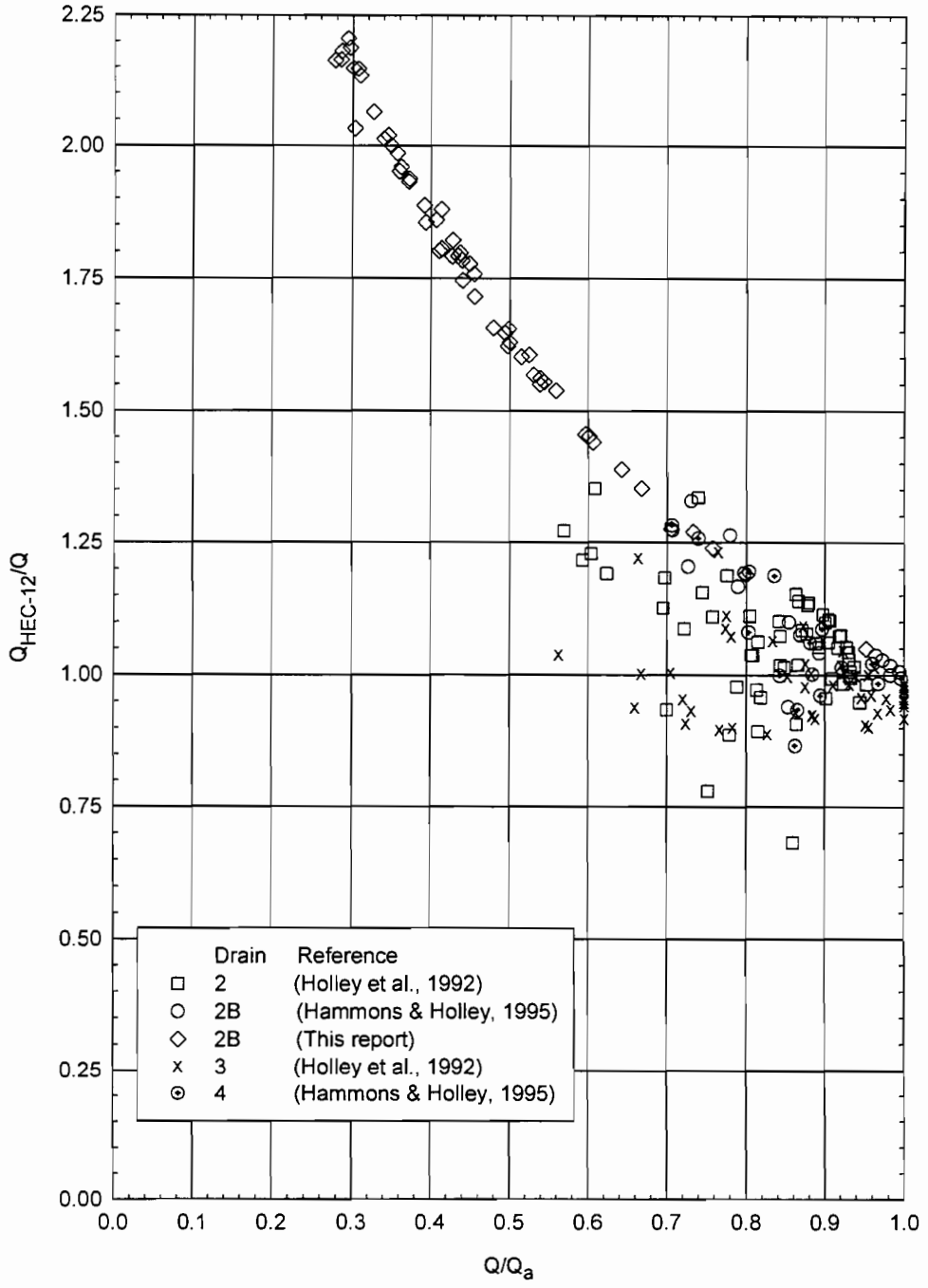

Figure 4.21 Ratios of Calculated and Measured Captured Flows for Weir Conditions (b) Plotted versus Capture Efficiency

However, for smaller values of Q/Q_a, Q_{HEC-12}/Q increases dramatically. Drains 2 and 2B are the only drains with values of Q/Q_a as small as about 0.3. These small values of Q/Q_a were possible under weir control because of the vertical length of the drain piping kept the drain pan from filling and creating orifice control. The high values of Q_{HEC-12}/Q for low Q/Q_a are probably related to the high values of R_f mentioned above. Significant splashover had to be occurring when Q/Q_a was small, but R_f did not seem to decrease in proportion to the observed splashover.

Values of R_f and R_s are shown in Figures 4.22 and 4.23. Again, these figures are only for weir control conditions. The smallest value of R_f for any of the drains is 0.82. All of the values of R_f for the data in this report are essentially one. All of the tests for Drain 2B in this report were done for one combination of S and S_x. The values for R_s vary widely, with the largest values naturally being for Drain 3 with the largest length in the flow direction.

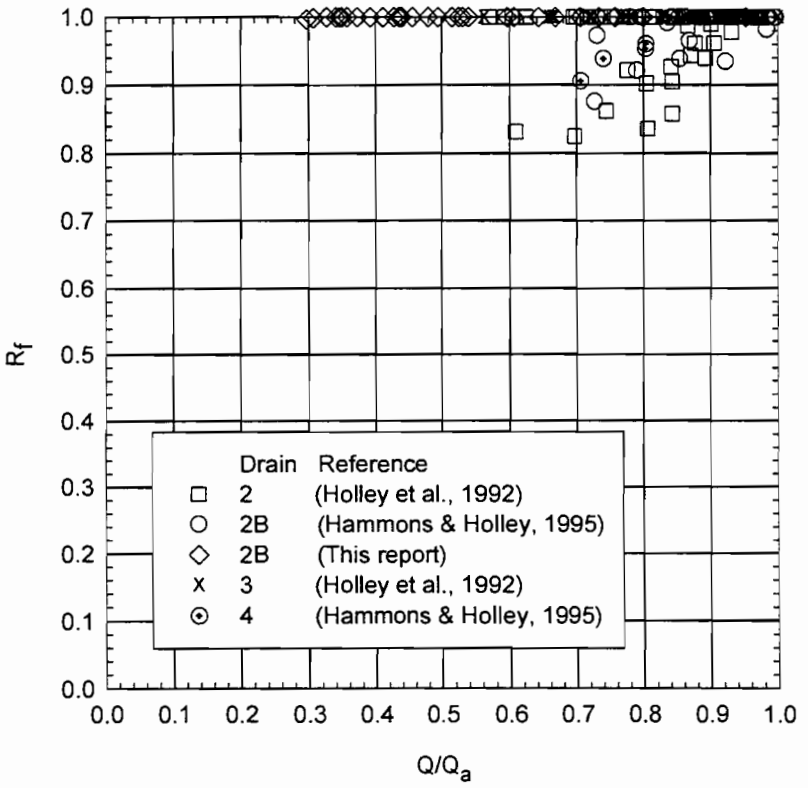

Figure 4.22 Frontal Flow Capture Efficiency for Weir Conditions

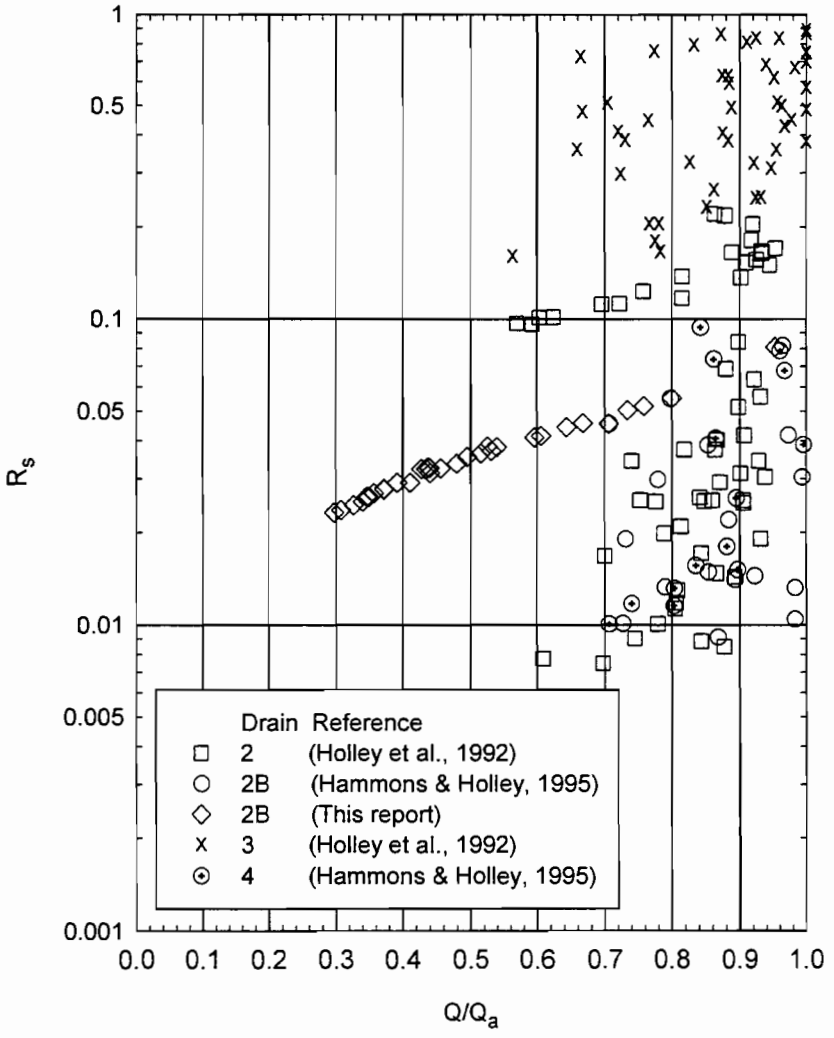

Figure 4.23 Side Flow Capture Efficiency for Weir Conditions

4.2.4 Orifice Flow

The identification of flows with orifice control was based on the orifice flow equation, namely,

$$Q = C_o A_o \sqrt{2gh_o} \tag{4.24}$$

where Q = flow captured by the drain, C_o = orifice coefficient for the exit from the drain pan = $C_{ov}C_{od}$ in Equation 2.6, A_o = area of the orifice = area of the drain pipe, and h_o = piezometric head difference across the orifice. The head difference across the orifice was taken as $y_c + L_v$ -

h_L, where y_c = depth of water on the roadway surface above the centerline of the orifice = $y_n(1 - W_c/T)$, W_c = width from the curb to the orifice centerline, T = ponded width in the approach flow = y_n/S_x, L_v = vertical distance from the top of the grate to the point of atmospheric pressure at the outlet from the drain or in the drain piping, and h_L = head loss from the roadway surface to the point of atmospheric pressure in the downstream part of the drain piping. Values of W_c and L_v are given in Tables B.3 - B.7. For piping configurations with an elbow followed by a vertical pipe, L_v was evaluated on the assumption that the last vertical pipe was not flowing full, so that atmospheric pressure occurred just before the elbow. No attempt was made to estimate the head loss for flow through the grate nor the head loss associated with the disturbed flow in the drainpan. The lack of adequate information to calculate these losses means that these losses effectively go into reducing the value of the discharge coefficient presented below. The head loss in the straight pipe was assumed to be negligible. Thus, the head loss was taken as the elbow loss, namely $NK_{EB}V_{pipe}^2/2g$ where N = number of elbows, K_{EB} = elbow loss coefficient which was taken as 0.9, and V_{pipe} = pipe velocity = Q/A_o. Substitution of these relationships into Equation 4.24 gives

$$Q = C_o A_o \sqrt{\frac{2g(y_c + L_v)}{1 + NK_{EB}C_o^2}} \tag{4.25}$$

Solving for C_o gives

$$C_o = \frac{V_{pipe}}{\sqrt{2g(y_c + L_v) - NK_{EB}V_{pipe}^2}} \tag{4.26}$$

For $L_v = 0$, N = 0, and $y_c = y_n(1 - W_c/T)$, Equation 4.25 gives

$$y_n \sim Q^2 \tag{4.27}$$

so that the slope of a graph of y_n vs. Q on log-log paper should be 2 for these conditions if C_o is constant for all flow rates. Values of L_v greater than zero give steeper slopes since the head losses from the piping and elbows are smaller than the increases in head from L_v. Thus, flows with orifice control were identified as those flows which were above the trend of the weir flow control discussed in Section 4.6.3 and had a y_n vs. Q variation with a slope of at least 2 on log-log paper.

Since most of the experiments have not been for the orifice control regime, only 27 cases could be identified as clearly being in the orifice regime. These cases, all of which were for Drain 2 and 2B, are indicated by an "O" in the Regime column in Tables B.3 - B.5. However, for the results for Drain 2B in this report, none of the orifice flows were used for tests with the swirl meter because of possible interference of the swirl meter with flow in the vicinity of the pipe entrance. For these 27 cases, C_o was calculated from Equation 4.26. These values of C_o are shown in Tables B.3 - B.5 and Figure 4.24. The plotting symbols are the pipe configuration for Drain 2 and for the data for Drain 2B from this report. For the data given by Hammons and Holley (1995), there was no piping attached to the drain.

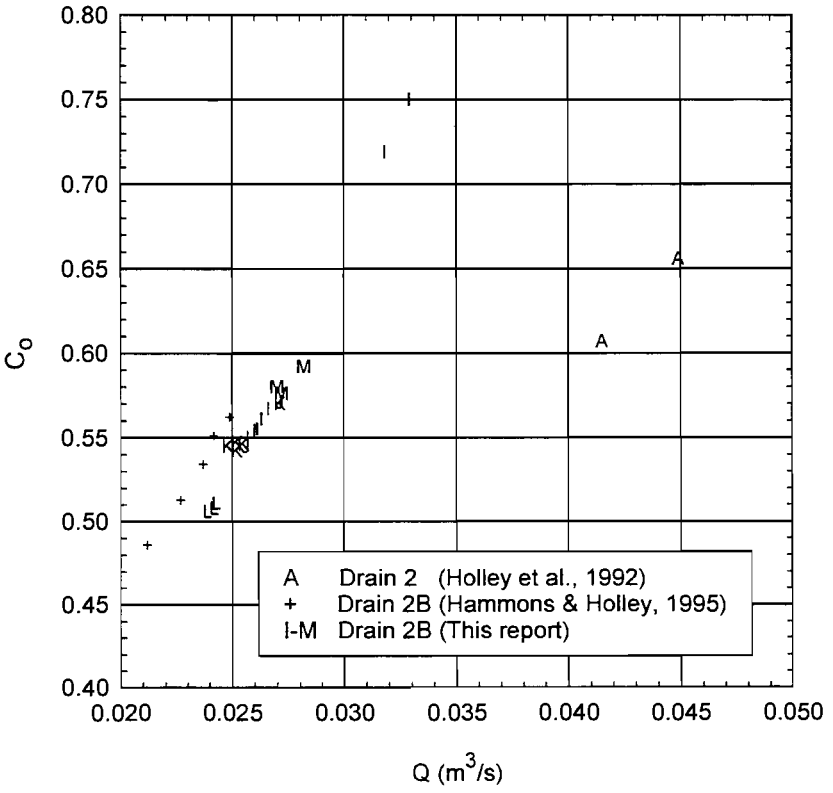

Figure 4.24 Orifice Coefficients Calculated from Discharge Measurements

It is apparent that C_o increases as Q increases and, even though there are only two points for Drain 2, it is also apparent that the relationship between C_o and Q is different for Drain 2 and

Drain 2B. Many different types of correlations were investigated to try to establish the reasons for the variation of C_o. These efforts included (a) varying the value of K_{EB}, (b) including head losses through the grate and in the drain pan, and (c) letting the head loss coefficient vary with the flow rate or with the length of vertical pipe. None of these efforts was successful in reducing the amount of variation of C_o. Thus, it was concluded that the types of measurements made during these experiments did not provide sufficient data for determining the cause of the variations of C_o with Q nor the cause of the differences between Drains 2 and 2B. For subsequent calculations, the average value of C_o, namely 0.57, was used. Tables B.3 - B.7 give the calculated values for Q_{orif}, which is the flow rate assuming that orifice control exists with C_o = 0.57.

For sag conditions, Johnson and Chang (1984) give C_o = 0.67 as the orifice coefficient for openings in a grate when the grate itself is acting as the orifice control. For sharp-edged metering orifices in pipelines, C_o for large Reynolds numbers increases from about 0.6 to about 0.7 as the ratio of the diameter of the orifice (D_o) to the diameter of the pipe (D_{pipe}) increases from 0.3 to 0.7. Similarly, C_o is about 0.6 for sharp-edged orifices discharging from a large tank or reservoir when D_o is small relative to the head on the orifice and when the orifice is away from any hydraulic influence of the boundaries of the tank. For small D_o/D_{pipe} and large Reynolds numbers in a pipe or for an orifice discharging from a large tank, C_o for an orifice with a rounded edge may be as high as 0.98. (These reference values of C_o are from Street et al., 1996). Since the orifice under consideration here has a rounded entrance (Figure 3.1) with a radius of curvature of 0.025 m, C_o would probably be 0.9 or higher for undisturbed approach flow in the absence of any hydraulic influence of the approach flow boundaries. The fact that all of the values of C_o are 0.75 or smaller is probably indicative of head losses for the flow through the grate and in the drain pan.

4.2.5 Comparison of Design Calculations and Measurements

For Drains 2, 2B, and 4, the calculation of the flow (Q_{calc}) captured by the drains consists of taking the minimum of Q_{HEC-12} and Q_{orif} in Tables B.3 - B.5 and B.7. For Drain 3, no calculations of Q_{orif} were made because of the rectangular drain piping (Section 4.6.2). Thus, for

Drain 3, Q_{HEC-12} was used as the calculated flow for cases which were identified as clearly having weir control; there was no calculated flow for the other conditions. The ratios of the calculated flows to the measured flows (Q_{calc}/Q) are shown in Figures 4.25a, b, and c. Figure 4.25a is a plot using Q as the abscissa while Figure 4.25b has Q/Q_a as the abscissa. Figure 4.25b also shows the average of Q_{calc}/Q for intervals of 0.5 of Q/Q_a and the average plus and minus one standard deviation. See Table B.8. Figure 4.25c is also a plot of Q_{calc}/Q vs. Q/Q_a, but the plotting symbols are just "W" and "O" to indicate whether weir flow (W) or orifice conditions (O) gave the smaller value of Q for each test. A similar notation of "W" or "O" is used in the tables in the column labeled "min Q".

For these tests, the following conclusions can be drawn:

a) For $Q/Q_a > 0.7$, the control was essentially always weir flow.

b) For $Q/Q_a < 0.6$, the control was essentially always orifice conditions.

c) For $Q/Q_a > 0.8$, Q_{calc} was within about 20% or less of Q.

d) Comparison of Figures 4.21b and 4.25b shows that the maximum value of Q_{calc}/Q is less than the maximum value of Q_{HEC-12}/Q for flows which were clearly operating with weir control. Thus, the smaller values of Q_{calc}/Q are at least partially due to the fact that the calculations erroneously indicate orifice control for some flows which were actually operating under weir control.

e) The errors in this calculation approach are predominately an overestimation of the flow which will be captured by a drain. For $0.25 < Q/Q_a < 0.95$, all of the average values of Q_{calc}/Q are greater than unity. For these tests, some of the errors were as large as 65% overestimation of the captured flow.

f) For each drain, the values of Q_{calc}/Q tend to increase as Q/Q_a decreases from unity in the region where weir control gives the minimum calculated Q. As Q/Q_a continues to decrease, orifice conditions eventually become the control, and the values of Q_{calc}/Q then start to decrease with decreasing Q/Q_a.

These errors in Q_{calc}/Q can be compared with the accuracy of empirical calibration equations in Holley et al. (1992), Hammons and Holley (1995), and this report. Generally, the error or uncertainty in the empirical equations is on the order of 5% or less. Comparison of this value with the values of Q_{calc}/Q in Figure 4.25 demonstrates both the need for experimental evaluation of drains before they are installed and the benefits of such tests.

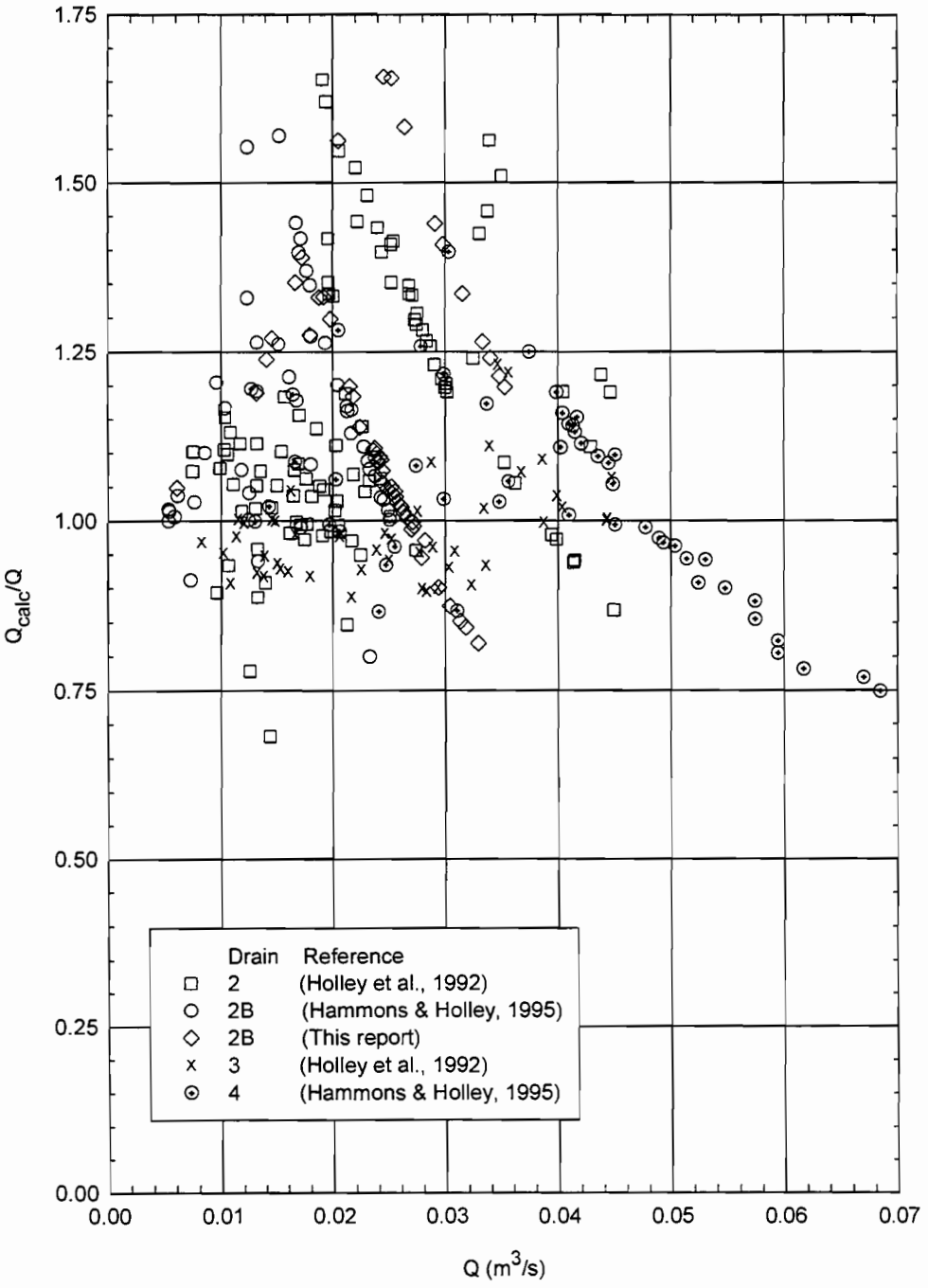

Figure 4.25 Ratios of Calculated and Measured Captured Flows (a) Plotted versus Captured Flow

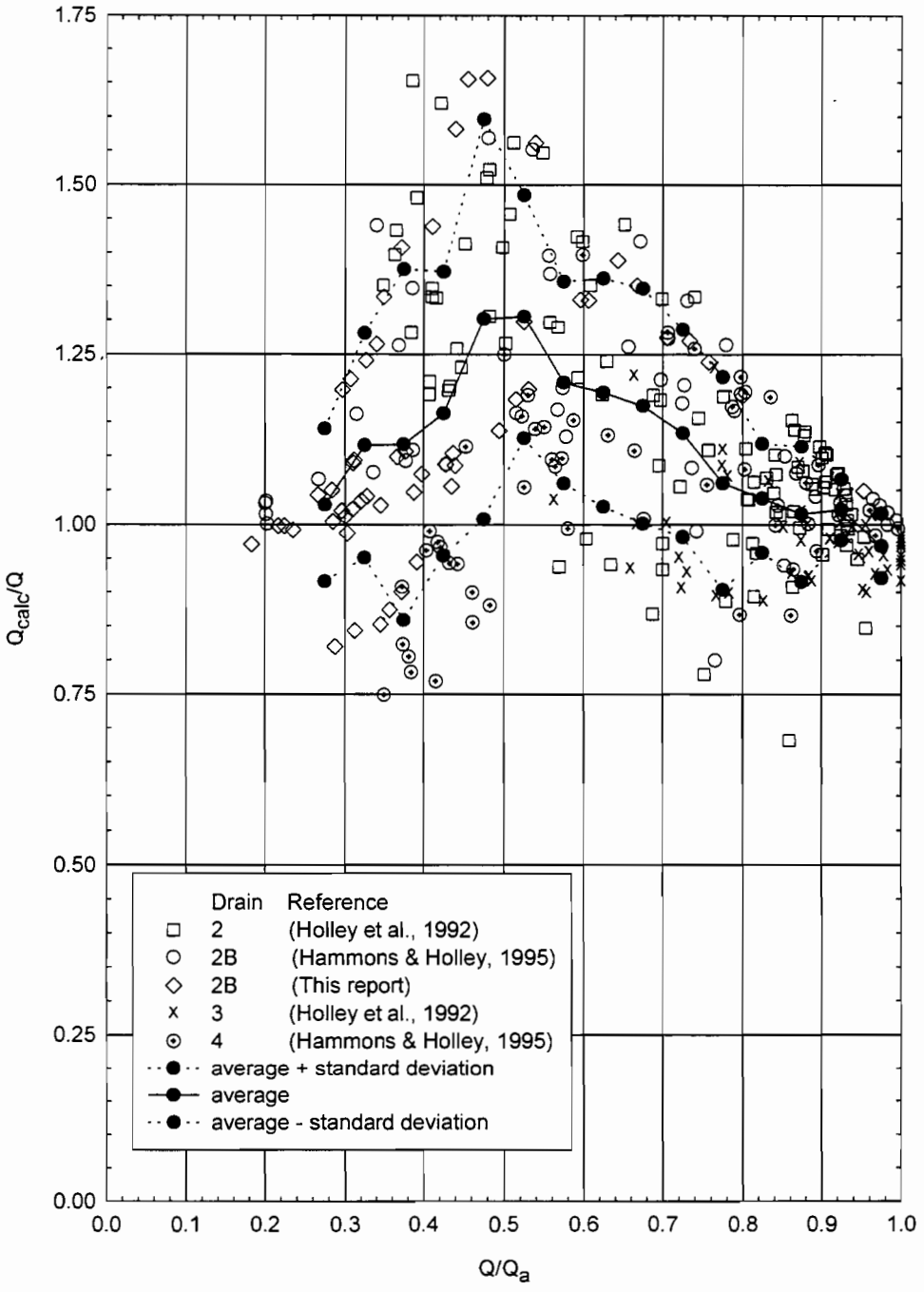

Figure 4.25 Ratios of Calculated and Measured Captured Flows (b) Plotted versus Captured Efficiency

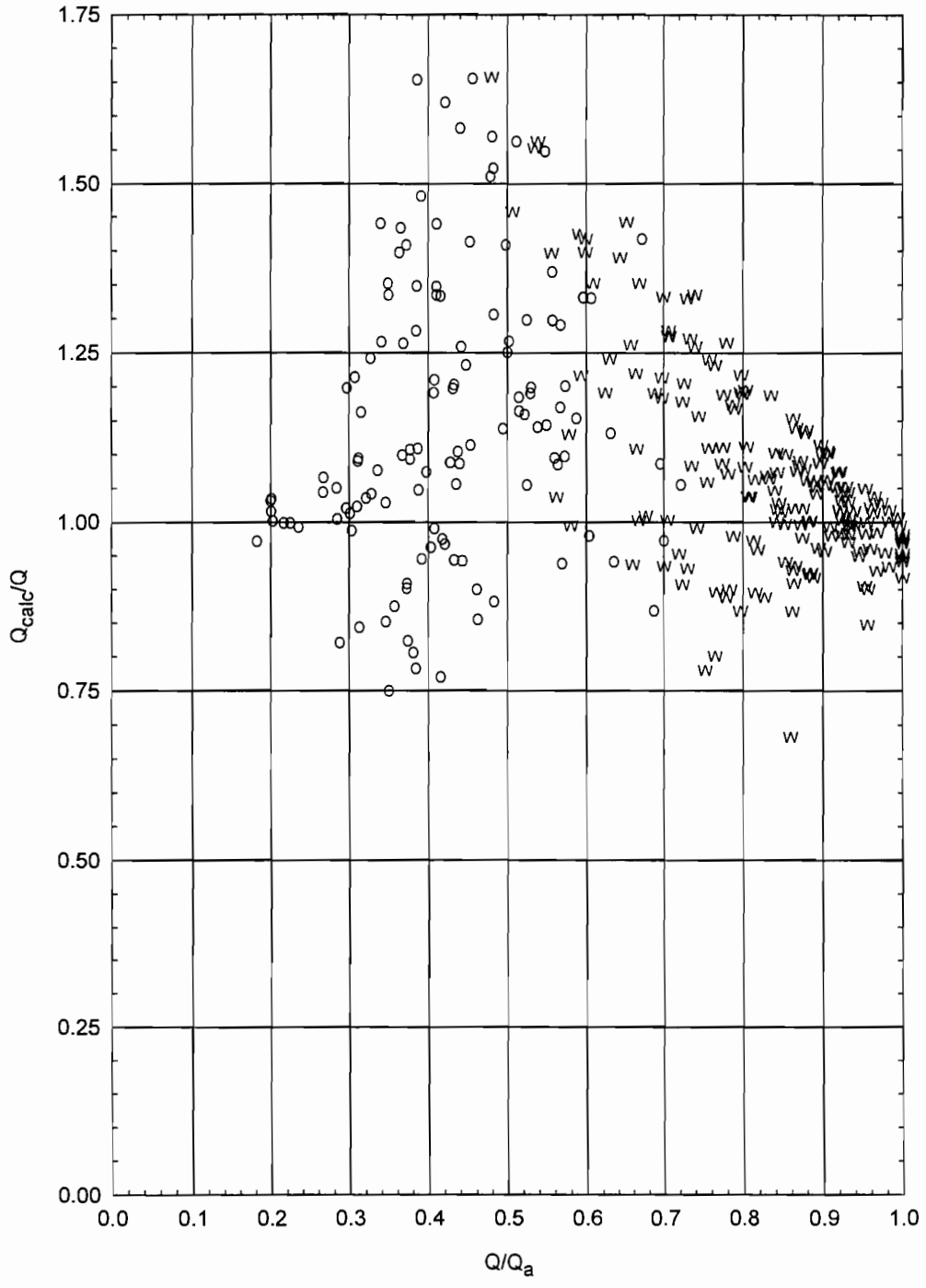

Figure 4.25 Ratios of Calculated and Measured Captured Flows (c) Plotted to Show Weir and Orifice Calculation Control

4.7 DESIGN RECOMMENDATIONS

A number of design recommendations can be drawn from the results discussed in this chapter. It is understood that these recommendations are not always feasible, but consideration should be given to these recommendations when they are within the design limitations.

- For almost all cases, attaching downspout piping directly to the drain pan outlet increased the capacity of the drain. (Only piping Configuration L, for which only three tests were performed for orifice control, showed that connecting piping to the drain caused a decrease in the captured flow rate compared to the captured flow rate for the drain with no piping. This statement assumes that the swirl meter was affecting the flow so that the results for Configurations L* and M* in Figure 4.11 can be discounted.) Also, drains with vertical piping connected directly to the bottom of the drain had larger captured flow rates than configurations with an elbow directly under the drain. Thus, it is straight vertical pipe with the vertical pipe as long as possible and connected directly to the drain pan orifice that increases the capacity of a drain. Since a vent is a necessary safety feature, it should be located below the first run of vertical pipe and above the first elbow when feasible.
- While under weir control, the drain showed a trend of a decreasing weir discharge coefficient going from the deeper to shallower portion of the drain. The drain pan should be made as deep as possible in order to keep the drain under weir control for higher gutter flows and to keep the weir length for the unsubmerged flow as large as possible, thus, increasing the drain capacity.
- Although not directly tested, increasing the pipe and drain orifice size would certainly increase the drain capacity by delaying the transition to orifice control. Even when under orifice control, the drain capacity would be increased due to the larger orifice area and the increased pipe capacity.
- Physical model studies should be conducted for determining the capacity of drains rather than relying on calculations from HEC-12 and orifice control. Comparison of measured flows and calculations taking the minimum of the flow calculated from HEC-12 and from orifice control showed that the calculations general overestimate the flow and that the error can be as much as 65%. On the other hand, calibration equations from physical model studies general has errors of 5% or less. The error in the calculations was 20% or less when the captured flow was at least 80% of the approach gutter flow.

CHAPTER 5. SUMMARY AND CONCLUSIONS

5.1 SUMMARY OF WORK

Full-scale hydraulic modeling of Drain 2B with various downspout piping configurations was performed in order to determine the effects of the piping configuration on the drain capacity. The objectives were as follows.

- Study the hydraulic flow behavior in Drain 2B and the downspout piping.
- Determine the relationship between the drain capacity and the downspout piping length.
- Determine the relationship between the drain capacity and the location of the first piping elbow.
- Present design recommendations based on the results.

The modeling of Drain 2B was performed on two separate models, the large model and the small model. The large model proved useful in obtaining detailed information about the drain behavior for various piping configurations. Through modeling of Drain 2B using the large model, all of the above objectives were achieved. The small model was constructed with the objective of studying vertical piping lengths up to 4.6 m. The inflow into the small model proved to be too small to provide useful information on the drain behavior.

A swirl meter was installed in the drain pan orifice for some of the piping configurations which were studied. The purpose of the swirl meter was to study the possible effects of vortex formation on the drain capacity.

The results from all experiments on Drains 2, 2B, 3, and 4 (Holley et al., 1992; Hammons and Holley, 1995) were analyzed to evaluate the practice of taking the design flow for a drain as the smaller of the flows for weir conditions using HEC-12 (Johnson and Chang, 1984) and flow calculated from the capacity of the orifice at the outlet from the drain pan.

5.2 RESULTS AND CONCLUSIONS

The drain piping was found to increase the drain capacity for the larger gutter flows due to the increase in the head across the drain orifice. The drain capacity was determined by one of two control regimes, weir control or orifice control, where "orifice" refers to the entrance into the

piping at the bottom of the drain pan. The drain piping determined which control regime occurred for a given approach flow rate. As long as the piping had the capacity to keep the drain pan from completely filling, the drain was under weir control. This control was characterized by a weir discharge coefficient which varied across the length of the grate. This weir discharge coefficient decreased toward the shallow portion of the drain pan due to submergence of the drain grate. When the drain became completely full, orifice control determined the drain capacity.

The drain capacity increased as the distance from the drain pan to the first piping elbow increased. This behavior occurred because the distance to the first elbow determined the total piezometric head from the piping system. Vertical piping which was located after a second elbow in the piping system did not flow full, so it did not add to the total piezometric head.

Results with a swirl meter installed at the beginning of the drain piping showed that the piping configuration affected the hydraulics of the flow in the drain pan, even under weir control. There are conflicting interpretations of whether the swirl meter had a significant influence on the drain capacity.

All of the above results were determined from tests using the large model. Tests using the small model proved inconclusive because of the problems encountered in using the small model. The model was too small for uniform flow to occur upstream of the drain. The elevation of the small model and the size of the piping leading to the headbox of the small model limited the maximum approach flow rate to less than that which was needed in order to effectively study the drain and piping systems.

Comparisons of calculations for weir control with the experimental results for Drain 2, 2B, 3 and 4 showed that the calculated weir (HEC-12) flow was within about 20% of the measured captured flow rates as long as the ratio of the captured flow to the approach gutter flow (Q/Q_a) was greater than about 0.8. However, for smaller values of Q/Q_a, the calculated weir flows were as much as 2.2 times larger than the measured captured flow for conditions which were known to be operating in the weir regime.

There were only 27 tests which could definitely be identified as being under orifice control, and all 27 cases were for Drains 2 and 2B. These tests were used to calculate orifice

coefficients (C_o) which were found to differ between Drain 2 and Drain 2B and to increase with increasing Q/Q_a for both drains. The values of C_o varied by almost a factor of two for Drain 2B. Nevertheless, no hydraulic explanation could be found for the variation. Thus, an average C_o of 0.57 was used for subsequent calculations.

For each test condition, HEC-12 and $C_o = 0.57$ were used to calculate the flow through the drain for weir control (Q_{HEC-12}) and orifice control (Q_{orif}). The calculated flow (Q_{calc}) was then taken as the minimum of Q_{HEC-12} and Q_{orif}. The controlling flow was essentially always weir flow for $Q/Q_a > 0.7$ while it was essentially always orifice flow for $Q/Q_a < 0.6$. The errors in this calculation approach are predominately an overestimation of the flow which was captured by a drain. For each drain, the values of Q_{calc}/Q tend to increase as Q/Q_a decreases from unity in the region where weir control gives the minimum calculated Q. As Q/Q_a continues to decrease, orifice conditions eventually become the control, and the values of Q_{calc}/Q then start to decrease with decreasing Q/Q_a. For $0.25 < Q/Q_a < 0.95$, average values of Q_{calc}/Q for intervals of 0.05 in Q/Q_a are all greater than unity. For these tests, some of the errors were as large as a 65% overestimation of the captured flow. The maximum error was no larger than 65% only because Q_{orif} was less than Q_{HEC-12} for some flows which were actually operating under weir control rather than orifice control.

These errors in Q_{calc}/Q can be compared with the accuracy of empirical calibration equations in Holley et al. (1992), Hammons and Holley (1995), and this report. Generally, the error or uncertainty in the empirical equations is on the order of 5% or less. Comparison of this value with possible errors of 65% in Q_{calc} demonstrates both the need for experimental evaluation of drains before they are installed and the benefits of such tests.

REFERENCES

Bennie, A. M. "Experiments on the Swirling Flow of Water in a Vertical Pipe and Bend." Proceedings of the Royal Society of London. Dec 1962.

Bos, M. G. Discharge Measurement Structures. Delft Hydraulics Laboratory, Publication No. 161. Delft, The Netherlands, 1989.

Daugherty, Robert L., Joseph B. Franzini and E. John Finnemore. Fluid Mechanics with Engineering Applications. New York: McGraw-Hill, 1985.

Eslon Thermoplastics. Products Catalog. Charlotte, NC, 1993.

Gordon, J. L. "Vortices at Intakes." Water Power. April 1970.

Grant, Douglas M. ISCO Open Channel Flow Measurement Handbook. Lincoln, Nebraska: 1992.

Gupta, Ram S. Hydrology and Hydraulic Systems. Englewood Cliffs, NJ: Prentice-Hall, 1989.

Hammons, M.A. and E.R. Holley, Hydraulic Characteristics of Flush Depressed Curb Inlets and Bridge Deck Drains. Project 0-1409, Center for Transportation Research, The University of Texas at Austin, 1995, 172 pp..

Henderson, F. M. Open Channel Flow. New York: MacMillan, 1966.

Holley, E. R., Carl Woodward, Aldo Brigneti, and Clemens Ott. Hydraulic Characteristics of Recessed Curb Inlets and Bridge Deck Drains. FHWA/TX-93+1267-1F, Center for Transportation Research, 1992.

Izzard, C. F. "Hydraulics of Runoff from Developed Surfaces," *Proceedings, 26th Annual Meeting,* Highway Research Board, 1946, pp. 129-150.

Jain, Akalank K., Kittur G. Ranga Raju and Ramachandra J. Garde. "Vortex Formation at Vertical Pipe Intakes." Journal of the Hydraulics Division. Oct 1978.

Johnson, F. L., and F. F. M. Chang. "Drainage of Highway Pavements." Hydraulic Engineering Circular No. 12. FHWA-TS-84-202, Federal Highway Administartion, 1984.

Kindsvater, C. E. and R. W. C. Carter. "Discharge Characteristics of Rectangular Thin-Plate Weirs." Journal of the Hydraulics Division. 1957.

Kitoh, Osami. "Swirling Flow Through a Bend." Journal of Fluid Mechanics. Feb 1987.

Knauss, Jost, ed. "Swirling Flow Problems at Intakes." Hydraulic Structures Design Manual, No 1. International Association for Hydraulic Research. Roterdam: Balkema, 1987.

Lugt, Hans J. Vortex Flow in Nature and Technology. New York: John Wiley & Sons, 1983.

Posey, C. J. and Hsieh-ching Hsu. "How the Vortex Affects Orifice Discharge." Engineering News Record. March 9, 1950.

Roberson, J. A. and C. T. Crowe. Engineering Fluid Mechanics. Boston: Houghton Mifflin, 1988.

Shimizu, Y. Flow and Loss of Multiple Bends. Dissertation, Nagoya University, 1975.

Street, R. L. et al. (1996) Elementary Fluid Mechanics, Wiley, New York, pp. 659-663.

Streeter, Victor L. and E. Benjamin Wylie. Fluid Mechanics. New York: McGraw-Hill, 1985.

APPENDIX A. LIST OF SYMBOLS

Symbol	Definition (Dimensions)
A_1	Area of venturi entrance (L^2)
A_2	Area of venturi throat (L^2)
A_o	Area of orifice (L^2)
B	V-notch weir approach channel width (L)
C_d	Venturi discharge coefficient
C_e	Effective weir discharge coefficient
C_{od} or C_o	Orifice discharge coefficient
C_{ov}	Velocity head correction coefficient for orifice
C_{wd}	Weir discharge coefficient
C_{wv}	Velocity head correction coefficient for weir
g	Acceleration due to gravity (L/T^2)
h_1	V-notch weir head (L)
h_e	Effective V-notch weir head (L)
h_{EB}	Elbow head loss (L)
h_L	Head loss (L)
h_o	Orifice head (L)
H_o	Total orifice head (L)
h_P	Straight pipe head loss (L)
h_w	Weir head (L)
H_w	Total weir head (L)
K_{EB}	Elbow loss coefficient
K_d	Channel and drain loss coefficient
L	Length of a grate in the flow direction (L)
L_e	Effective weir length (L)
L_t	Total grate length (L)

APPENDIX A. LIST OF SYMBOLS (continued)

Symbol	Definition (Dimensions)
L_v	Vertical distance from top of grate to lower point of atmospheric pressure (L)
N	Number of elbows in part of drain piping flowing full
n	Manning's roughness coefficient
P	V-notch weir crest height (L)
Q	Captured flow rate for any drain (L^3/T)
Q_2	Captured flow rate for Drain 2 (L^3/T)
Q_{2B}	Captured flow rate for Drain 2B (L^3/T)
Q_{HEC-12}	Captured flow rate from HEC-12 (L^3/T)
Q_{orif}	Captured flow rate from orifice control (L^3/T)
Q_a	Approach flow rate (L^3/T)
Q_{calc}	Minimum of Q_{HEC-12} and Q_{orif} (L^3/T)
Q_s	Side flow rate (L^3/T) = $Q_a - Q_w$
Q_w	Frontal flow rate for a grate (L^3/T)
Re	Reynolds number
R_f	Fraction of Q_w captured by a drain
R_s	Fraction of Q_s captured by a drain
S	Longitudinal slope (L/L)
S_x	Transverse slope (L/L)
T	Ponded width of approach flow (L)
V	Average velocity for approach flow (L/T)
V_o	Splashover velocity for a grate (L/T)
v_a or V_{pipe}	Axial flow velocity in drain pipe(L/T) = Q/A_o
v_t	Tangential flow velocity (L/T)
W	Width of a grate normal to the flow direction (L)

APPENDIX A. LIST OF SYMBOLS (continued)

W_c	Width from curb line to center of drain pan outlet (L)
y_c	Depth of water on roadway surface above centerline of orifice (L)
y_m	Measured depth at curb (L)
y_n	Normal depth at curb (L)
z_1	Elevation of approach flow surface at normal depth (L)
z_2	Elevation of pipe discharge (L)
α	Swirl angle
β, δ	Flow patterns in drain pan
θ	Weir notch angle
γ	Specific weight (F/L^3)
ν	Kinematic viscosity (FT/L^2)
Δh	Piezometric head across venturi (L)

APPENDIX B. EXPERIMENTAL DATA

The following tables provide all experimental data for tests run on Drain 2B in the analysis of the effects of the downspout piping on the drain capacity. Table B.1 contains the data for tests performed using the large model. All tests performed on the large model were at a longitudinal slope of 0.004 and a transverse slope of 0.0417. Table B.2 contains the data for the tests performed using the small model. No tests on the small model included the use of the swirl meter. Also, the approach flow rate was never directly measured for tests on the small model.

The definitions of the variables from left to right in Table B.1 are as follows. Config - piping configuration studied; Swirl Angle - swirl angle for swirl meter 1; Q_a - approach flow rate; Q_{2B} - captured flow rate; Q_{co} - carryover flow rate; y_m - measured depth in approach gutter; y_n - calculated normal depth in approach gutter; T - ponded width of approach flow. Blank values indicate unrecorded data. In Table B.2, the variables are defined as follows. S - longitudinal slope; S_x - transverse slope. Additional symbols in Tables B.3 - B.7 are C_o - orifice discharge coefficient; ; L - length of a grate in the flow direction (L); L_v - vertical distance from top of grate to lower point of atmospheric pressure (L); N - number of elbows in part of drain piping flowing full; Q - captured flow rate for any drain (L^3/T); Q_{HEC-12} - captured flow rate from HEC-12 (L^3/T); Q_{orif} - captured flow rate from orifice control (L^3/T); Q_{calc} - minimum of Q_{HEC-12} and Q_{orif} (L^3/T); Q_s - side flow rate (L^3/T) = Q_a - Q_w; Q_w - frontal flow rate for a grate (L^3/T); R_f - fraction of Q_w captured by a drain; R_s - fraction of Q_s captured by a drain; V_o - splashover velocity for a grate (L/T); W - width of a grate normal to the flow direction (L); W_c - width from curb line to center of drain pan outlet (L); y_c - depth of water on roadway surface above centerline of orifice (L);

Table B.1 Data for Drain 2B, Large Model Tests

TEST	Config	Swirl Angle	Q_a (m^3/s)	Q_{2B} (m^3/s)	Q_{co} (m^3/s)	y_m (m)	y_n (m)	T (m)
1	H		0.0511	0.0245	0.0281	0.0887	0.0878	2.10
2	H		0.0380	0.0205	0.0168	0.0753	0.0785	1.86
3	H		0.0600	0.0264	0.0355	0.0914	0.0932	
4	H		0.0186	0.0141	0.0042	0.0564	0.0601	1.40
5	H		0.0269	0.0173	0.0088	0.0651	0.0690	1.65
6	H		0.0553	0.0252	0.0311	0.0902	0.0904	2.16
7	H		0.0800	0.0298	0.0492	0.1030	0.1038	
8	H		0.1132	0.0348	0.0742	0.1180	0.1182	2.74
9	H		0.1188	0.0353	0.0763	0.1198	0.1204	2.74
10	H		0.0708	0.0291	0.0414	0.0989	0.0991	2.32
11	H		0.0901	0.0315	0.0583	0.1087	0.1085	2.50
12	H		0.1040	0.0340	0.0681	0.1151	0.1145	2.68
13	H		0.0978	0.0333	0.0625	0.1120	0.1119	2.59
14	I		0.0423	0.0218	0.0214	0.0814	0.0817	0.88
15	I		0.0250	0.0167	0.0077	0.0632	0.0671	1.54
16	I		0.0743	0.0257	0.0497	0.1015	0.1009	1.52
17	I		0.0874	0.0263	0.0629	0.1088	0.1073	0.94
18	I		0.0839	0.0260	0.0576	0.1065	0.1057	0.61
19	I		0.0881	0.0261	0.0609	0.1084	0.1076	0.79
20	I		0.0933	0.0266	0.0662	0.1108	0.1100	0.82
21	I		0.0561	0.0240	0.0329	0.0917	0.0909	0.73
22	I		0.1143	0.0329	0.0776	0.1187	0.1186	1.19
23	I		0.0905	0.0313	0.0587	0.1088	0.1087	1.28
24	I		0.0851	0.0304	0.0543	0.1068	0.1062	0.70
25	I		0.0789	0.0294	0.0501	0.1032	0.1033	0.98
26	I		0.0712	0.0279	0.0445	0.0997	0.0994	1.16
27	I		0.1017	0.0318	0.0669	0.1134	0.1136	0.88
28	I		0.0613	0.0244	0.0381	0.0940	0.0939	1.37
29	J		0.0255	0.0180	0.0085	0.0646	0.0677	1.58
30	J		0.0165	0.0132	0.0031	0.0543	0.0576	1.31
31	J		0.0064	0.0061	0.0005	0.0375	0.0402	0.94
32	J		0.0628	0.0237	0.0393	0.0908	0.0948	
33	J		0.0405	0.0215	0.0202	0.0788	0.0804	1.89
34	J		0.0797	0.0256	0.0539	0.1030	0.1037	2.50
35	J		0.1205	0.0271	0.0873	0.1207	0.1210	2.87
36	K		0.0639	0.0248	0.0406	0.0948	0.0954	2.29
37	K		0.0310	0.0188	0.0123	0.0700	0.0727	1.71
38	K		0.0453	0.0224	0.0245	0.0832	0.0839	1.98
39	K		0.0561	0.0244	0.0333	0.0908	0.0909	2.13
40	K		0.0956	0.0255	0.0677	0.1111	0.1110	2.59
41	K		0.0887	0.0252	0.0622	0.1079	0.1079	2.53
42	K		0.0768	0.0252	0.0517	0.1010	0.1022	
43	K		0.0199	0.0146	0.0052	0.0585	0.0616	1.46
44	K		0.1251	0.0271	0.0925	0.1218	0.1227	2.87
45	L		0.0377	0.0198	0.0192	0.0753	0.0783	1.89
46	L		0.0651	0.0239	0.0424	0.0963	0.0961	2.29
47	L		0.0776	0.0242	0.0534	0.1027	0.1026	2.44
48	L		0.0781	0.0243	0.0537	0.1027	0.1029	2.41

Table B.1 Data for Drain 2B, Large Model Tests (continued)

TEST	Config	Swirl Angle	Q_a (m^3/s)	Q_{2B} (m^3/s)	Q_{co} (m^3/s)	y_m (m)	y_n (m)	T (m)
49	L*	0.584	0.0737	0.0239	0.0504	0.0992	0.1007	2.38
50	L*	0.547	0.0568	0.0235	0.0353	0.0905	0.0913	2.19
51	L*	0.245	0.0423	0.0211	0.0229	0.0803	0.0817	
52	L*	0.042	0.0369	0.0201	0.0181	0.0753	0.0777	1.86
53	L*	0.398	0.0501	0.0225	0.0294	0.0861	0.0871	2.07
54	L*	0.659	0.0864	0.0239	0.0612	0.1058	0.1068	2.53
55	L*	0.680	0.1180	0.0247	0.0882	0.1187	0.1201	2.83
56	L*	0.673	0.1532	0.0251	0.1282	0.1355	0.1324	3.20
57	L*	0.435	0.0779	0.0236	0.0537	0.1021	0.1028	2.41
58	M		0.0322	0.0192	0.0130	0.0725	0.0738	1.74
59	M		0.0891	0.0270	0.0622	0.1096	0.1081	2.56
60	M		0.0546	0.0240	0.0329	0.0898	0.0899	2.16
61	M		0.1155	0.0272	0.0835	0.1195	0.1191	2.83
62	M		0.0540	0.0236	0.0319	0.0887	0.0896	2.13
63	M		0.1541	0.0282	0.1259	0.1369	0.1327	3.20
64	M*	-0.013	0.0311	0.0187	0.0127	0.0735	0.0728	1.71
65	M*	0.379	0.0497	0.0226	0.0292	0.0885	0.0868	2.07
66	M*	0.576	0.0616	0.0239	0.0392	0.0959	0.0941	2.26
67	M*	0.585	0.0715	0.0243	0.0483	0.1018	0.0995	2.38
68	M*	0.660	0.0947	0.0244	0.0687	0.1117	0.1106	2.62
69	M*	0.666	0.1217	0.0251	0.0913	0.1224	0.1215	2.80
70	M*	0.668	0.1217	0.0251	0.0941	0.1236	0.1215	2.90
71	M*	0.670	0.1482	0.0252	0.1230	0.1343	0.1308	3.20
72	M*	0.622	0.0890	0.0240	0.0620	0.1071	0.1080	2.53
73	M*	0.038	0.0338	0.0189	0.0165	0.0760	0.0752	1.77
74	N*	0.117	0.0679	0.0281	0.0402	0.0975	0.0976	2.29
75	N*	-0.087	0.0472	0.0235	0.0254	0.0846	0.0852	2.01
76	N*	0.255	0.0883	0.0318	0.0556	0.1073	0.1077	2.53
77	N*	0.394	0.1209	0.0364	0.0793	0.1204	0.1212	2.83
78	N*	0.636	0.1403	0.0426	0.0978	0.1399	0.1281	3.20
79	N*	0.494	0.1347	0.0386	0.0961	0.1283	0.1262	3.17
80	O*	0.545	0.0796	0.0268	0.0524	0.1029	0.1036	2.38
81	O*	0.443	0.0641	0.0261	0.0393	0.0954	0.0955	2.23
82	O*	-0.117	0.0397	0.0214	0.0200	0.0786	0.0798	1.89
83	O*	0.593	0.0871	0.0275	0.0583	0.1068	0.1071	2.53
84	O*	0.650	0.1214	0.0288	0.0869	0.1195	0.1214	2.80
85	O*	0.588	0.0939	0.0277	0.0637	0.1094	0.1102	2.59
86	O*	0.550	0.0814	0.0270	0.0526	0.1027	0.1045	2.41
87	P*	-0.165	0.0452	0.0226	0.0241	0.0823	0.0838	1.98
88	P*	0.000	0.0611	0.0261	0.0356	0.0925	0.0938	2.26
89	P*	0.186	0.0844	0.0306	0.0531	0.1050	0.1059	2.53
90	P*	0.300	0.0749	0.0295	0.0450	0.0991	0.1013	2.41
91	P*	0.432	0.1192	0.0351	0.0774	0.1189	0.1205	2.83
92	P*	0.332	0.1122	0.0348	0.0719	0.1271	0.1178	2.74
93	P*	0.426	0.1516	0.0422	0.1094	0.1353	0.1319	3.20
94	P*	0.424	0.1398	0.0399	0.1000	0.1288	0.1280	3.20

Table B.2 Data for Drain 2B, Small Model Tests

TEST	Config	S	S_x	Q_{2B} (m^3/s)	Q_{co} (m^3/s)	y_m (m)
1	K	0.004	0.0417	0.0170	0.0086	0.0652
2	K	0.004	0.0417	0.0218	0.0215	0.0735
3	K	0.004	0.0417	0.0228	0.0247	0.0751
4	K	0.004	0.0417	0.0152	0.0050	0.0552
5	K	0.004	0.0417	0.0251	0.0377	0.0840
6	K	0.004	0.0417	0.0256	0.0407	0.0852
7	K	0.004	0.0417	0.0254	0.0419	0.0861
8	K	0.004	0.0417	0.0264	0.0415	0.0832
9	K	0.004	0.0417	0.0242	0.0429	0.0860
10	K	0.004	0.0417	0.0229	0.0452	0.0835
11	K	0.02	0.0417	0.0218	0.0460	0.0796
12	K	0.02	0.0417	0.0206	0.0349	0.0744
13	K	0.02	0.0417	0.0182	0.0283	0.0639
14	K	0.02	0.0417	0.0202	0.0314	0.0747
15	K	0.02	0.0417	0.0188	0.0296	0.0661
16	R	0.02	0.0417	0.0206	0.0488	0.0770
17	R	0.02	0.0417	0.0185	0.0367	0.0721
18	R	0.02	0.0417	0.0169	0.0283	0.0663

Table B.3 Calculations for Weir and Orifice Control for Drain 2 (Holley et al., 1992)

Weir (HEC-12) Calculations
P-1-7/8-4 Grate
W = 0.927 m
L = 0.197 m
V_o = 0.67 m/s

Orifice Calculations
D_o = 0.152 m
W_c = 0.140 m

Configuration	L_v m	No. of Elbows
A	0.561	0
B	0.638	1
C	1.552	1
D	1.476	0
E	0.638	1
F	0.638	1
G	0.561	1

Test No.	S	S_x	y_n m	Q_a m³/s	Q m³/s	Q_w m³/s	R_f	R_s	Q_{HEC-12} m³/s	$(C_o)_{calc}$	Q_{orif} m³/s	min Q	Q_{calc}/Q	Con- fig.	Regime	Fig. 4-20
1	0.001	0.08	0.166	0.0653	0.0449	0.0519	1.000	0.116	0.0534	0.656	0.0390	O	0.868	A	O	
2	0.001	0.08	0.166	0.0651	0.0271	0.0517	1.000	0.117	0.0533		0.0361	O	1.333	B	T	
3	0.001	0.08	0.157	0.0562	0.0254	0.0460	1.000	0.124	0.0473		0.0359	O	1.413	B	T	
4	0.001	0.06	0.135	0.0505	0.0252	0.0382	1.000	0.112	0.0396		0.0354	O	1.408	B	T	
5	0.001	0.06	0.155	0.0728	0.0280	0.0505	1.000	0.097	0.0527		0.0359	O	1.282	B	T	
6	0.001	0.06	0.149	0.0652	0.0268	0.0465	1.000	0.101	0.0484		0.0358	O	1.335	B	T	
7	0.001	0.08	0.166	0.0652	0.0268	0.0518	1.000	0.117	0.0534		0.0361	O	1.347	B	T	
8	0.001	0.08	0.158	0.0570	0.0399	0.0465	1.000	0.123	0.0478		0.0388	O	0.972	A	T	
9	0.001	0.08	0.166	0.0653	0.0415	0.0519	1.000	0.116	0.0534	0.606	0.0390	O	0.941	A	O	
10	0.001	0.06	0.149	0.0653	0.0394	0.0466	1.000	0.101	0.0485		0.0386	O	0.979	A	W	D
11	0.001	0.06	0.136	0.0506	0.0352	0.0383	1.000	0.112	0.0397		0.0382	O	1.086	A	W	D
12	0.001	0.06	0.155	0.0726	0.0413	0.0504	1.000	0.097	0.0526		0.0388	O	0.938	A	W	D
13	0.001	0.06	0.136	0.0515	0.0324	0.0388	1.000	0.111	0.0402		0.0525	W	1.240	C	T	
14	0.001	0.06	0.150	0.0666	0.0338	0.0472	1.000	0.100	0.0492		0.0528	W	1.457	C	T	
15	0.001	0.06	0.156	0.0731	0.0350	0.0507	1.000	0.097	0.0529		0.0528	O	1.510	C	T	
16	0.001	0.08	0.156	0.0557	0.0330	0.0457	1.000	0.124	0.0470		0.0528	W	1.424	C	T	
17	0.001	0.08	0.167	0.0663	0.0339	0.0525	1.000	0.116	0.0541		0.0530	O	1.562	C	T	
18	0.001	0.06	0.135	0.0502	0.0362	0.0380	1.000	0.112	0.0394		0.0382	O	1.055	D	W	D
19	0.001	0.08	0.157	0.0566	0.0428	0.0463	1.000	0.123	0.0475		0.0587	W	1.109	D	W	E
20	0.001	0.08	0.166	0.0648	0.0446	0.0516	1.000	0.117	0.0531		0.0588	W	1.190	D	T	
21	0.001	0.06	0.149	0.0648	0.0404	0.0463	1.000	0.101	0.0482		0.0586	W	1.191	D	W	D
22	0.001	0.06	0.156	0.0739	0.0438	0.0511	1.000	0.096	0.0533		0.0587	W	1.216	D	W	D
23	0.001	0.06	0.134	0.0489	0.0273	0.0373	1.000	0.114	0.0386		0.0354	O	1.297	E	T	
24	0.001	0.08	0.158	0.0570	0.0275	0.0465	1.000	0.123	0.0478		0.0359	O	1.306	E	T	
25	0.001	0.08	0.166	0.0650	0.0287	0.0516	1.000	0.117	0.0532		0.0361	O	1.258	E	T	
26	0.001	0.06	0.149	0.0650	0.0290	0.0464	1.000	0.101	0.0482		0.0358	O	1.231	E	T	
27	0.001	0.06	0.155	0.0727	0.0297	0.0505	1.000	0.097	0.0526		0.0359	O	1.210	E	T	
28	0.001	0.06	0.133	0.0483	0.0274	0.0369	1.000	0.114	0.0382		0.0354	O	1.290	F	T	
29	0.001	0.08	0.157	0.0564	0.0283	0.0462	1.000	0.123	0.0474		0.0359	O	1.266	F	T	
30	0.001	0.08	0.170	0.0695	0.0301	0.0544	1.000	0.114	0.0562		0.0362	O	1.203	F	T	
31	0.001	0.06	0.153	0.0695	0.0300	0.0488	1.000	0.099	0.0508		0.0358	O	1.197	F	T	
32	0.001	0.06	0.156	0.0741	0.0302	0.0512	1.000	0.096	0.0534		0.0359	O	1.191	F	T	
33	0.001	0.06	0.130	0.0457	0.0220	0.0353	1.000	0.117	0.0366		0.0335	O	1.522	G	T	
34	0.001	0.08	0.160	0.0590	0.0231	0.0478	1.000	0.121	0.0492		0.0342	O	1.481	G	T	
35	0.001	0.08	0.166	0.0655	0.0239	0.0520	1.000	0.116	0.0536		0.0343	O	1.433	G	T	
36	0.001	0.06	0.150	0.0670	0.0243	0.0474	1.000	0.100	0.0494		0.0340	O	1.397	G	T	
37	0.001	0.06	0.155	0.0723	0.0252	0.0503	1.000	0.097	0.0524		0.0341	O	1.352	G	T	
38	0.001	0.06	0.093	0.0184	0.0172	0.0168	1.000	0.166	0.0171		0.0344	W	0.994	E	W	D

Table B.3 Calculations for Weir and Orifice Control for Drain 2 (Holley et al., 1992) - continued

Test	S	S_x	y_n	Q_a	Q	Q_w	R_f	R_s	Q_{HEC-12}	$(C_o)_{calc}$	Q_{orif}	min	Q_{calc}/Q	Con-	Regime	Fig.
No.			m	m^3/s	m^3/s	m^3/s			m^3/s		m^3/s	Q		fig.		4-20
39	0.001	0.06	0.102	0.0237	0.0224	0.0209	1.000	0.151	0.0213		0.0347	W	0.949	E	W	D
40	0.001	0.06	0.112	0.0304	0.0274	0.0255	1.000	0.137	0.0262		0.0349	W	0.956	E	W	D
41	0.001	0.08	0.088	0.0120	0.0103	0.0119	1.000	0.220	0.0119		0.0343	W	1.153	E	W	E
42	0.001	0.08	0.119	0.0269	0.0251	0.0249	1.000	0.164	0.0253		0.0350	W	1.006	E	W	E
43	0.001	0.06	0.092	0.0180	0.0168	0.0165	1.000	0.167	0.0167		0.0370	W	0.998	A	W	D
44	0.001	0.06	0.098	0.0215	0.0198	0.0192	1.000	0.157	0.0195		0.0372	W	0.984	A	W	D
45	0.001	0.06	0.111	0.0297	0.0242	0.0251	1.000	0.138	0.0257		0.0375	W	1.062	A	W	D
46	0.001	0.08	0.095	0.0147	0.0135	0.0145	1.000	0.205	0.0145		0.0370	W	1.073	A	W	E
47	0.001	0.08	0.118	0.0262	0.0232	0.0243	1.000	0.166	0.0246		0.0377	W	1.059	A	W	E
48	0.001	0.06	0.090	0.0170	0.0162	0.0157	1.000	0.171	0.0159		0.0325	W	0.982	G	W	D
49	0.001	0.06	0.100	0.0226	0.0205	0.0200	1.000	0.154	0.0204		0.0328	W	0.993	G	W	D
50	0.001	0.08	0.108	0.0205	0.0188	0.0196	1.000	0.182	0.0198		0.0329	W	1.051	G	W	E
51	0.001	0.08	0.089	0.0123	0.0108	0.0122	1.000	0.218	0.0122		0.0324	W	1.131	G	W	E
52	0.001	0.08	0.122	0.0287	0.0200	0.0263	1.000	0.160	0.0267		0.0332	W	1.332	G	T	
53	0.001	0.04	0.085	0.0222	0.0213	0.0174	1.000	0.128	0.0180		0.0325	W	0.847	G	T	
54	0.001	0.02	0.052	0.0118	0.0096	0.0082	1.000	0.117	0.0086		0.0317	W	0.894	G	W	B
55	0.005	0.01	0.034	0.0167	0.0144	0.0096	1.000	0.026	0.0098		0.0312	W	0.682	G	W	F
56	0.005	0.01	0.034	0.0167	0.0126	0.0096	1.000	0.026	0.0098		0.0312	W	0.779	G	W	F
57	0.005	0.02	0.043	0.0162	0.0140	0.0126	1.000	0.037	0.0127		0.0314	W	0.908	G	W	G
58	0.005	0.02	0.043	0.0162	0.0133	0.0126	1.000	0.037	0.0127		0.0314	W	0.958	G	W	G
59	0.005	0.04	0.064	0.0233	0.0217	0.0209	1.000	0.046	0.0210		0.0319	W	0.970	G	T	
60	0.005	0.04	0.067	0.0263	0.0218	0.0232	1.000	0.044	0.0233		0.0320	W	1.068	G	T	
61	0.005	0.06	0.068	0.0180	0.0166	0.0178	1.000	0.063	0.0178		0.0319	W	1.075	G	W	I
62	0.005	0.06	0.076	0.0245	0.0228	0.0238	1.000	0.056	0.0238		0.0322	W	1.043	G	W	I
63	0.005	0.06	0.086	0.0340	0.0222	0.0319	1.000	0.048	0.0320		0.0324	W	1.442	G	T	
64	0.005	0.08	0.067	0.0130	0.0117	0.0130	1.000	0.084	0.0130		0.0318	W	1.114	G	W	J
65	0.005	0.08	0.080	0.0211	0.0186	0.0211	1.000	0.069	0.0211		0.0322	W	1.136	G	W	J
66	0.01	0.01	0.029	0.0152	0.0107	0.0099	1.000	0.017	0.0100		0.0311	W	0.934	G	W	K
67	0.01	0.02	0.036	0.0140	0.0118	0.0120	1.000	0.025	0.0120		0.0313	W	1.014	G	W	L
68	0.01	0.02	0.042	0.0215	0.0175	0.0169	1.000	0.021	0.0170		0.0314	W	0.972	G	W	L
69	0.01	0.02	0.044	0.0242	0.0191	0.0186	1.000	0.020	0.0187		0.0315	W	0.978	G	W	L
70	0.01	0.04	0.049	0.0162	0.0150	0.0158	1.000	0.034	0.0158		0.0315	W	1.052	G	W	M
71	0.01	0.04	0.055	0.0215	0.0202	0.0205	1.000	0.030	0.0205		0.0317	W	1.015	G	W	M
72	0.01	0.06	0.058	0.0170	0.0154	0.0170	1.000	0.042	0.0170		0.0317	W	1.102	G	W	N
73	0.01	0.06	0.069	0.0266	0.0197	0.0262	1.000	0.034	0.0263		0.0320	W	1.335	G	W	N
74	0.01	0.08	0.062	0.0147	0.0132	0.0147	1.000	0.052	0.0147		0.0317	W	1.114	G	W	O
75	0.01	0.08	0.076	0.0261	0.0226	0.0261	0.987	0.040	0.0257		0.0321	W	1.139	G	W	O
76	0.02	0.01	0.026	0.0171	0.0133	0.0117	1.000	0.010	0.0118		0.0310	W	0.887	G	W	P
77	0.02	0.02	0.034	0.0168	0.0146	0.0148	1.000	0.015	0.0148		0.0312	W	1.019	G	W	Q
78	0.02	0.02	0.038	0.0225	0.0182	0.0188	1.000	0.013	0.0188		0.0313	W	1.036	G	W	Q
79	0.02	0.04	0.038	0.0113	0.0103	0.0113	1.000	0.026	0.0113		0.0312	W	1.105	G	W	R
80	0.02	0.04	0.048	0.0218	0.0203	0.0214	0.978	0.019	0.0209		0.0315	W	1.029	G	W	R
81	0.02	0.04	0.059	0.0375	0.0205	0.0347	0.946	0.015	0.0329		0.0318	O	1.547	G	T	
82	0.02	0.06	0.045	0.0117	0.0106	0.0117	0.990	0.031	0.0116		0.0313	W	1.098	G	W	S
83	0.02	0.06	0.054	0.0195	0.0177	0.0195	0.961	0.025	0.0187		0.0316	W	1.062	G	W	S
84	0.02	0.08	0.060	0.0195	0.0170	0.0195	0.944	0.029	0.0184		0.0317	W	1.084	G	W	T
85	0.02	0.08	0.068	0.0272	0.0211	0.0272	0.922	0.025	0.0251		0.0319	W	1.188	G	W	T
86	0.04	0.02	0.026	0.0123	0.0111	0.0118	0.990	0.011	0.0117		0.0310	W	1.054	G	T	
87	0.04	0.02	0.032	0.0203	0.0177	0.0183	0.962	0.009	0.0177		0.0311	W	0.995	G	T	

Table B.3 Calculations for Weir and Orifice Control for Drain 2 (Holley et al., 1992) - continued

Test No.	S	S_x	y_n m	Q_a m³/s	Q m³/s	Q_w m³/s	R_f	R_s	Q_{HEC-12} $(C_o)_{calc}$ m³/s	Q_{orif} m³/s	min Q	Q_{calc}/Q	Con- fig.	Regime	Fig. 4-20
88	0.04	0.02	0.043	0.0461	0.0194	0.0357	0.909	0.006	0.0325	0.0315	O	1.620	G	T	
89	0.04	0.04	0.037	0.0148	0.0132	0.0148	0.939	0.014	0.0139	0.0312	W	1.052	G	W	W
90	0.04	0.04	0.045	0.0252	0.0203	0.0250	0.902	0.011	0.0225	0.0314	W	1.111	G	W	W
91	0.04	0.06	0.058	0.0327	0.0196	0.0327	0.849	0.013	0.0278	0.0317	W	1.417	G	T	
92	0.04	0.06	0.050	0.0228	0.0192	0.0228	0.879	0.015	0.0201	0.0315	W	1.046	G	T	
93	0.04	0.08	0.039	0.0089	0.0075	0.0089	0.927	0.026	0.0083	0.0311	W	1.102	G	W	Y
94	0.06	0.02	0.024	0.0113	0.0099	0.0111	0.961	0.008	0.0107	0.0309	W	1.078	G	W	a
95	0.06	0.04	0.040	0.0229	0.0171	0.0229	0.862	0.009	0.0197	0.0313	W	1.156	G	W	b
96	0.06	0.04	0.046	0.0322	0.0196	0.0319	0.832	0.008	0.0265	0.0314	W	1.352	G	W	b
97	0.06	0.06	0.033	0.0088	0.0075	0.0088	0.905	0.017	0.0080	0.0310	W	1.073	G	W	c
98	0.06	0.06	0.045	0.0205	0.0165	0.0205	0.836	0.012	0.0171	0.0313	W	1.037	G	W	c
99	0.08	0.04	0.033	0.0155	0.0131	0.0155	0.858	0.009	0.0133	0.0311	W	1.018	G	W	g
100	0.08	0.04	0.038	0.0226	0.0157	0.0226	0.825	0.007	0.0186	0.0312	W	1.183	G	W	g
101	0.08	0.04	0.051	0.0495	0.0191	0.0480	0.744	0.005	0.0357	0.0316	O	1.653	G	T	

Table B.4 Calculations for Weir and Orifice Control for Drain 2B (Hammons and Holley, 1996)

Weir (HEC-12) Calculations
P-1-7/8-4 Grate
W = 0.927 m
L = 0.197 m
V_o = 0.67 m/s

Orifice Calculations
D_o = 0.152 m
W_c = 0.832 m
L_v = 0.257 m
No. of Elbows = 0

Test No.	S	S_x	y_n m	Q_a m³/s	Q m³/s	Q_w m³/s	R_f	R_s	Q_{HEC-12} m³/s	$(C_o)_{calc}$	Q_{orif} m³/s	min Q	Q_{calc}/Q	Regime	Fig. 4-20
2B01	0.004	0.0208	0.043	0.0156	0.0133	0.0124	1.000	0.039	0.0125		0.0245	W	0.940	W	G
2B02	0.004	0.0208	0.033	0.0072	0.0073	0.0066	1.000	0.055	0.0066		0.0240	W	0.912	W	G
2B03	0.004	0.0208	0.050	0.0231	0.0172	0.0168	1.000	0.033	0.0170		0.0248	W	0.990	T	
2B04	0.004	0.0208	0.060	0.0374	0.0216	0.0240	1.000	0.027	0.0244		0.0252	W	1.129	T	
2B05	0.01	0.0208	0.051	0.0374	0.0212	0.0271	1.000	0.014	0.0272	0.488	0.0248	O	1.169	O	
2B06	0.01	0.0208	0.043	0.0245	0.0181	0.0195	1.000	0.018	0.0195		0.0245	W	1.083	T	
2B07	0.01	0.0208	0.035	0.0141	0.0125	0.0124	1.000	0.022	0.0125		0.0241	W	1.001	W	L
2B08	0.02	0.0208	0.031	0.0140	0.0125	0.0130	1.000	0.014	0.0130		0.0239	W	1.041	W	Q
2B09	0.02	0.0208	0.044	0.0356	0.0204	0.0281	0.968	0.009	0.0273		0.0245	O	1.201	T	
2B10	0.02	0.0208	0.037	0.0232	0.0168	0.0199	0.992	0.011	0.0198		0.0242	W	1.178	T	
2B11	0.04	0.0208	0.033	0.0232	0.0162	0.0210	0.930	0.007	0.0196		0.0240	W	1.213	T	
2B12	0.04	0.0208	0.027	0.0136	0.0118	0.0132	0.965	0.009	0.0127		0.0238	W	1.075	W	V
2B13	0.04	0.0208	0.019	0.0055	0.0054	0.0055	1.000	0.013	0.0055		0.0234	W	1.017	W	V
2B14	0.06	0.0208	0.018	0.0055	0.0054	0.0055	0.983	0.010	0.0054		0.0234	W	1.000	W	a
2B15	0.06	0.0208	0.034	0.0306	0.0170	0.0275	0.864	0.005	0.0237		0.0241	W	1.396	T	
2B16	0.06	0.0208	0.030	0.0231	0.0152	0.0216	0.886	0.005	0.0192		0.0239	W	1.261	T	
2B17	0.06	0.0417	0.039	0.0231	0.0124	0.0231	0.831	0.008	0.0192		0.0236	W	1.552	T	
2B18	0.06	0.0417	0.023	0.0059	0.0054	0.0059	0.935	0.014	0.0055		0.0228	W	1.014	W	b
2B19	0.06	0.0417	0.032	0.0132	0.0096	0.0132	0.876	0.010	0.0115		0.0232	W	1.205	W	b
2B20	0.04	0.0417	0.034	0.0131	0.0103	0.0131	0.922	0.013	0.0121		0.0233	W	1.167	W	W
2B21	0.04	0.0417	0.031	0.0100	0.0085	0.0100	0.939	0.015	0.0094		0.0232	W	1.100	W	W
2B22	0.04	0.0417	0.048	0.0317	0.0152	0.0314	0.853	0.009	0.0268		0.0239	O	1.569	T	
2B23	0.02	0.0417	0.054	0.0317	0.0177	0.0306	0.933	0.014	0.0286		0.0242	O	1.369	T	
2B24	0.02	0.0417	0.029	0.0059	0.0059	0.0059	1.000	0.030	0.0059		0.0231	W	1.006	W	R
2B25	0.02	0.0417	0.043	0.0169	0.0124	0.0169	0.973	0.019	0.0164		0.0237	W	1.329	W	R
2B26	0.01	0.0417	0.049	0.0169	0.0132	0.0167	1.000	0.030	0.0167		0.0240	W	1.264	W	M
2B27	0.01	0.0417	0.037	0.0078	0.0076	0.0078	1.000	0.042	0.0078		0.0234	W	1.028	W	M
2B28	0.01	0.0417	0.057	0.0256	0.0172	0.0243	1.000	0.025	0.0244		0.0243	O	1.417	T	
2B29	0.004	0.0417	0.068	0.0255	0.0181	0.0229	1.000	0.045	0.0230		0.0248	W	1.273	W	H
2B30	0.004	0.0417	0.058	0.0166	0.0132	0.0157	1.000	0.055	0.0157		0.0244	W	1.192	W	H
2B31	0.004	0.0417	0.040	0.0064	0.0061	0.0064	1.000	0.082	0.0064		0.0236	W	1.037	W	H
2B32	0.005	0.0208	0.060	0.0420	0.0217	0.0271	1.000	0.022	0.0274		0.0252	O	1.164	T	
2B33	0.005	0.0208	0.068	0.0304	0.0232	0.0179	1.000	0.059	0.0186		0.0256	W	0.800	T	
2B34	0.01	0.0208	0.060	0.0588	0.0227	0.0379	0.998	0.012	0.0381	0.514	0.0252	O	1.109	O	
2B35	0.02	0.0208	0.062	0.0887	0.0237	0.0563	0.910	0.006	0.0514	0.535	0.0253	O	1.066	O	
2B36	0.04	0.0208	0.049	0.0676	0.0213	0.0500	0.848	0.004	0.0425		0.0247	O	1.162	T	
2B37	0.06	0.0208	0.041	0.0524	0.0193	0.0427	0.818	0.004	0.0350		0.0244	O	1.263	T	
2B38	0.06	0.0417	0.052	0.0492	0.0167	0.0479	0.752	0.006	0.0360		0.0241	O	1.440	T	
2B39	0.04	0.0417	0.055	0.0466	0.0180	0.0448	0.821	0.008	0.0368		0.0243	O	1.348	T	
2B40	0.02	0.0417	0.073	0.0691	0.0232	0.0600	0.875	0.010	0.0526		0.0250	O	1.076	T	
2B41	0.01	0.0417	0.075	0.0539	0.0231	0.0460	0.964	0.018	0.0445		0.0251	O	1.088	T	
2B42	0.004	0.0417	0.095	0.0628	0.0237	0.0473	1.000	0.031	0.0478		0.0259	O	1.093	T	
2B43	0.04	0.0417	0.079	0.1224	0.0245	0.1021	0.715	0.005	0.0731		0.0253	O	1.031	T	
2B44	0.06	0.0417	0.073	0.1235	0.0250	0.1067	0.635	0.004	0.0678		0.0250	O	1.001	T	

Table B.4 Calculations for Weir and Orifice Control for Drain 2B (Hammons and Holley, 1996) - continued

Test	S	S_x	y_n	Q_a	Q	Q_w	R_f	R_s	Q_{HEC-12}	$(C_o)_{calc}$	Q_{orif}	min	Q_{calc}/Q	Regime	Fig.
No.			m	m^3/s	m^3/s	m^3/s			m^3/s		m^3/s	Q			4-20
2B45	0.06	0.0208	0.056	0.1203	0.0242	0.0813	0.728	0.003	0.0593	0.551	0.0250	O	1.034	O	
2B46	0.04	0.0208	0.061	0.1238	0.0249	0.0790	0.788	0.003	0.0625	0.562	0.0252	O	1.015	O	

Table B.5 Calculations for Weir and Orifice Control for Drain 2B (Smith and Holley, 1996)

Weir (HEC-12) Calculations
P-1-7/8-4 Grate
W = 0.927 m
L = 0.197 m
V_o = 0.67 m/s

Orifice Calculations
D_o = 0.152 m
W_c = 0..832 m

Configuration	L_v m	No. of Elbows
H	1.003	1
I	0.359	1
J	0.359	1
K	0.257	0
L	0.359	1
M	0.359	1

Test No.	S	S_x	y_n m	Q_a m³/s	Q m³/s	Q_w m³/s	R_f	R_s	Q_{HEC-12} m³/s	$(C_o)_{calc}$	Q_{orif} m³/s	min Q	Q_{calc}/Q	Con- fig.	Regime	Fig. 4-20
1	0.004	0.0417	0.088	0.0511	0.0245	0.0402	1.000	0.034	0.0406		0.0417	W	1.657	H	W	H
2	0.004	0.0417	0.079	0.0380	0.0205	0.0318	1.000	0.038	0.0320		0.0415	W	1.562	H	W	H
3	0.004	0.0417	0.093	0.0600	0.0264	0.0456	1.000	0.031	0.0461		0.0418	O	1.582	H	W	H
4	0.004	0.0417	0.060	0.0186	0.0141	0.0174	1.000	0.052	0.0175		0.0411	W	1.239	H	W	H
5	0.004	0.0417	0.069	0.0269	0.0173	0.0239	1.000	0.044	0.0240		0.0413	W	1.389	H	W	H
6	0.004	0.0417	0.090	0.0553	0.0252	0.0428	1.000	0.032	0.0432		0.0417	O	1.655	H	W	H
7	0.004	0.0417	0.104	0.0800	0.0298	0.0569	1.000	0.028	0.0576		0.0420	O	1.408	H	W	H
8	0.004	0.0417	0.118	0.1132	0.0348	0.0739	0.999	0.024	0.0747		0.0423	O	1.214	H	W	H
9	0.004	0.0417	0.120	0.1188	0.0353	0.0765	0.996	0.023	0.0772		0.0423	O	1.198	H	W	H
10	0.004	0.0417	0.099	0.0708	0.0291	0.0519	1.000	0.029	0.0524		0.0419	O	1.439	H	W	H
11	0.004	0.0417	0.109	0.0901	0.0315	0.0623	1.000	0.026	0.0630		0.0421	O	1.335	H	W	H
12	0.004	0.0417	0.115	0.1040	0.0340	0.0694	1.000	0.025	0.0702		0.0422	O	1.241	H	W	H
13	0.004	0.0417	0.112	0.0978	0.0333	0.0662	1.000	0.025	0.0670		0.0421	O	1.265	H	W	H
14	0.004	0.0417	0.082	0.0423	0.0218	0.0346	1.000	0.036	0.0349		0.0258	O	1.184	I	W	H
15	0.004	0.0417	0.067	0.0250	0.0167	0.0225	1.000	0.046	0.0226		0.0253	W	1.352	I	W	H
16	0.004	0.0417	0.101	0.0743	0.0257	0.0538	1.000	0.028	0.0544	0.550	0.0264	O	1.028	I	O	
17	0.004	0.0417	0.107	0.0874	0.0263	0.0609	1.000	0.027	0.0616	0.561	0.0266	O	1.012	I	O	
18	0.004	0.0417	0.106	0.0839	0.0260	0.0590	1.000	0.027	0.0597	0.554	0.0266	O	1.022	I	O	
19	0.004	0.0417	0.108	0.0881	0.0261	0.0612	1.000	0.026	0.0620	0.556	0.0266	O	1.020	I	O	
20	0.004	0.0417	0.110	0.0933	0.0266	0.0639	1.000	0.026	0.0647	0.567	0.0267	O	1.004	I	O	
21	0.004	0.0417	0.091	0.0561	0.0240	0.0433	1.000	0.032	0.0437		0.0261	O	1.088	I	W	H
22	0.004	0.0417	0.119	0.1143	0.0329	0.0744	0.998	0.024	0.0752	0.751	0.0270	O	0.820	I	O	
23	0.004	0.0417	0.109	0.0905	0.0313	0.0625	1.000	0.026	0.0632		0.0267	O	0.852	I	W	H
24	0.004	0.0417	0.106	0.0851	0.0304	0.0597	1.000	0.027	0.0603		0.0266	O	0.874	I	W	H
25	0.004	0.0417	0.103	0.0789	0.0294	0.0563	1.000	0.028	0.0569		0.0265	O	0.901	I	W	H
26	0.004	0.0417	0.099	0.0712	0.0279	0.0521	1.000	0.029	0.0526		0.0264	O	0.945	I	W	H
27	0.004	0.0417	0.114	0.1017	0.0318	0.0682	1.000	0.025	0.0690	0.720	0.0268	O	0.843	I	O	
28	0.004	0.0417	0.094	0.0613	0.0244	0.0464	1.000	0.031	0.0469		0.0262	O	1.074	I	T	
29	0.004	0.0417	0.068	0.0255	0.0180	0.0228	1.000	0.046	0.0230		0.0254	W	1.275	J	W	H
30	0.004	0.0417	0.058	0.0165	0.0132	0.0157	1.000	0.055	0.0157		0.0250	W	1.189	J	W	H
31	0.004	0.0417	0.040	0.0064	0.0061	0.0064	1.000	0.081	0.0064		0.0245	W	1.049	J	W	H
32	0.004	0.0417	0.095	0.0628	0.0237	0.0473	1.000	0.031	0.0478		0.0262	O	1.107	J	T	
33	0.004	0.0417	0.080	0.0405	0.0215	0.0335	1.000	0.037	0.0337		0.0258	O	1.199	J	W	H
34	0.004	0.0417	0.104	0.0797	0.0256	0.0567	1.000	0.028	0.0574	0.545	0.0265	O	1.035	J	O	
35	0.004	0.0417	0.121	0.1205	0.0271	0.0774	0.996	0.023	0.0780	0.572	0.0270	O	0.998	J	O	
36	0.004	0.0417	0.095	0.0639	0.0248	0.0479	1.000	0.030	0.0484	0.545	0.0260	O	1.047	K	O	
37	0.004	0.0417	0.073	0.0310	0.0188	0.0269	1.000	0.042	0.0271		0.0250	O	1.330	K	W	H
38	0.004	0.0417	0.084	0.0453	0.0224	0.0366	1.000	0.035	0.0369		0.0255	O	1.138	K	W	H

Table B.5 Calculations for Weir and Orifice Control for Drain 2B (Smith and Holley, 1996) - continued

Test No.	S	S_x	y_n m	Q_a m³/s	Q m³/s	Q_w m³/s	R_f	R_s	Q_{HEC-12} m³/s	$(C_o)_{calc}$	Q_{orif} m³/s	min Q	Q_{calc}/Q	Con-fig.	Regime	Fig. 4-20
39	0.004	0.0417	0.091	0.0561	0.0244	0.0433	1.000	0.032	0.0437		0.0258	O	1.056	K	W	H
40	0.004	0.0417	0.111	0.0956	0.0255	0.0651	1.000	0.026	0.0659	0.547	0.0266	O	1.043	K	O	
41	0.004	0.0417	0.108	0.0887	0.0252	0.0615	1.000	0.026	0.0623	0.543	0.0265	O	1.050	K	O	
42	0.004	0.0417	0.102	0.0768	0.0252	0.0552	1.000	0.028	0.0558	0.548	0.0262	O	1.041	K	O	
43	0.004	0.0417	0.062	0.0199	0.0146	0.0185	1.000	0.050	0.0185		0.0245	W	1.270	K	W	H
44	0.004	0.0417	0.123	0.1251	0.0271	0.0795	0.994	0.023	0.0801	0.571	0.0271	O	0.998	K	O	
45	0.004	0.0417	0.078	0.0377	0.0198	0.0316	1.000	0.038	0.0318		0.0257	O	1.298	L	W	H
46	0.004	0.0417	0.096	0.0651	0.0239	0.0486	1.000	0.030	0.0491	0.506	0.0263	O	1.099	L	O	
47	0.004	0.0417	0.103	0.0776	0.0242	0.0556	1.000	0.028	0.0562	0.509	0.0265	O	1.094	L	O	
48	0.004	0.0417	0.103	0.0781	0.0243	0.0559	1.000	0.028	0.0565	0.511	0.0265	O	1.090	L	O	
49	0.004	0.0417	0.101	0.0737	0.0239	0.0535	1.000	0.029	0.0540		0.0262			L*	*	
50	0.004	0.0417	0.091	0.0568	0.0235	0.0437	1.000	0.032	0.0441		0.0258			L*	W	H
51	0.004	0.0417	0.082	0.0423	0.0211	0.0346	1.000	0.036	0.0349		0.0254			L*	W	H
52	0.004	0.0417	0.078	0.0369	0.0201	0.0310	1.000	0.039	0.0312		0.0252			L*	W	H
53	0.004	0.0417	0.087	0.0501	0.0225	0.0396	1.000	0.034	0.0400		0.0256			L*	W	H
54	0.004	0.0417	0.107	0.0864	0.0239	0.0604	1.000	0.027	0.0610		0.0264			L*	*	
55	0.004	0.0417	0.120	0.1180	0.0247	0.0761	0.997	0.023	0.0769		0.0269			L*	*	
56	0.004	0.0417	0.132	0.1532	0.0251	0.0922	0.983	0.021	0.0919		0.0274			L*	*	
57	0.004	0.0417	0.103	0.0779	0.0236	0.0558	1.000	0.028	0.0564		0.0263			L*	*	
58	0.004	0.0417	0.074	0.0322	0.0192	0.0278	1.000	0.041	0.0279		0.0256	O	1.331	M	W	H
59	0.004	0.0417	0.108	0.0891	0.0270	0.0617	1.000	0.026	0.0625	0.580	0.0266	O	0.987	M	O	
60	0.004	0.0417	0.090	0.0546	0.0240	0.0424	1.000	0.033	0.0428		0.0261	O	1.086	M	W	H
61	0.004	0.0417	0.119	0.1155	0.0272	0.0750	0.998	0.024	0.0757	0.576	0.0270	O	0.992	M	O	
62	0.004	0.0417	0.090	0.0540	0.0236	0.0420	1.000	0.033	0.0424		0.0261	O	1.104	M	W	H
63	0.004	0.0417	0.133	0.1541	0.0282	0.0926	0.983	0.021	0.0923	0.592	0.0274	O	0.971	M	O	
64	0.004	0.0417	0.073	0.0311	0.0187	0.0270	1.000	0.042	0.0271		0.0250			M*	W	H
65	0.004	0.0417	0.087	0.0497	0.0226	0.0394	1.000	0.034	0.0397		0.0256			M*	W	H
66	0.004	0.0417	0.094	0.0616	0.0239	0.0466	1.000	0.031	0.0470		0.0259			M*	*	
67	0.004	0.0417	0.100	0.0715	0.0243	0.0523	1.000	0.029	0.0528		0.0261			M*	*	
68	0.004	0.0417	0.111	0.0947	0.0244	0.0646	1.000	0.026	0.0654		0.0266			M*	*	
69	0.004	0.0417	0.122	0.1217	0.0251	0.0779	0.995	0.023	0.0785		0.0270			M*	*	
70	0.004	0.0417	0.122	0.1217	0.0251	0.0779	0.995	0.023	0.0785		0.0270			M*	*	
71	0.004	0.0417	0.131	0.1482	0.0252	0.0900	0.985	0.021	0.0899		0.0274			M*	*	
72	0.004	0.0417	0.108	0.0890	0.0240	0.0617	1.000	0.026	0.0624		0.0265			M*	*	
73	0.004	0.0417	0.075	0.0338	0.0189	0.0289	1.000	0.040	0.0291		0.0251			M*	W	H
74	0.004	0.0417	0.098	0.0679	0.0281	0.0502	1.000	0.030	0.0507		0.0260			N*	W	H
75	0.004	0.0417	0.085	0.0472	0.0235	0.0378	1.000	0.035	0.0381		0.0255			N*	W	H
76	0.004	0.0417	0.108	0.0883	0.0318	0.0613	1.000	0.026	0.0621		0.0265			N*	W	H
77	0.004	0.0417	0.121	0.1209	0.0364	0.0775	0.996	0.023	0.0782		0.0270			N*	W	H
78	0.004	0.0417	0.128	0.1403	0.0426	0.0865	0.988	0.022	0.0866		0.0273			N*	W	H
79	0.004	0.0417	0.126	0.1347	0.0386	0.0839	0.990	0.022	0.0842		0.0272			N*	W	H
80	0.004	0.0417	0.104	0.0796	0.0268	0.0567	1.000	0.028	0.0573		0.0263			O*	*	
81	0.004	0.0417	0.096	0.0641	0.0261	0.0480	1.000	0.030	0.0485		0.0260			O*	W	H
82	0.004	0.0417	0.080	0.0397	0.0214	0.0329	1.000	0.037	0.0332		0.0253			O*	W	H
83	0.004	0.0417	0.107	0.0871	0.0275	0.0607	1.000	0.027	0.0614		0.0264			O*	*	
84	0.004	0.0417	0.121	0.1214	0.0288	0.0778	0.995	0.023	0.0784		0.0270			O*	*	
85	0.004	0.0417	0.110	0.0939	0.0277	0.0642	1.000	0.026	0.0650		0.0266			O*	*	
86	0.004	0.0417	0.105	0.0814	0.0270	0.0577	1.000	0.027	0.0583		0.0263			O*	*	
87	0.004	0.0417	0.084	0.0452	0.0226	0.0365	1.000	0.035	0.0368		0.0255			P*	W	H
88	0.004	0.0417	0.094	0.0611	0.0261	0.0463	1.000	0.031	0.0468		0.0259			P*	W	H

Table B.5 Calculations for Weir and Orifice Control for Drain 2B (Smith and Holley, 1996) - continued

Test No.	S	S_x	y_n m	Q_a m³/s	Q m³/s	Q_w m³/s	R_f	R_s	Q_{HEC-12} m³/s	$(C_o)_{calc}$	Q_{orif} m³/s	min Q	Q_{calc}/Q	Con-fig.	Regime	Fig. 4-20
89	0.004	0.0417	0.106	0.0844	0.0306	0.0593	1.000	0.027	0.0600		0.0264			P*	W	H
90	0.004	0.0417	0.101	0.0749	0.0295	0.0541	1.000	0.028	0.0547		0.0262			P*	W	H
91	0.004	0.0417	0.121	0.1192	0.0351	0.0767	0.996	0.023	0.0774		0.0270			P*	W	H
92	0.004	0.0417	0.118	0.1122	0.0348	0.0734	0.999	0.024	0.0742		0.0269			P*	W	H
93	0.004	0.0417	0.132	0.1516	0.0422	0.0915	0.984	0.021	0.0913		0.0274			P*	W	H
94	0.004	0.0417	0.128	0.1398	0.0399	0.0862	0.988	0.022	0.0864		0.0273			P*	W	H

Table B.6 Calculations for Weir and Orifice Control for Drain 3 (Holley et al., 1992)

Weir (HEC-12) Calculations
P-1-7/8-4 Grate
W = 0.610 m
L = 0.915 m
V_o = 1.88 m/s

Test	S	S_x	y_n	Q_a	Q	Q_w	R_f	R_s	Q_{HEC-12}	Q_{calc}/Q	Regime	Fig.
No.			m	m^3/s	m^3/s	m^3/s			m^3/s			4-20
1	0.001	0.02	0.064	0.0183	0.0167	0.0079	1.000	0.810	0.0164	0.979	W	B
2	0.001	0.02	0.0287	0.0371	0.083	0.0128	1.000	0.756	0.0312	1.086	W	B
3	0.001	0.02	0.0356	0.0536	0.095	0.0164	1.000	0.724	0.0434	1.219	W	B
4	0.001	0.04	0.0447	0.0537	0.123	0.0239	1.000	0.794	0.0475	1.063	W	C
5	0.001	0.04	0.0475	0.0871	0.148	0.0333	1.000	0.756	0.0740		T	
6	0.001	0.04	0.0289	0.0301	0.099	0.0159	1.000	0.833	0.0277	0.960	W	C
7	0.001	0.06	0.0277	0.0277	0.112	0.0180	1.000	0.866	0.0264	0.953	W	D
8	0.001	0.06	0.0443	0.0479	0.138	0.0269	1.000	0.835	0.0445	1.003	W	D
9	0.001	0.08	0.0252	0.0252	0.121	0.0189	1.000	0.888	0.0245	0.972	W	E
10	0.001	0.08	0.0386	0.0443	0.149	0.0289	1.000	0.860	0.0421	1.090	W	E
11	0.005	0.01	0.0115	0.0163	0.035	0.0066	1.000	0.508	0.0115	1.002	W	F
12	0.005	0.01	0.0146	0.0219	0.039	0.0080	1.000	0.476	0.0146	1.001	W	F
13	0.005	0.02	0.0113	0.0130	0.041	0.0079	1.000	0.627	0.0111	0.976	W	G
14	0.005	0.02	0.0161	0.0182	0.047	0.0100	1.000	0.591	0.0148	0.924	W	G
15	0.005	0.04	0.0083	0.0083	0.045	0.0072	1.000	0.751	0.0080	0.968	W	H
16	0.005	0.04	0.0323	0.0339	0.077	0.0217	1.000	0.615	0.0292	0.904	W	H
17	0.005	0.06	0.0250	0.0250	0.080	0.0201	1.000	0.696	0.0235	0.941	W	I
18	0.005	0.06	0.0336	0.0341	0.090	0.0257	1.000	0.665	0.0313	0.933	W	I
19	0.005	0.06	0.0443	0.0501	0.104	0.0345	1.000	0.626	0.0443	1.000	W	I
20	0.005	0.06	0.0424	0.0745	0.120	0.0462	1.000	0.583	0.0627		T	
21	0.005	0.08	0.0206	0.0206	0.083	0.0187	1.000	0.745	0.0201	0.976	W	J
22	0.005	0.08	0.0387	0.0412	0.107	0.0331	1.000	0.682	0.0386	0.997	W	J
23	0.01	0.01	0.0102	0.0141	0.029	0.0066	1.000	0.409	0.0097	0.952	W	K
24	0.01	0.01	0.0151	0.0229	0.035	0.0092	1.000	0.358	0.0141	0.936	W	K
25	0.01	0.02	0.0138	0.0156	0.039	0.0099	1.000	0.492	0.0127	0.917	W	L
26	0.01	0.02	0.0303	0.0415	0.056	0.0199	1.000	0.384	0.0282	0.930	W	L
27	0.01	0.04	0.0180	0.0180	0.053	0.0145	1.000	0.571	0.0165	0.917	W	M
28	0.01	0.04	0.0293	0.0307	0.065	0.0219	1.000	0.511	0.0264	0.900	W	M
29	0.01	0.04	0.0451	0.0688	0.088	0.0399	1.000	0.421	0.0521		T	
30	0.01	0.06	0.0416	0.0688	0.102	0.0477	1.000	0.476	0.0577		T	
31	0.01	0.06	0.0256	0.0256	0.071	0.0219	1.000	0.586	0.0241		T	
32	0.01	0.08	0.0337	0.0366	0.090	0.0321	1.000	0.586	0.0348		T	
33	0.01	0.08	0.0357	0.0423	0.095	0.0361	1.000	0.570	0.0396		T	
34	0.02	0.01	0.0108	0.0150	0.026	0.0076	1.000	0.297	0.0098	0.907	W	P
35	0.02	0.02	0.0132	0.0150	0.034	0.0105	1.000	0.382	0.0122	0.922	W	Q
36	0.02	0.02	0.0216	0.0262	0.041	0.0158	1.000	0.325	0.0192	0.887	W	Q
37	0.02	0.04	0.0139	0.0139	0.042	0.0125	1.000	0.483	0.0132	0.947	W	R
38	0.02	0.04	0.0225	0.0233	0.051	0.0191	1.000	0.426	0.0209	0.927	W	R
39	0.02	0.06	0.0308	0.0315	0.067	0.0276	1.000	0.447	0.0294	0.954	W	S
40	0.02	0.06	0.0404	0.0461	0.077	0.0378	1.000	0.405	0.0412	1.019	W	S
41	0.02	0.08	0.0275	0.0286	0.072	0.0272	1.000	0.498	0.0279	1.013	W	T
42	0.02	0.08	0.0347	0.0453	0.086	0.0405	1.000	0.446	0.0427	1.231	W	T
43	0.02	0.08	0.0368	0.0749	0.103	0.0613	1.000	0.391	0.0666		T	
44	0.04	0.02	0.0154	0.0178	0.032	0.0130	1.000	0.264	0.0143	0.928	W	V

Table B.6 Calculations for Weir and Orifice Control for Drain 3 (Holley et al., 1992)

Test	S	S_x	y_n	Q_a	Q	Q_w	R_f	R_s	Q_{HEC-12}	Q_{calc}/Q	Regime	Fig.
No.			m	m^3/s	m^3/s	m^3/s			m^3/s			4-20
45	0.04	0.02	0.0283	0.0369	0.041	0.0224	1.000	0.205	0.0254	0.895	W	V
46	0.04	0.02	0.0399	0.0709	0.053	0.0357	1.000	0.161	0.0414	1.036	W	V
47	0.04	0.04	0.0149	0.0156	0.039	0.0145	1.000	0.358	0.0149	0.999	W	W
48	0.04	0.04	0.0239	0.0252	0.047	0.0217	1.000	0.310	0.0228	0.956	W	W
49	0.04	0.06	0.0207	0.0207	0.050	0.0201	1.000	0.380	0.0203	0.981	W	X
50	0.04	0.06	0.0334	0.0362	0.062	0.0329	1.000	0.322	0.0340	1.017	W	X
51	0.04	0.08	0.0295	0.0362	0.069	0.0348	1.000	0.358	0.0353		T	
52	0.04	0.08	0.0333	0.0828	0.094	0.0709	1.000	0.278	0.0742		T	
53	0.06	0.02	0.0120	0.0141	0.027	0.0113	1.000	0.232	0.0120	0.996	W	a
54	0.06	0.02	0.0279	0.0357	0.038	0.0230	1.000	0.166	0.0251	0.899	W	a
55	0.06	0.04	0.0246	0.0264	0.044	0.0234	1.000	0.250	0.0241	0.981	W	b
56	0.06	0.04	0.0368	0.0471	0.055	0.0374	1.000	0.205	0.0394	1.071	W	b
57	0.06	0.06	0.0307	0.0350	0.057	0.0327	1.000	0.269	0.0333		T	
58	0.06	0.06	0.0305	0.0653	0.072	0.0555	1.000	0.217	0.0577		T	
59	0.08	0.04	0.0163	0.0176	0.036	0.0168	1.000	0.248	0.0170	1.044	W	g
60	0.08	0.04	0.0339	0.0437	0.050	0.0363	1.000	0.180	0.0376	1.110	W	g
61	0.08	0.04	0.0362	0.1008	0.069	0.0695	1.000	0.131	0.0736		T	

Table B.7 Calculations for Weir and Orifice Control for Drain 4 (Hammons and Holley, 1996)

Weir (HEC-12) Calculations
45° Tilt Bar Grate
W = 0.994 m
L = 0..297 m
V_o = 1.01 m/s

Orifice Calculations
D_o = 0.203 m
W_c = 0.907 m
L_v = 0.299 m
No. of Elbows = 0

Test No.	S	S_x	y_n m	Q_a m^3/s	Q m^3/s	Q_w m^3/s	R_f	R_s	Q_{HEC-12} m^3/s	Q_{orif} m^3/s	min Q	Q_{calc}/Q	Regime	Fig. 4-20
4_01	0.004	0.0417	0.120	0.1188	0.0574	0.0814	1.000	0.032	0.0827	0.0506	O	0.881	T	
4_02	0.004	0.0417	0.103	0.0786	0.0450	0.0594	1.000	0.039	0.0602	0.0494	O	1.097	T	
4_03	0.004	0.0417	0.081	0.0412	0.0348	0.0355	1.000	0.051	0.0358	0.0479	W	1.028	T	
4_04	0.01	0.0417	0.069	0.0428	0.0337	0.0394	1.000	0.028	0.0395	0.0470	W	1.173	T	
4_05	0.01	0.0417	0.084	0.0709	0.0417	0.0602	1.000	0.022	0.0604	0.0481	O	1.153	T	
4_06	0.01	0.0417	0.101	0.1188	0.0548	0.0907	1.000	0.018	0.0912	0.0493	O	0.900	T	
4_07	0.02	0.0417	0.089	0.1188	0.0514	0.0976	0.928	0.011	0.0908	0.0484	O	0.943	T	
4_08	0.02	0.0417	0.075	0.0753	0.0399	0.0671	0.968	0.014	0.0651	0.0475	O	1.190	T	
4_09	0.02	0.0417	0.058	0.0374	0.0298	0.0363	1.000	0.019	0.0363	0.0462	W	1.217	T	
4_10	0.04	0.0417	0.051	0.0376	0.0278	0.0373	0.938	0.012	0.0350	0.0457	W	1.258	W	W
4_11	0.04	0.0417	0.066	0.0748	0.0375	0.0701	0.871	0.009	0.0611	0.0468	O	1.250	T	
4_12	0.04	0.0417	0.078	0.1171	0.0489	0.1027	0.821	0.007	0.0844	0.0477	O	0.974	T	
4_13	0.06	0.0417	0.072	0.1171	0.0477	0.1061	0.742	0.005	0.0788	0.0473	O	0.990	T	
4_14	0.06	0.0417	0.066	0.0928	0.0420	0.0868	0.774	0.006	0.0672	0.0468	O	1.114	T	
4_15	0.06	0.0417	0.053	0.0506	0.0303	0.0499	0.847	0.008	0.0423	0.0459	W	1.397	T	
4_16	0.06	0.0208	0.048	0.0774	0.0404	0.0606	0.876	0.008	0.0532	0.0469	O	1.159	T	
4_17	0.06	0.0208	0.039	0.0471	0.0356	0.0407	0.925	0.010	0.0377	0.0463	W	1.058	T	
4_18	0.06	0.0208	0.047	0.0744	0.0410	0.0588	0.880	0.008	0.0518	0.0468	O	1.143	T	
4_19	0.04	0.0208	0.053	0.0853	0.0448	0.0625	0.926	0.010	0.0581	0.0473	O	1.054	T	
4_20	0.04	0.0208	0.060	0.1171	0.0493	0.0794	0.896	0.009	0.0714	0.0477	O	0.967	T	
4_21	0.04	0.0208	0.048	0.0657	0.0415	0.0510	0.950	0.011	0.0486	0.0469	O	1.131	T	
4_22	0.02	0.0208	0.053	0.0605	0.0402	0.0443	1.000	0.019	0.0446	0.0473	W	1.108	T	
4_23	0.02	0.0208	0.058	0.0777	0.0435	0.0535	1.000	0.017	0.0539	0.0476	O	1.095	T	
4_24	0.02	0.0208	0.070	0.1248	0.0504	0.0760	0.983	0.014	0.0753	0.0484	O	0.962	T	
4_25	0.01	0.0208	0.079	0.1243	0.0574	0.0688	1.000	0.021	0.0700	0.0491	O	0.855	T	
4_26	0.01	0.0208	0.067	0.0788	0.0445	0.0495	1.000	0.026	0.0502	0.0482	O	1.085	T	
4_27	0.01	0.0208	0.061	0.0605	0.0410	0.0407	1.000	0.029	0.0413	0.0478	W	1.008	T	
4_28	0.004	0.0208	0.061	0.0390	0.0310	0.0261	1.000	0.064	0.0269	0.0478	W	0.867	T	
4_29	0.004	0.0208	0.079	0.0776	0.0450	0.0431	1.000	0.048	0.0448	0.0491	W	0.994	T	
4_30	0.004	0.0208	0.093	0.1198	0.0531	0.0586	1.000	0.040	0.0611	0.0500	O	0.942	T	
4_31	0.004	0.0208	0.112	0.1956	0.0685	0.0824	1.000	0.032	0.0860	0.0513	O	0.749	T	
4_32	0.004	0.0417	0.135	0.1612	0.0670	0.1022	1.000	0.028	0.1039	0.0515	O	0.769	T	
4_33	0.06	0.0208	0.062	0.1558	0.0594	0.1034	0.795	0.006	0.0825	0.0479	O	0.805	T	
4_34	0.06	0.0417	0.077	0.1405	0.0524	0.1237	0.716	0.005	0.0887	0.0476	O	0.908	T	
4_35	0.06	0.0417	0.034	0.0158	0.0127	0.0158	0.961	0.013	0.0152	0.0445	W	1.195	W	b
4_36	0.06	0.0417	0.043	0.0290	0.0205	0.0290	0.906	0.010	0.0263	0.0451	W	1.282	W	b
4_37	0.06	0.0208	0.028	0.0186	0.0167	0.0181	1.000	0.015	0.0181	0.0454	W	1.087	W	a
4_38	0.06	0.0208	0.035	0.0341	0.0274	0.0310	0.954	0.012	0.0296	0.0459	W	1.081	W	a
4_39	0.004	0.0208	0.043	0.0155	0.0131	0.0128	1.000	0.094	0.0130	0.0465	W	0.999	W	G
4_40	0.004	0.0208	0.054	0.0279	0.0240	0.0203	1.000	0.074	0.0208	0.0473	W	0.866	W	G
4_41	0.004	0.0417	0.055	0.0149	0.0143	0.0146	1.000	0.079	0.0146	0.0461	W	1.021	W	H
4_42	0.004	0.0417	0.063	0.0213	0.0206	0.0202	1.000	0.068	0.0203	0.0466	W	0.984	W	H
4_43	0.01	0.0417	0.062	0.0323	0.0298	0.0308	1.000	0.031	0.0308	0.0466	W	1.032	T	
4_44	0.01	0.0417	0.052	0.0198	0.0197	0.0196	1.000	0.039	0.0196	0.0458	W	0.994	W	M

Table B.7 Calculations for Weir and Orifice Control for Drain 4 (Hammons and Holley, 1996) - continued

Test No.	S	S_x	y_n m	Q_a m³/s	Q m³/s	Q_w m³/s	R_f	R_s	Q_{HEC-12} m³/s	Q_{orif} m³/s	min Q	Q_{calc}/Q	Regime	Fig. 4-20
4_45	0.04	0.0417	0.040	0.0197	0.0165	0.0197	0.992	0.016	0.0195	0.0449	W	1.187	W	W
4_46	0.04	0.0208	0.033	0.0230	0.0203	0.0215	1.000	0.018	0.0215	0.0458	W	1.061	W	V
4_47	0.04	0.0208	0.051	0.0766	0.0413	0.0575	0.936	0.011	0.0540	0.0471	O	1.140	T	
4_48	0.04	0.0208	0.067	0.1605	0.0617	0.1003	0.863	0.008	0.0870	0.0483	O	0.782	T	
4_49	0.02	0.0208	0.076	0.1587	0.0594	0.0904	0.963	0.012	0.0879	0.0489	O	0.823	T	
4_50	0.02	0.0208	0.040	0.0285	0.0255	0.0244	1.000	0.026	0.0245	0.0463	W	0.961	W	Q
4_51	0.01	0.0208	0.046	0.0286	0.0247	0.0228	1.000	0.041	0.0231	0.0467	W	0.934	W	L

Table B.8 Statistics for Ratios of Calculated and Measured Captured Flows

Range of Q_{calc}/Q	Average minus Std. Dev.	Average Q_{calc}/Q	Average plus Std. Dev.	Standard Deviation	No. of Points
0.25-0.30	0.92	1.03	1.14	0.112	7
0.30-0.35	0.95	1.12	1.28	0.165	18
0.35-0.40	0.86	1.12	1.38	0.258	22
0.40-0.45	0.95	1.16	1.37	0.209	24
0.45-0.50	1.01	1.30	1.60	0.294	13
0.50-0.55	1.13	1.31	1.48	0.179	15
0.55-0.60	1.06	1.21	1.36	0.149	20
0.60-0.65	1.03	1.19	1.36	0.168	8
0.65-0.70	1.00	1.17	1.35	0.173	15
0.70-0.75	0.98	1.13	1.29	0.152	18
0.75-0.80	0.90	1.06	1.22	0.156	20
0.80-0.85	0.96	1.04	1.12	0.080	19
0.85-0.90	0.92	1.02	1.11	0.099	33
0.90-0.95	0.98	1.02	1.07	0.044	29
0.95-1.00	0.92	0.97	1.02	0.047	28

APPENDIX C - PHOTOGRAPHS

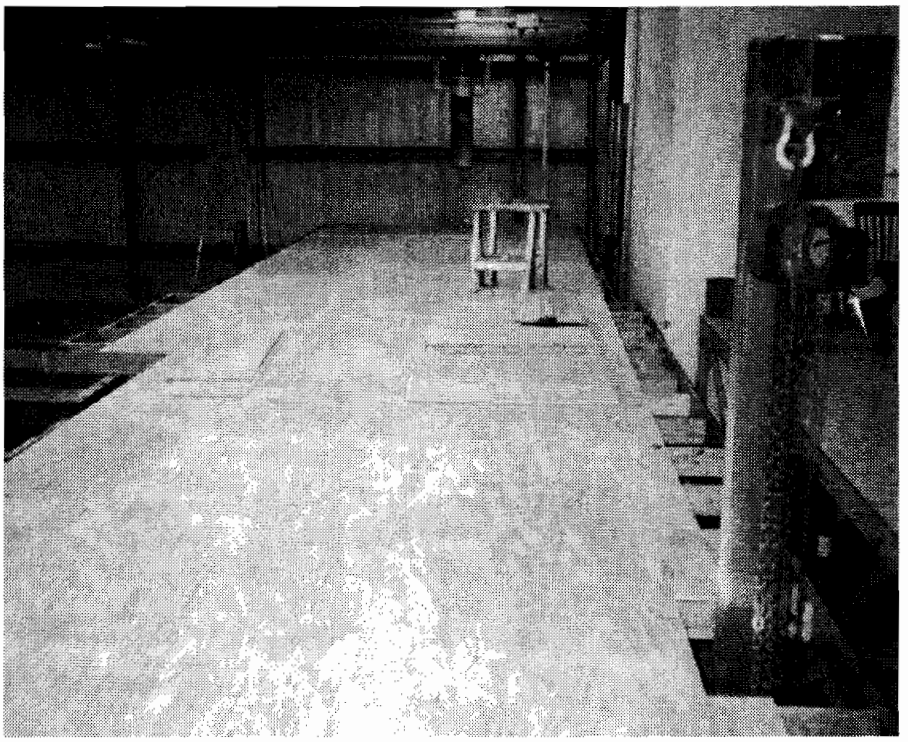

Figure C.1 Large Model During Construction

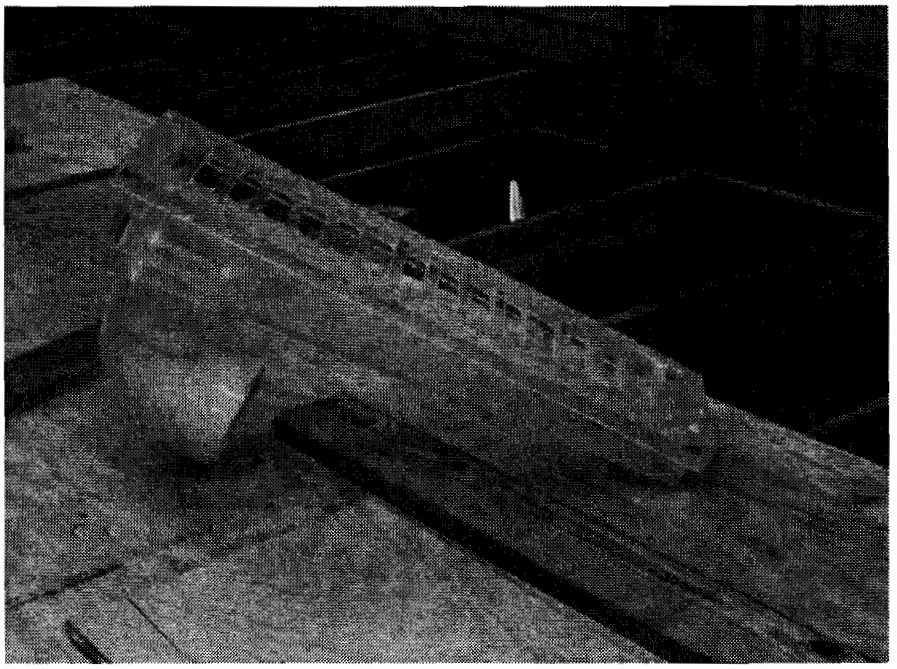

Figure C.2 Plexiglas Model of Drain 2B

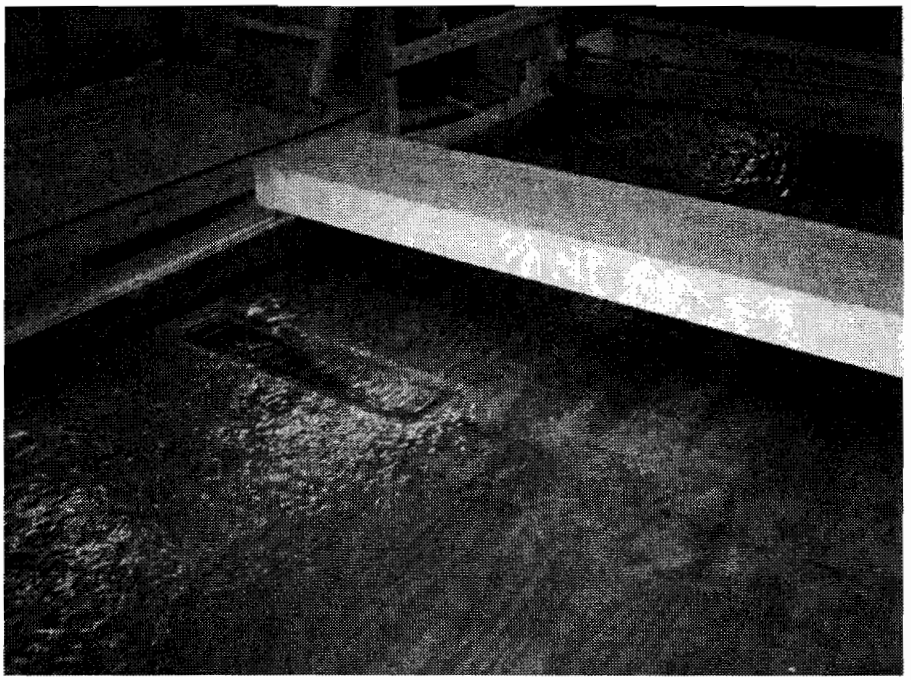

Figure C.3 Typical Test with Drain 2B, Looking Downstream

Figure C.4 Drain 2B with Partially Submerged Conditions Near Curb
(Flow from Left to Right, Looking Toward Curb)

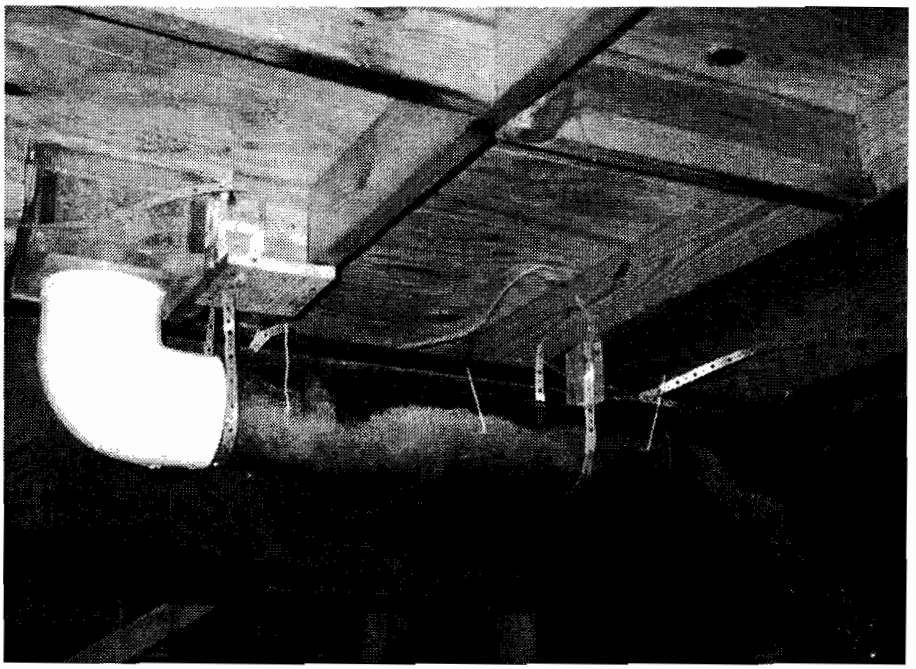

Figure C.5 Piping Configuration I
(Horizontal Pipe Not Full)

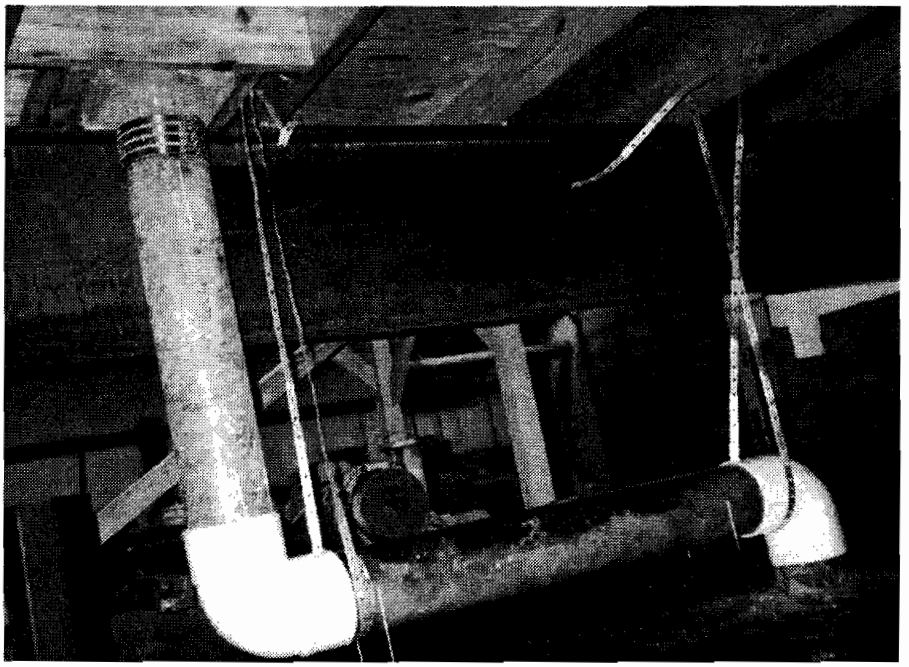

Figure C.6 Piping Configuration H
(Horizontal Pipe Not Full, Note Air Bubbles in Vertical Pipe)

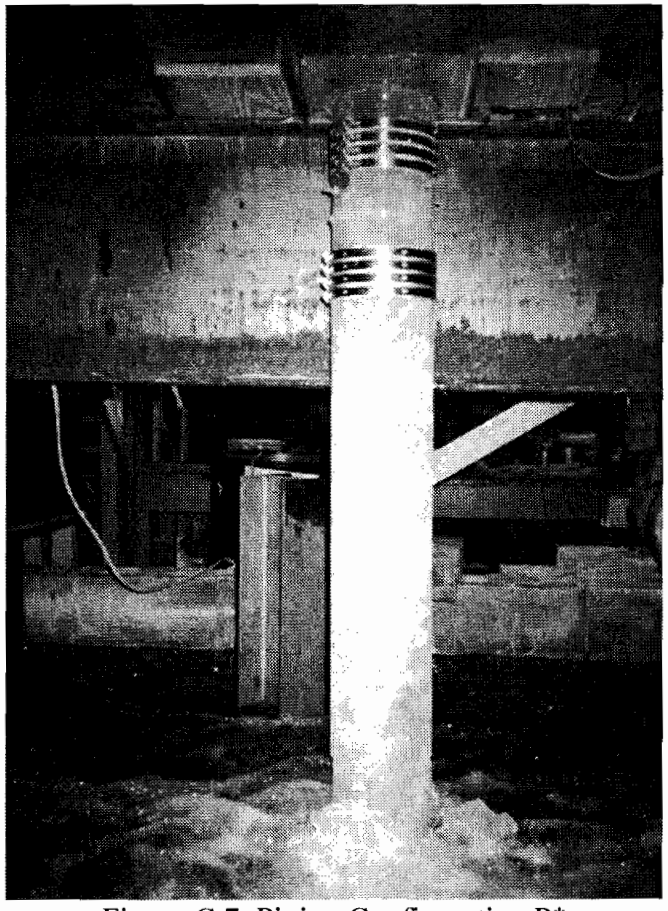

Figure C.7 Piping Configuration P*

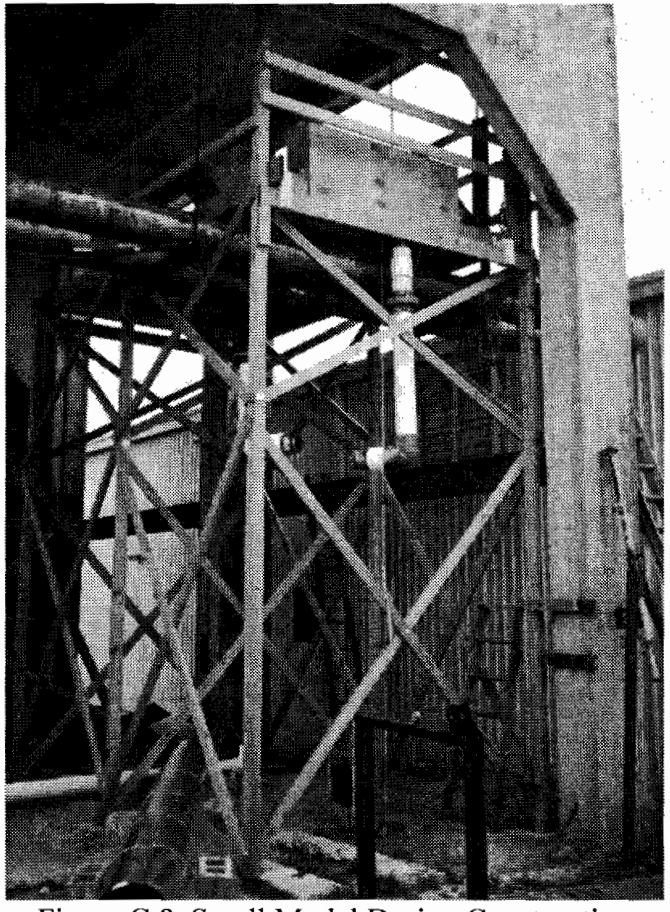

Figure C.8 Small Model During Construction